Nature versus Nurture: How Parent Galaxy Environments Affect the Rates and Properties of their Type Ia Supernovae

by

Melissa Lynn Graham
B.Sc., Queen's University, 2004

A Dissertation Submitted in Partial Fulfillment of the
Requirements for the Degree of

DOCTOR OF PHILOSOPHY

in the Department of Physics and Astronomy

Nature versus Nurture: How Parent Galaxy Environments Affect the Rates and Properties of their Type Ia Supernovae

by

Melissa Lynn Graham
B.Sc., Queen's University, 2004

Supervisory Committee

Dr. C. J. Pritchet, Supervisor
(Department of Physics and Astronomy, University of Victoria)

Dr. F. D. A. Hartwick, Departmental Member
(Department of Physics and Astronomy, University of Victoria)

Dr. S. L. Ellison, Departmental Member
(Department of Physics and Astronomy, University of Victoria)

Dr. D. A. VandenBerg, Departmental Member
(Department of Physics and Astronomy, University of Victoria)

Dr. R. Illner, Outside Member
(Department of Mathematics, University of Victoria)

Supervisory Committee

Dr. C. J. Pritchet, Supervisor
(Department of Physics and Astronomy, University of Victoria)

Dr. F. D. A. Hartwick, Departmental Member
(Department of Physics and Astronomy, University of Victoria)

Dr. S. L. Ellison, Departmental Member
(Department of Physics and Astronomy, University of Victoria)

Dr. D. A. VandenBerg, Departmental Member
(Department of Physics and Astronomy, University of Victoria)

Dr. R. Illner, Outside Member
(Department of Mathematics, University of Victoria)

ABSTRACT

Supernovae of Type Ia, SNe Ia, are currently the most powerful tool of modern cosmology, but their progenitor scenario is not yet well constrained. Recent studies of SN Ia rates in radio-loud early-type galaxies, and members of rich clusters, suggest a possible influence on SN Ia explosions *outside* of the established correlation with the age of the parent galaxy's stellar population (via the current specific star formation rate, sSFR). These rates were used to show that the characteristics of SN Ia progenitor systems may be inconsistent with theoretical expectations of the most popular scenarios. The astrophysical question of this thesis is: do parent galaxy and environment influence the rates and properties of Type Ia supernovae, and, if so, how? Towards this end, we combine the database of Type Ia supernovae from the Canada-France-Hawaii Telescope's Supernova Legacy Survey with publicly available catalogs including: galaxy photometric and spectroscopic redshifts, radio and infrared sources, and members of galaxy groups and clusters. This is the most comprehensive set of multi-wavelength host properties and environment parameters for intermediate redshift Type Ia supernovae yet compiled. We present the SNLS SN Ia rate per unit mass in a variety of parent galaxy and environment samples. We also statistically assess the probability of discrepancies between our rates, those of previous works

at low redshift, rates in the general population of galaxies, and predictions of established empirical SN Ia rate models. In general, we do not find statistically significant evidence for SN Ia rate enhancements over the general population in galaxies which are radio-loud, infrared-bright, or associated with galaxy groups and clusters. In cases where we do find a suggestive rate enhancement, it is always with $\lesssim 2\sigma$ confidence. These rates agree with established empirical rate models, which in turn are consistent with theoretical expectations of the most plausible progenitor scenarios. Furthermore, we find the properties of SNLS SNe Ia in these types of hosts and environments are consistent with the predictions of these scenarios. We conclude that, aside from the established correlation with host sSFR, no conclusive evidence is observed with SNLS data for strictly environmental effects on SN Ia rates. This supports their continued status as cosmological standard candles.

Contents

List of Tables

List of Figures

ACKNOWLEDGMENTS

I would like to thank the following colleagues, teachers, and administrators:

My supervisor, Chris Pritchet, and my closest colleagues, David Sand and Eric Hsiao. SNLS team members: Mark Sullivan, Andy Howell, Don Neill, Kathy Perrett, Alex Conley, Ray Carlberg, Sebastien Fabbro, Reynald Pain, Isobel Hook, and Julien Guy. MEGaCS team members: Henk Hoekstra and Chris Bildfell. PSSS team members and DAO staff: Dave Balam, Russ Robb, Alex Parker, Sarah Sadavoy, Aaron Maxwell, David Bohlender, and Dmitry Monin.

My professors, and senior graduate students in Victoria: David Hartwick, Don VandenBerg, Sara Ellison, Luc Simard, Jon Willis, Stephen Gwyn, Gregg Poole, James Clem, and Karun Thanjavur. My professors and TAs in Kingston: Gregg Wade at the RMC; Larry Widrow, Judith Irwin, Rupinder Brar, and Douglas McNeil at Queens.

Staff and faculty at the University of Victoria: Stephenson Yang, Michel LeFèvre, Susan Gnucci, Monica Lee, Chantal Laliberté, Michelle Shen, Alex VanNetten, Cynthia Korpan, Charles Card, Bob Kowalewski, Tony Burke, and Reinhard Illner. Staff at CFHT: The Queued Service Observations team, especially Todd Burdullis; Jean-Charles Cuillandre, Daniel Devost, Adam Draginda, and Teddy George.

Olivier Ilbert and Henry McCracken for early access to and correspondence regarding the photometric redshift galaxy catalog, Lisbeth Olsen for early access the optical cluster catalog, and Enrico Cappellaro for access to the C99 galaxy and supernova samples. Dan Maoz, Colin Borys, Dave Patton, Douglas Scott, and Stephane Arnouts for their scientific advice, and anonymous referees for constructive correspondence.

Technical acknowledgments for data and data products:

This work is based in part on observations obtained with MegaPrime/MegaCam, a joint project of CFHT and CEA/DAPNIA, at the CFHT which is operated by the National Research Council (NRC) of Canada, the Institut National des Science de l'Univers of the Centre National de la Recherche Scientifique (CNRS) of France, and the University of Hawaii. This work is based in part of data products produced at the Canadian Astronomy Data Centre as part of the CFHT Legacy Survey, a collaborative project of NRC and CNRS.

The SNLS spectroscopic follow-up program is based in part on observations obtained at the Gemini Observatory, which is operated by the Association of Universities for Research in Astronomy, Inc., under a cooperative agreement with the NSF on behalf of the Gemini

partnership: the National Science Foundation (United States), the Science and Technology Facilities Council (United Kingdom), the National Research Council (Canada), CONICYT (Chile), the Australian Research Council (Australia), Ministério da Ciência e Tecnologia (Brazil) and Ministerio de Ciencia, Tecnología e Innovación Productiva (Argentina) Gemini identification numbers of the programs under which these observations were taken are: GS-2003B-Q-8, GN-2003B-Q-9, GS-2004A-Q-11, GN-2004A-Q-19, GS-2004B-Q-31, GN-2004B-Q-16, GS-2005A-Q-11, GN-2005A-Q-11, GS-2005B-Q-6, GN-2005B-Q-7, GN-2006A-Q-7 and GN-2006B-Q-10. The SNLS spectroscopic follow-up program is also based in part on observations made with the European Southern Observatory Very Large Telescope at in Paranal, Chile (some under program ID 175.A-0839); with the W. M. Keck Observatory which is operated as a scientific partnership among the California Institute of Technology, the University of California, and the National Aeronautics and Space Administration; and with the 6.5 meter Magellan Telescopes located at Las Campanas Observatory, Chile.

This research has made use of data products from the Very Large Array. The VLA is operated by the National Radio Astronomy Observatory, a facility of the National Science Foundation operated under cooperative agreement by Associated Universities, Inc. This research has made use of the NASA/IPAC Extragalactic Database (NED) and Infrared Science Archive (IRSA), which are operated by the Jet Propulsion Laboratory, California Institute of Technology, under contract with the National Aeronautics and Space Administration. This research has made use of the VizieR catalogue access tool, CDS, Strasbourg, France. This research has made use of data products from the Two Micron All Sky Survey, which is a joint project of the University of Massachusetts and the Infrared Processing and Analysis Center/California Institute of Technology, funded by the National Aeronautics and Space Administration and the National Science Foundation. MENeaCS follow-up is based in part on observations at the Bok Telescope and the MMT, operated by the Steward Observatory and the University of Arizona. The MMT is a joint facility of the Smithsonian Institution and the University of Arizona.

This work has been financially supported by NSERC and the University of Victoria. I gratefully acknowledge the financial support of the Province of British Columbia through the Ministry of Advanced Education, and the Criswick fund and the Faculty of Graduate Studies for travel grants to present research.

Chapter 1

Introduction

After millions to billions of years fusing hydrogen and helium into heavier elements, the evolutionary life cycles of many stars end in a sudden and catastrophic death called a supernova. These stellar explosions expel matter at high velocities, scattering enriched material into the interstellar medium where it can be recycled into new stars and planets.

1.1 The Astrophysical Problem

Supernovae are broadly classified based on their observational qualities, and the most homogeneous class of supernovae are called Type Ia. They are all events of approximately the same intrinsic brightness, and observable to great distances. These two qualities make Type Ia supernovae (SNe Ia) modern cosmology's favored standard candle. SNe Ia are widely accepted to be the deaths of white dwarf stars which have accreted sufficient mass from their binary companion to initiate a thermonuclear explosion. However, the specific physical progenitor systems and explosion mechanisms for SNe Ia remain unconstrained.

There is an established correlation between the SN Ia rate and galaxy star formation rate (SFR), in which the specific SN Ia rate is higher in star-forming galaxies. Based on this, the SN Ia rate is commonly expressed as the sum of two components: an "A" component proportional to stellar mass, and a "B" component proportional to SFR. As such, it is commonly referred to as the "A+B" model. Recently, several works have shown the specific SN Ia rate to be enhanced in elliptical galaxies with strong radio emission, or residing in rich galaxy clusters. If the probability of SN Ia explosions is indeed directly influenced by radio emission or environment density, it is an effect *outside* of this established correlation. Furthermore, these enhanced SN Ia rates have been shown to suggest the physical progenitor scenario has certain characteristics that are not currently expected by theoreti-

cal models. This may challenge their use as modern cosmological standard candles. **The main goal of this thesis is to verify and analyze the influence of parent galaxy and environment characteristics on the rates and properties of SNe Ia**.

1.2 Our Approach to a Solution

We meet these goals by combining a database of Type Ia supernovae generated by the Supernova Legacy Survey (SNLS) at the Canada-France-Hawaii Telescope (CFHT), with publicly available catalogs of galaxies, their photometric and spectroscopic redshifts, radio and infrared sources, galaxy groups, and rich galaxy clusters. This collection and synthesis of data catalogs has resulted in the most comprehensive multi-wavelength coverage of intermediate redshift SN Ia parent galaxies to date.

Most of the publications which established the aforementioned SN Ia rate trends are based on low redshift surveys intentionally targeted at galaxies or clusters, some of which lack spectroscopic confirmation of SN events. The supernova, galaxy, and multi-wavelength source catalogs we use have neither of these issues. The highest cost of working with a deeper redshift SN survey is the loss of completeness in the multi-wavelength source catalogs, and we will be clear about how we deal with this in our analysis.

The specific correlations between SN Ia rate, and host radio power or environment density are important because they contribute to understanding the physical nature of SNe Ia, and their suitability as standard candles. The plethora of data available has also enabled our investigation into the less constrained rates in small groups, and relatively unknown SN Ia rates in galaxies with strong infrared emission. To capitalize on the large, deep, uniformly sampled volume of the SNLS fields we have developed two new techniques to parametrize the amount of clustering in a galaxy's local environment, on any desired size scale. We use these parametrizations to compare the SN Ia rates in under-dense, over-dense, and field environments without relying on strict definitions of galaxy groups or clusters. Such an analysis was not possible with previous low-volume, galaxy-targeted surveys.

1.3 A Summary of Our Main Results

The main results of this thesis can be summarized as follows:

1. We show the SNLS SN Ia rate in elliptical galaxies with powerful radio emission is consistent with the "A+B" model, especially when dust-obscured infrared SFR

is considered. This marks the first time infrared SFR is incorporated into the "B" component (proportional to SFR). We also find the characteristics of SNe Ia in radio elliptical galaxies support a continuum of progenitor ages, consistent with expectations of theoretical models.

2. We make the first observation that the SN Ia rate in elliptical Luminous Infrared Galaxies is enhanced by several times over the rate in all ellipticals, at a confidence level of $\lesssim 2\sigma$. We show it is consistent with the "A+B" model, especially when dust-obscured star formation is incorporated.

3. We determine the SN Ia rate in members of small galaxy groups and pairs to be consistent with the field rate for a variety of host and group properties, and also consistent with the "A+B" model. We also show the radio and infrared emission of hosts in groups is not significantly different from field hosts.

4. We find the SNLS SN Ia rate in cluster elliptical galaxies is not strongly supportive of a rate enhancement, is ultimately consistent with the rate in SNLS field ellipticals, but also consistent with the rates in local galaxy clusters. We constrain the SNLS SN Ia cluster rate to agree with the "A+B" model to within a factor of 2.

5. We show the number of SNe Ia observed in environments clustered on small scales is greater than predicted by "A+B", and vice versa in environments with significant clustering on large scales. We find this is suggestive – but ultimately statistically inconclusive – evidence that environment can influence the SN Ia rate.

6. We find no evidence that residence in an under-dense or void environment has a measurable influence on a galaxy's specific SN Ia rate.

These results are a timely and relevant contribution to ongoing efforts to constrain the progenitor scenarios of Type Ia supernovae, but our work does not stop there. Our interest in constraining the influence of environment on the SN Ia rate led to our involvement in the Multi-Epoch Nearby Cluster Survey. MENeaCS will yield the largest sample of cluster supernovae yet observed, and provide better constraints on the cluster SN Ia rate. In Appendix A we present the MENeaCS real-time analysis pipeline for data reduction, SN detection, and flux calibration. We also describe our technique for determining our detection efficiencies, which are necessary for all rates calculations. Appendix A will be useful for anyone conducting their own supernova survey.

At the time of writing, large scale automated surveys for supernovae such as PanSTARRS, Skymapper, and the Palomar Transient Factory are currently online and monitoring the transient sky. Future automated surveys are planned on even larger scales; for example, the Large Synoptic Survey Telescope is poised to come online within five years. Within the decade, tens of thousands of supernovae will be found every month. This thesis lays the necessary groundwork for interpreting such data.

1.4 Thesis Agenda

A one-sentence synopsis of each chapter is provided for the convenience of the reader:

Chapter 1 introduces the main astrophysical problem, and provides a brief preview of how this thesis will solve it.

Chapter 2 gives the reader a deeper background to Type Ia supernovae, with a focus on the recent scientific publications which motivate this work.

Chapter 3 documents the variety of supernova, galaxy, and multi-wavelength source catalogs which are compiled, edited, and used for this thesis.

Chapter 4 covers our analysis of the rates and properties of Type Ia supernovae in galaxies with radio and infrared emission, including the first ever SN Ia rate in Luminous Infrared Galaxies, first published as Graham et al. (2010).

Chapter 5 contains our derivation of the SN Ia rate in galaxy groups, an analysis of the radio properties of group hosts, and the ratio between Ia and core collapse supernovae in groups.

Chapter 6 presents our calculation of the SN Ia rate in galaxy clusters first published as Graham et al. (2008), with updated catalogs and a review of recent, relevant publications.

Chapter 7 describes two new parametrizations for environment clustering, and uses them to derive the SN Ia rate in over- and under-dense environments on multiple size scales.

Chapter 8 summarizes and discusses the scientific impact of our key results.

Chapter 2

Motivation

The main scientific goal of this thesis is to determine whether parent galaxy environments affect the rates and properties of Type Ia supernovae, and, if so, how. The purpose of this chapter is to explain how the answer to this is directly related to understanding the physical nature of SNe Ia, and why the problem is important enough to merit study. We begin with a general introduction to supernovae in § 2.1, then focus on the relevant details of Type Ia supernovae in § 2.2. Finally, in § 2.3 we discuss several recently detected correlations between galaxy properties, environment, and SN Ia rates – and their implications – which form the main motivation for this thesis work.

2.1 Supernovae

The stellar explosions that we call supernovae were first identified as a separate class by Baade & Zwicky (1934), who noted that the were distinct from the fainter recurrent novae in the Milky Way and Andromeda. Based on the brightness and duration of two nearby and well observed events – the bright "nova" of 1885 in the Andromeda galaxy, and the "nova" of 1572 discovered by Tycho Brahe – they postulated that supernovae are otherwise ordinary stars which explosively eject most of their mass. Baade & Zwicky also deduced that supernovae radiate nearly as much light as their entire host galaxy, and occur at a rate of about one every few centuries in every galaxy. In 1934 accurate light curves and spectroscopy were not available, but over time, as observations mounted, Baade & Zwicky were proved correct.

In modern astronomy, supernovae are empirically divided into two main types based on their optical spectra (Filippenko 1997): Type II supernovae show hydrogen and helium, Type Ib show helium but not hydrogen, and Type Ic and Ia show neither element. Type

Ia supernovae (SNe Ia) show a distinctive silicon absorption line at 6150 Å and the lines of iron-peak elements, especially at late times. Type Ib and Ic both show features of intermediate mass elements (oxygen, magnesium, and calcium). The shape and color of supernova light curves also differ between types, and SNe Ia are the most photometrically homogeneous class of SN.

The properties and rates of Type II and Ib/c supernovae indicate they are explosions induced by collapse of iron cores in massive stars, $\gtrsim 8$ and $\gtrsim 20 M_{\odot}$ respectively (Smartt 2009). The existence of core collapse supernovae (CC SN) was verified by direct observations of the predicted neutrino flux from Type II SN 1987A in the Large Magellanic Cloud (Hirata et al. 1987). The scenario of a massive progenitor is consistent with the host population of core collapse supernovae (CC SNe), because they are predominantly galaxies known to contain a young stellar component and/or showing active star formation (late-type galaxies such as spirals). CC SN are only rarely seen in galaxies with mainly old stellar populations, such as early-type galaxies or ellipticals (Hakobyan et al. 2008). Recently, the massive star progenitor scenario has been directly confirmed with high resolution pre-explosion images for the most common subset of CC SNe, called Type II-plateau for their light curve shape (Li et al. 2007).

Type Ia supernovae – the subject of this thesis – are an entirely different kind of stellar explosion. Their optical properties indicate they are most likely the thermonuclear explosions of carbon-oxygen white dwarf (COWD) stars (Hillebrandt & Niemeyer 2000). These white dwarfs are the end-point of stellar evolution of initially low mass ($2 \lesssim M_{\odot} \lesssim 8$) stars which were unable to burn carbon in their cores, and lost their outer layers during a planetary nebula phase. COWDs are supported by electron degeneracy pressure, a stable support system up to the Chandrasekhar limit of $\sim 1.4\ M_{\odot}$. SNe Ia are likely COWDs in binary systems which have accreted a sufficient amount of mass from their companion to reach or approach this limit and initiate a runaway thermonuclear reaction (Nomoto et al. 1984; Woosley & Weaver 1986). The elements present in their spectra, their near-uniform peak absolute brightness, and their presence in elliptical galaxies are all consistent with this scenario. Despite a general consensus about *what* is exploding, several models exist for the accretion mode, companion type, timescale, and the explosion mechanism itself (Hillebrandt & Niemeyer 2000; Höflich et al. 2003). Direct observations of a Type Ia progenitor system have yet to be confirmed, because white dwarfs are much fainter than the massive progenitors of SNe II.

2.2 Type Ia Supernovae

Type Ia supernovae are often called "standardizable candles" because of the empirical correlation between decline rate and peak luminosity: fainter SNe Ia decline faster, and vice versa (Phillips 1993). This relation is used by cosmological surveys to correct all SNe Ia to a standard brightness via the Δm_{15} parameter (decline in magnitude during the 15 days after maximum light), or the "stretch" parameter, s (Perlmutter et al. 1997). Stretch is applied to the time axis of an observed light curve as $t = s\,t_o$, and to the peak magnitude as $m = m_o + \alpha(s - 1)$, where $\alpha \sim 1.5$, and typically $0.8 < s < 1.1$. This empirical technique was used by SN Ia survey teams to discover the accelerated expansion of the Universe and the existence of dark energy, and has since been used to constrain the nature of dark energy (Riess et al. 1998; Perlmutter et al. 1999; Wood-Vasey et al. 2007; Astier et al. 2006).

There are, of course, exceptions to every rule, and not all SN Ia light curves can be easily calibrated with a stretch value $0.8 < s < 1.1$. These peculiar SNe Ia are broadly classified as sub-luminous and over-luminous, or SN 1991bg-like and SN 1991T-like after exemplary members of each category (Branch et al. 1993). For the sub-luminous SNe Ia, the stretch factor still works and some may be included in cosmological analyses. Aside from calibrating the light curves for cosmological analysis, stretch is important because SN Ia peak luminosity is directly associated with the mass of nickel-56 synthesized during the explosion (Arnett 1982).

The SN Ia light curve stretch is correlated with host type: brighter, slower-declining SNe Ia occur more often in late-type galaxies with younger stellar populations, and vice versa for fainter, quickly-declining SNe Ia (Hamuy et al. 1996; Sullivan et al. 2006a). This suggests SNe Ia which yield more nickel-56 are associated with younger progenitor systems. However, the correlation is not necessarily only with age; elliptical galaxies contain more metals which also affect the amount of nickel-56 synthesized (Howell et al. 2009). Furthermore, since late-type galaxies have old stellar populations as well as young, the progenitors of SNe Ia could originate solely from old stars, and the correlation may not be with age at all.

The Two-Component "A+B" Model for SN Ia Rates

One way to ascertain whether the parent population of SNe Ia is young or old is with a measurement of the SN Ia delay time: the amount of time between star formation and COWD explosion. The timescales for stars of initial mass $2 \lesssim M_\odot \lesssim 8$ to evolve into COWD are 0.05–1 $\times 10^9$ years, which constrains the theoretical minimum delay time. A

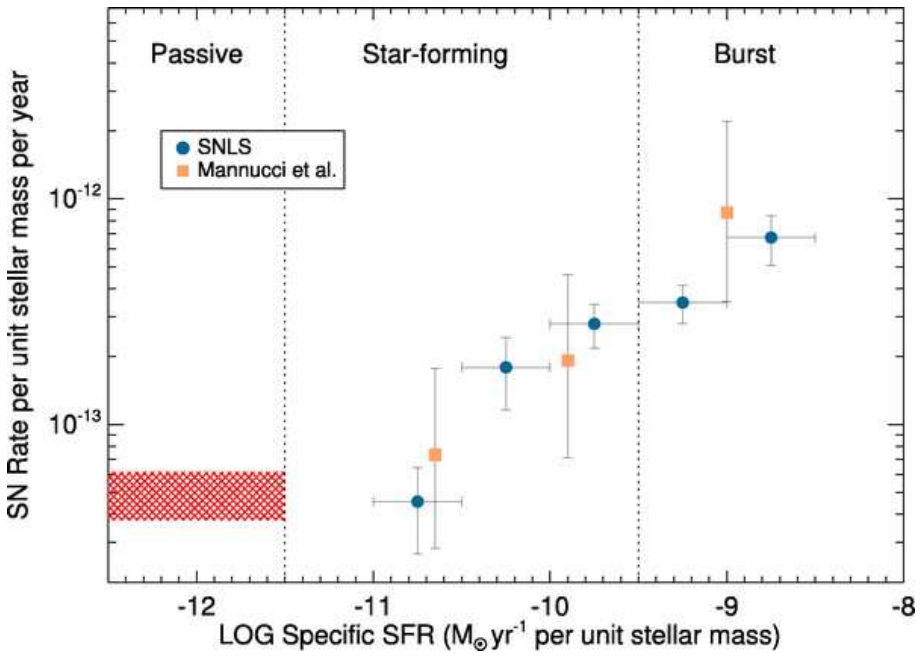

Figure 2.1 The SN Ia rate per unit mass as a function of host galaxy's specific star formation rate in passive (early-type or ellipticals), star-forming and burst (late-types, spirals or irregulars) galaxies. Includes data from Mannucci et al. (2005, orange squares) and the SNLS (blue circles). Passive galaxies shown with red hatched region because their specific SFR is ~ 0. (Source: Sullivan et al. 2006a).

Hubble Space Telescope SN survey to z $\sim$ 1.6 found a downturn in the universal SN Ia rate at redshifts z $\gtrsim$ 1. In combination with the universal star formation history (SFH) which peaks around z $\sim$ 2, this indicated a characteristic delay time of $\sim$ 2 Gyr for all Type Ia supernovae (Dahlen et al. 2004).

In contrast to this long delay time, the SN Ia rate *per unit mass* was found to be higher in bluer galaxies, as it is for CC SN; in other words, the *specific* SN Ia rate is correlated with host star formation rate (Mannucci et al. 2005). This indicates some SNe Ia are physically associated with young stellar populations, and have much shorter delay times of $<$ 1 Gyr. Based on this, a galaxy's SN Ia rate is commonly expressed as the sum of a "delayed" component from old stellar populations and a "prompt" component from young stellar populations. These components are parametrized as "A" and "B", proportional to a galaxy's mass and SFR respectively, as shown in Figure 2.1 (Scannapieco & Bildsten 2005; Sullivan et al. 2006a). We will refer to this as the two-component "A+B" model throughout this thesis.

The Single and Double Degenerate Progenitor Scenarios

At this point, the accretion mechanism is a necessary addition to this discussion. The case in which a white dwarf accretes from a main sequence or red giant companion is the called the "single degenerate" (SD) scenario, and the one in which two white dwarfs merge is the "double degenerate" (DD) scenario. The very brightest SNe Ia are likely to be DD systems with a combined mass in excess of 1.4 $M_{\odot}$ (Howell et al. 2006), but such supernovae are outside of the general relation between stretch and host star formation rate (SFR). Intuitively, one might expect these two scenarios to yield different distributions of delay times, with longer delay times required for the DD evolution of two stars into COWDs which then lose angular momentum to gravitational radiation and merge. However, theoretical delay time distributions have been shown remarkably similar for the SD and DD scenarios (Greggio et al. 2008).

It has recently been shown that the observed specific SN Ia rate is $\sim$ 1% of the specific white dwarf creation rate (Pritchet et al. 2008). This provides strong support for the SD model, except for one detail: the 1% efficiency factor is constant over a range of galaxy SFR, but it should theoretically be lower for low-mass systems. For example, lower mass stars produce lower mass COWD, which must then accrete more (or faster) to reach $\sim$ 1.4 $M_{\odot}$. Thus, Pritchet et al. (2008) surmise that either one or more scenarios in addition to the SD must exist in old stellar populations, or that no SNe Ia come from SD systems.

Direct observation of a SN Ia progenitor system has yet to be confirmed. Efforts to

identify the COWDs companion star are underway; this would confirm the single degenerate scenario. For Brahe's 1572 SN Ia, Ruiz-Lapuente et al. (2004) have excluded the possibility of a red giant companion, but find a nearby main sequence star has a peculiar velocity consistent with its being the remaining companion.

2.3 Galaxy Properties, Environment, and SN Ia Rates

The ultimate progenitor scenario(s), distribution of delay times, and the root causes of correlations between stretch, age, and metallicity all remain open questions in the field of Type Ia supernovae. They are essential to understand, and we will use the empirical relation between stretch and age in our analysis, but solving these mysteries is not the immediate goal of this work.

Several studies have shown the specific SN Ia rate to be higher in galaxies with radio emission and/or residing in rich galaxy clusters. These enhancements could not entirely be attributed to the "A+B" model, and may indicate additional environmental influences on the evolution and production of Type Ia supernovae. In some cases these rates imply a distribution of delay times inconsistent with previous studies and theoretical predictions. These findings may be difficult to reconcile with the use of SNe Ia as cosmological standard candles. The next few sections review the discovered correlations between galaxy properties, environment, and SN Ia rates. The main goal of this thesis is the verification and analysis of these relations in the Supernova Legacy Survey data set.

2.3.1 SNe Ia in Radio and Infrared Galaxies

The correlation between specific SN Ia rate and galaxy color found by Mannucci et al. (2005) is based on the supernova catalog of Cappellaro et al. (1999, hereafter C99). This catalog is a combination of visual and photographic searches of nearby galaxies (Cappellaro et al. 1993; Cappellaro et al. 1997; Evans et al. 1989). When the C99 SN Ia catalog was combined with 1.4 GHz survey data from the Very Large Array (VLA), the specific SN Ia rate was found to be 2–7 times enhanced in radio-loud over radio-quiet early-type galaxies (Della Valle et al. 2005, hereafter DV05). This was surprising because the SN Ia rate in early-type galaxies is expected to be simply proportional to host mass.

DV05 define radio-loud galaxies to have $L_{1.4\,\mathrm{GHz}} > 10^{29}$ ergs s^{-1} Hz^{-1}, the faint-end limit of the radio luminosity function, and radio-quiet to have $L_{1.4\,\mathrm{GHz}} < 4{\times}10^{27}$ ergs s^{-1} Hz^{-1}. We will use this convention for our thesis, but note the exact limits are not universal

(Zamfir et al. 2008). In radio-loud galaxies, the radio continuum radiation is generated by synchrotron emission; these are photons emitted by accelerated charged particles spiraling around magnetic field lines, such as electrons accelerated by AGN jet winds (Binney & Merrifield 1998). How might these processes for radio emission also enhance the SN Ia rate per unit mass? AGN jet winds could increase the accretion rate of ISM onto a white dwarf (Capetti 2002), a process thought to trigger classical nova eruptions (Livio et al. 2002; Madrid et al. 2007). However, DV05 reject this explanation for the enhanced specific SN Ia rate in radio-loud galaxies. They find galaxy interactions are most likely to cause the radio emission, *and* to supply the necessary SN Ia progenitors via stellar capture of a young population during dwarf accretion, or star formation induced by major mergers (Della Valle et al. 2005). This conclusion was based in part on the fact that some of the C99 SNe Ia in radio-loud early-type hosts had low Δm_{15} values, similar to SNe Ia in late-type galaxies. One final detail to remark upon here is that, since AGN activity is not suspected of directly influencing the probability of a SN Ia explosion, the SN Ia rate is not expected to be proportional to $L_{1.4\,\mathrm{GHz}}$.

By setting up a hypothetical galaxy interaction and AGN activity model with a recurring star formation model of ten 10^8 year long episodes, each separated by 10^9 years, Mannucci et al. (2006) find the enhanced specific SN Ia rate in radio-loud early-type galaxies is best fit by a *bimodal* delay-time distribution (DTD) in which half of all SNe Ia belong to the "prompt" (B) component, with delay times is constrained to $\lesssim 10^8$ years. They suggest this implies two physical populations of SN Ia progenitors. This is quite dissimilar from theoretically predicted delay time distributions for the single and double degenerate scenarios (Greggio et al. 2008). However, Mannucci et al. (2006) also note a broad single-population DTD could not be ruled out. As the existence of this extremely prompt component relies on a rate enhancement found with 21 photometrically identified SNe Ia from C99, we will look to confirm this in the large database of spectroscopically-typed SNe Ia from the CFHT SNLS in Chapter 4.

The existence of bright infrared counterparts for radio galaxies has been well documented, and often attributed to dust-obscured star formation coeval with the AGN (Magliocchetti et al. 2008; Mainieri et al. 2008). We will also look for obscured star formation in the radio-loud SN Ia host galaxies. Dust extinction in starbursts hinders SN detection: only one SN Ia has been detected, and the SN Ia rate remains unconstrained in starburst galaxies (Mannucci et al. 2003; Mannucci et al. 2007). In Chapter 4 we also use infrared catalogs to calculate the SN Ia rate in bright and luminous infrared galaxies, which are known to experience bursts of star formation up to $100 - 1000\ M_\odot\ y^{-1}$.

2.3.2 SNe Ia in Galaxy Pairs, Groups, and Clusters

As discussed above, the root cause of the enhanced rate in low redshift radio-loud early-type galaxies was suspected to be repeated galaxy interactions or mergers
(Della Valle et al. 2005), and such events are most common in pairs and groups of galaxies where the velocity dispersions are lower than rich clusters (Hickson 1997). A previous measure of the SN Ia rate in galaxy groups by Navasardyan et al. (2001) found it to be higher in galaxy pairs than in groups, and higher in groups than in isolated galaxies (with large uncertainties). They suggested this may result from star formation in interacting galaxies, but could not confirm it. In Chapter 5, we derive the specific SN Ia rate in groups from the CFHT SNLS, and in Chapter 7 explore the SN Ia rate in under-dense environments and isolated galaxies.

The SN Ia rate in galaxy clusters is expected to be lower than in the field due to the morphology-density relation (Postman & Geller 1984): cluster galaxies are predominantly of early-type with little or no star formation, and the two-component "A+B" model predicts a lower SN Ia rate per unit mass in early-type galaxies. However, since clusters contain only a small fraction of the stellar mass of the Universe, it is conceivable that some hitherto undetected influence in such exotic environments could affect the SN Ia rate. For example, the fraction of binary stars, or the rate of mass accretion onto the white dwarf, could be enhanced. The recent discovery of an enhanced nova rate in the core of the elliptical galaxy M87 is evidence for the latter (Madrid et al. 2007). A second example is the detected SN Ia rate enhancement in radio-loud early-type galaxies (Della Valle et al. 2005); luminous ellipticals in the centers of large clusters tend to show radio emission.

Based on their analysis of two SNe found in an archival survey of Hubble Space Telescope cluster images, Gal-Yam et al. 2002 find the SN Ia rate in cluster and field galaxies to agree at both low and high redshifts. The Wise Observatory Optical Transient Survey targeting 140 Abell clusters (WOOTS; Gal-Yam et al. 2008) found six cluster SNe Ia, and confirmed the SN Ia rate per unit mass in low redshift galaxy clusters to be consistent with the rate in early-type galaxies (Sharon et al. 2007). Recently, Mannucci et al. (2008) analyzed the C99 sample of low redshift SNe ($z < 0.04$) and found the specific SN Ia rate in cluster early-type galaxies is enhanced by a factor of $\gtrsim 3$ over field early-type galaxies. They show this is a distinct effect from the one in radio-loud early-type galaxies by demonstrating their SN Ia rate in radio-loud *cluster* ellipticals is enhanced over radio-loud *field* ellipticals. Though they find the cluster enhancement can mostly be attributed to the known correlation between specific SN Ia rate and galaxy color (Mannucci et al. 2005), their galaxies are morphologically typed, and their photometry is not precise enough to

unambiguously confirm this, or to make a statistical comparison with predictions of the "A+B" model.

In Chapter 6 we combine the CFHT SNLS database with the publicly available cluster catalogs for SNLS fields (Ilbert et al. 2006; Olsen et al. 2007), which are ideal for extending these investigations to higher redshifts. In Chapter 7 we apply statistical parametrizations of clustering to catalogs of CFHTLS Deep field galaxies, and examine the influence of environment density on the SN Ia rate per unit mass. Additional motivations for the study of Type Ia supernovae in clusters are presented in Appendix A, in which we discuss the Multi-Cluster Nearby Supernova Survey.

2.4 Summary

Current studies of correlations between SN Ia rates and properties, and the properties and environment of their parent galaxies, are a timely and relevant contribution to the larger discussion regarding the physical nature of Type Ia supernovae, and their use as cosmological standardizable candles. Much of the current results in this area come from low-redshift, galaxy-targeted surveys such as C99.

For this work we use the intermediate redshift database of spectroscopically classified SNe from the Canada-France-Hawaii Telescope's Supernova Legacy Survey (CFHT SNLS). The SNLS survey area overlaps popular fields covered by multi-wavelength surveys, in which galaxy structures have been identified and published. In Chapter 3 we describe the images and/or source catalogs available at radio, infrared, and optical wavelengths, as well as catalogs of photometric and spectroscopic redshifts for galaxies, and lists of identified groups and clusters. The main strength of this work lies in its simultaneous combination of multi-wavelength data sets to make a thorough investigation of how parent galaxy environments affect the rates and properties of Type Ia supernovae.

Chapter 3

Data Catalogs

The Canada-France-Hawaii Telescope Legacy Survey (CFHTLS) is a large project jointly run by a Canada-France collaboration. Observations were made from 2003 to 2008, with a few additional observations in 2009, for a total of over 450 nights with CFHT's wide field optical camera, MegaCam. CFHTLS had three components: Deep, Wide, and Very Wide, each with their own specific survey strategies and science goals. The Deep component's main science goal was the Supernova Legacy Survey (SNLS); its survey included 4 one square degree fields spread out roughly in right ascension such that at any given time of year, 2-3 were visible at all times. CFHTLS Deep field center coordinates are listed in Table 3.1. In all cases we assume a standard flat cosmology of $H_0 = 70$ km s^{-1} Mpc^{-1}, $\Omega_M = 0.3$, and $\Omega_\Lambda = 0.7$.

CFHTLS Deep is also an excellent data set for studies of structure formation and galaxy evolution, and the 4 fields were chosen to overlap with other deeply observed regions of sky. In pursuit of their own science goals, third parties have covered some Deep fields (in whole or in part) with multi-wavelength surveys, or processed the images to identify galaxy groups and clusters. In many cases their catalogs are publicly available. The main goals of this thesis are to make a comprehensive analysis of the multi-wavelength characteristics of SN Ia parent galaxies and their environments at intermediate redshifts, and to test whether the SN Ia rate per unit mass varies in distinctive populations. Towards this end, we have gathered and integrated as many of these overlapping surveys as possible. They are listed for convenience in Table 3.2.

In this chapter we describe the origin and specifics of each catalog used for this work, and how they were integrated with each other. We begin with a description of the SNLS in § 3.1. We present the optical photometry and spectroscopy catalogs for Deep field galaxies based on observations at CFHT and the European Southern Observatory's Very Large Tele-

Table 3.1 Locations of CFHTLS Deep fields in J2000 coordinates.

Field	Right Ascension [h:m:s]	Declination [d:m:s]
D1	2:26:00	-04:30:00
D2	10:00:29	+02:12:21
D3	14:17:54	+52:30:31
D4	22:15:31	-17:44:05

scope in § 3.2. The CFHTLS Deep fields 1 and 2 are covered by radio surveys from the Very Large Array and infrared surveys from the Spitzer space telescope described in § 3.3 and 3.4. Chapter 4 also includes a re-analysis of the Cappellaro et al. (1999) set of supernovae, which is described in § 3.5 (not related to CFHTLS). In § 3.6 and 3.7 we describe optical galaxy group and cluster samples used in Chapters 5 and 6. (A description of the CFHT Multi-Epoch Nearby Cluster Survey, not associated with the CFHTLS, is presented separately in Appendix A.)

3.1 CFHT Supernova Legacy Survey

The Supernova Legacy Survey (SNLS[1]) is the main science goal of the CFHTLS Deep component. Over five years (2003-2008), the CFHTLS Deep Survey monitored four 1 square degree fields (D1–D4) with a 3–5 night cadence in four MegaCam filters (g_M, r_M, i_M, z_M) to a depth $i_M \simeq 25$; this imaging was paired with a strong spectroscopic campaign to follow up all potential SN Ia candidates. As SNLS is a joint Canada-France collaboration, both sides run their own detection pipelines and SN Ia light-curve fitting techniques, adding redundancy and reliability to the survey. After final reductions it will have discovered and classified hundreds of SNe Ia, and provide the best direct constraints on the dark energy equation of state parameter *w* (Astier et al. 2006; Komatsu et al. 2009).

The SNLS catalog of SNe Ia is private, and available for use within the collaboration only. The number of SNe Ia spectroscopically classified and available for use in this thesis in fields D1–4 are: 105, 101, 120, and 86 respectively. In following sections we discuss further restrictions on the SN Ia catalog, including requiring a host identified in the galaxy catalog, and limits on the discovery date or redshift. In June 2007, CFHT lost its i_M-band filter, which upset SNLS survey completeness. At various points in our analysis, we divide

[1] http://legacy.astro.utoronto.ca

Table 3.2 Compiled data catalogs.

Description	Deep Fields	Telescope	Survey Name	Reference
Type Ia Supernovae	D1–4	CFHT	SNLS	Astier et al. (2004)
Photometric redshifts	D1–4	CFHT	CFHTLS	Coupon et al. (2009)
Spectroscopic redshifts	D1	VLT	VVDS	LeFèvre et al. (2005)
	D2	VLT	zCOSMOS	Lilly et al. (2009)
Radio source fluxes	D1	VLA	VLA-VIRMOS	Bondi et al. (2003)
	D2	VLA	VLA-COSMOS	Schinnerer et al. (2007)
Infrared source fluxes	D1	Spitzer	SWIRE	Lonsdale et al. (2003)
	D2	Spitzer	S-COSMOS	Sanders et al. (2007)
Groups of galaxies	D1–4	CHFT, VLT		Knobel et al. (2009)
Clusters of galaxies	D1–4	CFHT		Olsen et al. (2007)

the SNLS SN Ia database into SNLS-2006 and SNLS-2008 containing only SNe Ia discovered up to and including 2006 and 2008 respectively. We will not list the characteristics of every SNLS SN Ia used in this project, but do present the relevant "SNe of interest" as required in each chapter. We use SN Ia stretch values from the SiFTO light curve fitting technique of Conley et al. (2008), most recently presented in the SNLS collaboration paper Guy et al. (2010). At the time of writing, SiFTO stretch values were only available for SNe Ia detected in the first three years of SNLS (i.e. up to 2006).

3.2 CFHTLS Deep Field Optical Galaxy Catalogs

Here we describe the optical photometric and spectroscopic galaxy catalogs generated by third parties for the CFHTLS Deep fields 1–4. We list all restrictions we have applied to these catalogs, and why. We explain how we match these catalogs with each other, and with the catalog of SNLS SNe Ia. This section also describes how we derived the SN Ia correction factor C, which accounts for SNLS detection efficiencies. To assist in the understanding of C, we also present the equations which incorporate C into our calculations of SNe Ia rates and predicted numbers of SNe Ia from the "A+B" model.

3.2.1 Photometric Redshift Catalog

The Terapix[2] astronomical data reduction center at the Institut d'Astrophysique de Paris has produced accurate ($\sigma_{\Delta z/(1+z)}$ = 0.028–0.030 out to z $\leq$ 1.5) photometric redshifts for $\geq$ 80000 galaxies in each of the four CFHTLS Deep fields. They do this by incorporating VIMOS VLT Deep Survey spectroscopic redshifts (discussed below) to calibrate their spectral energy distribution (SED) and redshift fitting routine. Our analysis now uses the most recently published galaxy catalog from Coupon et al. (2009).

Before the C09 catalog was available, our analysis used an earlier version of this catalog from Ilbert et al. (2006). We found that, in their optimization of the photo-z calculation, the accuracies of the SEDs are compromised (Olivier Ilbert, private communication) and the distribution of SED types is discontinuous. To solve this we applied the 51 SEDs interpolated from Coleman et al. (1980) and Kinney et al. (1996) templates, made by Stephen Gwyn at the Canadian Astronomical Data Center[3] (Gwyn 2001), to the catalog galaxies. The Gwyn templates, shown in Figure 3.1, are numbered from 0 to 100 (bottom

[2] http://terapix.iap.fr

[3] http://www.cadc.hia.nrc.gc.ca/community/CFHTLS–SG/docs/cfhtls.html

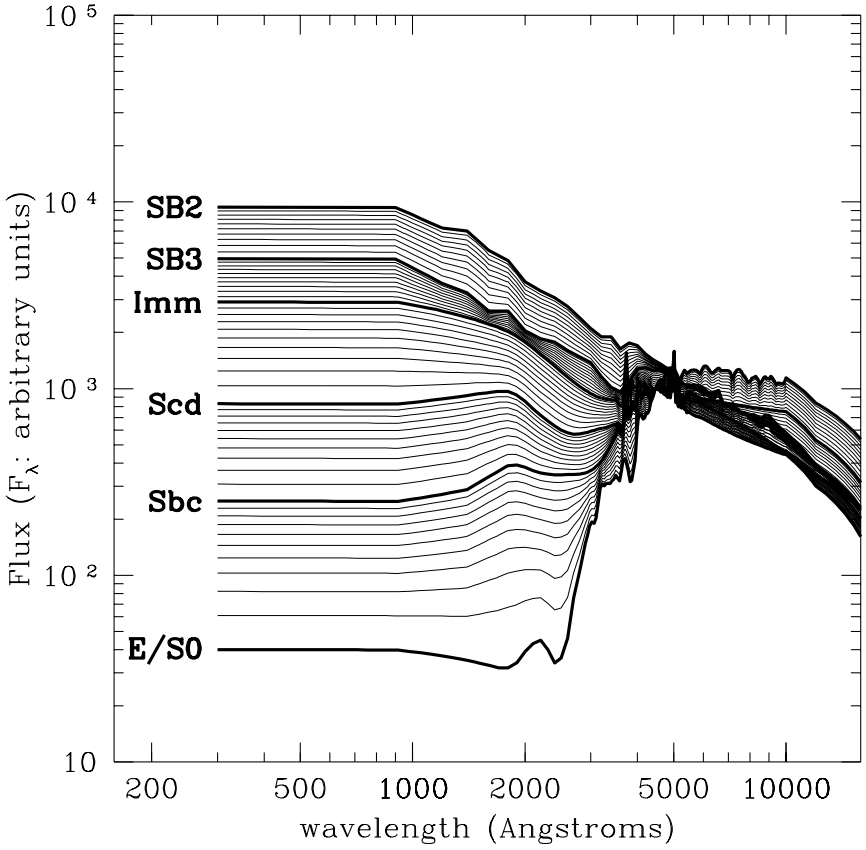

Figure 3.1 The 51 spectral energy distribution templates interpolated by Stephen Gwyn from the original SEDs (heavy lines). (Source: Gwyn 2001).

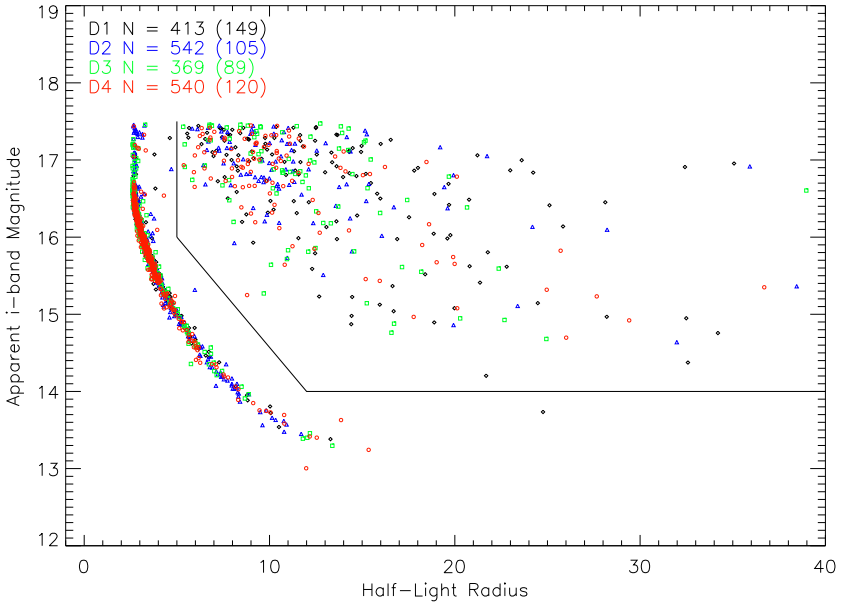

Figure 3.2 Apparent i-band magnitude versus half-light radius in pixels for C09 objects with flag values equal to 8 or 12 in D1–4 (black diamonds, blue triangles, green squares, and red circles respectively). Stars lie to the left of and below the black line. Top left lists the total number of sources plotted in each field, and in brackets the number of real galaxies identified.

to top). These SED types include E/S0 (ellipticals and lenticulars, 0-8), Sbc and Scd (spiral galaxies, 10-24 and 26-48), Irr (irregular galaxies, 50-78), and SB (starbursts, 80+, which have a SFR per unit mass, or sSFR $\gtrsim 30 \times 10^{-10}$ y^{-1}). When, in later sections and chapters, we refer to "early-type" galaxies this refers to E/S0, and "late-type" refers to all other types. We estimate galaxy stellar masses (corrected for dying stars) and star formation rates (SFR) using fits of this library of SEDs to the models of Buzzoni (2005). We correct these for systematic offsets (of about a factor of 2) to agree with the PEGASE models (Sullivan et al. 2006b). Based on this we estimate a $\sim$ 40–50% uncertainty in the mass and SFR values.

To ensure catalog purity we restrict the catalog to only reliable galaxy photometric redshifts which meet the following conditions, similar to suggestions by C09 but more relaxed to increase completeness:

- there must be no second redshift solutions (indicative of catastrophic failures)
- the object parameter must be equal to 0 (object is a galaxy, not a star)
- at least 3 pass-bands must have contributed to the photometric redshift fit
- $i_M \leq 25$
- $0 < z < 1.5$.

C09 suggest excluding all sources with a Terapix flag value > 0, to avoid stars and galaxies on masked regions around foreground stars. However, we find that (after applying restrictions listed above) the objects with flag values equal to 8 and 12 are a mix of foreground stars, and a non-insignificant fraction of the brightest field galaxies which are not near the masked regions. We need to keep these in our galaxy sample, but reject the stars. The stars, as unresolved point sources, lay along the curve in the plot of magnitude versus half-light radius (also called effective radius, it is the radius which encloses half of the galaxy's light) shown in Figure 3.2. We use this plot to identify and recover the bright galaxies. We also cap the absolute V-band magnitude at $V > -25$ to reject the few remaining outliers (incorrect photometric redshifts).

3.2.2 SN Ia Host Galaxy Associations

We identify SN Ia hosts as the nearest C09 galaxy within 5″ (a maximum host offset) and with $\Delta z_{phot} = 0.15$ (a generous initial margin between galaxy photometric and SN Ia spectroscopic redshift). In cases where the two nearest galaxies are both at large offset, between

3″ and 5″ away, the second closest will be chosen if its Δz_{phot} is $\leq 0.5\times$ that of the nearest galaxy (only one SN Ia-host match is made this way). In D1–4, 23, 25, 34, and 32 SNe Ia have no catalog galaxy meeting these criteria and cannot be used; this mainly includes SNe Ia on masked regions and in hosts of $i_M > 25$.

To remove SN Ia–host matches which are likely to be chance alignments, we apply iterative outlier rejection to the residual dispersion between host photometric and SN Ia spectroscopic redshifts for each deep field. For this we clip at 3σ, and stop when fewer than 1% of the sample are rejected (i.e. usually only one or two iterations). This process results in photometric redshift uncertainties of $\sigma_{D1} = 0.026$, $\sigma_{D2} = 0.028$, $\sigma_{D3} = 0.026$, and $\sigma_{D4} = 0.027$. Only 2 SN Ia-host matches are rejected, one each in D1 and D2. Host matching and outlier rejection together leave 81, 75, 86, and 54 usable SNe Ia in fields D1–4 respectively.

Some surveys will use physical separations, galaxy half-light radius, or elliptical isophotes to make their host–SN Ia associations, but we have used a relatively simple 5″ radius to make our associations. Has this affected our results? The majority of SNLS SNe Ia have z=0.2–0.8. At these redshifts, 5″ translates into physical host offsets of R=16–38 kpc, which is adequate to encompass the majority of galaxies. If we increase this standard angular maximum host offset to 10″, we associate 8 more SNe Ia with Coupon et al. host galaxies in the $z \leq 0.6$ redshift bin – an additional $\sim$ 6%. However, the clipped mean process then returns a slightly higher uncertainty of $\sigma \sim 0.028$ for all fields, and the probability of fallacious associations increases. In general we consider a minimized threat of misidentified host galaxies as preferable to an additional 8 SNe Ia in our sample, and retain the simple 5″ host–SN Ia matching radius.

3.2.3 Predicted SN Ia Rates from "A+B" and the Correction Factor

For each C09 galaxy, we calculate a SN Ia rate per year (R_{Ia}) based on the two-component "A+B" model, incorporating the time dilation correction to our observed frame of reference:

$$R_{Ia} = \frac{A \times M \; + \; B \times SFR}{1+z}, \tag{3.1}$$

where M is stellar mass ($M_\odot$), SFR is star formation rate ($M_\odot\ y^{-1}$), and the A and B values are from Sullivan et al. (2006): $A = 5.3 \pm 1.1 \times 10^{-14}$ SNe y^{-1} $M_\odot^{-1}$ and $B = 3.9 \pm 0.7 \times 10^{-4}$ SNe y^{-1} $(M_\odot\ y^{-1})^{-1}$. Thus, R_{Ia} is the number of SNe Ia expected in a galaxy per year of observing.

Table 3.3 SN Ia Rate Correction Factor C.

Field	z Range	2003	2004	2005	2006	2007	2008	≤2006	≤2008
D1	0.0-0.6	0.299	0.373	0.299	0.336	0.112	0.000	1.306	1.418
	0.6-0.8	0.169	0.295	0.084	0.338	0.127	0.000	0.886	1.013
	0.8-1.0	0.080	0.160	0.107	0.053	0.080	0.000	0.401	0.481
D2	0.0-0.6	0.000	0.345	0.460	0.383	0.268	0.115	1.188	1.572
	0.6-0.8	0.000	0.147	0.110	0.147	0.293	0.147	0.403	0.843
	0.8-1.0	0.000	0.025	0.074	0.025	0.074	0.074	0.124	0.272
D3	0.0-0.6	0.286	0.205	0.205	0.327	0.409	0.123	1.023	1.555
	0.6-0.8	0.000	0.304	0.380	0.228	0.380	0.038	0.912	1.329
	0.8-1.0	0.000	0.087	0.117	0.000	0.087	0.000	0.204	0.292
D4	0.0-0.6	0.169	0.253	0.295	0.211	0.126	0.000	0.927	1.054
	0.6-0.8	0.161	0.215	0.268	0.107	0.161	0.000	0.752	0.913
	0.8-1.0	0.067	0.133	0.133	0.033	0.033	0.000	0.367	0.400

The total number of SNe Ia which actually exploded per year (based on the "A+B" model) in the *entire* SNLS sample of N_{gal} galaxies is thus $\sum_{j=1}^{j=N_{gal}} R_{Ia,j}$. We can use this total SN Ia frequency to derive a correction factor, C, between it and the number of SNLS SNe Ia observed, N_{obs}:

$$C = \frac{N_{obs}}{\sum_{j=1}^{j=N_{gal}} R_{Ia,j}}. \tag{3.2}$$

This factor C accounts for SNLS survey recovery efficiencies such as detection and spectroscopic completeness, and observing season length ($\sim$ 6 months). In this way it is similar to the product of of ϵ_{yr}, C_{SPEC}, and S of Neill et al. (2006). Since these efficiencies vary between deep fields, with redshift, and over time (Perrett et al. 2010), we calculate a C value for each deep field, for three redshift ranges, for each year individually, and also for the SNLS-2006 and SNLS-2008 samples explained in § 3.1. As pointed out in Perrett et al. (2010), the SNLS completeness is constant out to $z \sim 0.6$ and then drops to 50% by $z \sim 1.0$, so we use three redshift bins of $z \leq 0.6$, $0.6 < z \leq 0.8$, and $0.8 < z \leq 1.0$.

It is important to note that when multiple years are considered together, N_{obs} is the total number over all years, yet $\sum_{j=1}^{j=N_{gal}} R_{Ia,j}$ is always in units of SN per year. This is most sensible for the methods in which this correction factor C is applied, as we will now discuss. To calculate the observed SN Ia rate per year per unit mass in any sub-sample of galaxies, $sSNR_{Ia}$, we use:

$$sSNR_{Ia} = \frac{\sum_{i=1}^{i=N_{obs}} 1/C_i}{\sum_{j=1}^{j=N_{gal}} M_j/(1+z_j)}, \tag{3.3}$$

where N_{obs} is the total number of SNe Ia in the sub-sample, and dividing by the correction factor converts the number of SNe Ia observed into a SNe Ia frequency per year. The denominator $\sum_{j=1}^{j=N_{gal}} M_j/(1+z_j)$ is the total galaxy stellar mass in the sub-sample, with the (1+z) time dilation factor for each galaxy which converts the units for $sSNR_{Ia}$ from observed to rest-frame time. Aside from the observed SN Ia rates, in our sub-samples of galaxies we also often calculate the total number of SNe Ia predicted to be observed by the "A+B" model:

$$N_{A+B} = \sum_{j=0}^{j=N_{gal}} C_j \times R_{Ia,j}. \tag{3.4}$$

In this case, the correction factor C converts the expected SNe Ia frequency in the sub-sample to the total number expected to be observed in the chosen timeframe, Deep field, and redshift range. We can then statistically compare the number of SNe Ia observed in any sub-sample to this predicted number as follows: the Poisson probability of observing $x = N_{obs}$ given an expected number $\mu = N_{A+B}$ is expressed by P_p (Bevington & Robinson 2003):

$$P_P(x;\mu) = \mu^x \frac{e^{-\mu}}{x!}. \tag{3.5}$$

We use this to calculate the *summed* Poisson probability, P_{SUM}, as follows. When $N_{obs} > N_{A+B}$, P_{SUM} is the probability of observing $x = N_{obs}$ *or more*, and equal to the integral of P_P from $x = N_{obs}$ to $x = \infty$. When $N_{obs} < N_{A+B}$, P_{SUM} is the probability of observing $x = N_{obs}$ *or less*, and equal to the integral from $x = 0$ to $x = N_{obs}$. The summed Poisson probability, P_{SUM}, assesses whether the observed number of SNe Ia is consistent with the "A+B" model in any given galaxy subset. Probabilities of $P_{SUM} \leq 0.05$ are considered statistically significant results.

It is important to note that this correction factor, C, is derived based on the observed number of SNe Ia in the *whole survey*, but always applied to much smaller sub-samples of galaxies. As such, it is not a circular correction, and the number of SNe Ia predicted in a given sub-sample will not always equal the number observed. This correction method assumes the SNLS detection efficiency and spectroscopic completeness are independent of galaxy type, but this is a reasonable (and mostly true) assumption. The advantage of using C is that biases in the photometric galaxy catalog are automatically accounted for.

3.2.4 Spectroscopic Redshift Catalog

Two recent surveys to obtain a large number of spectroscopic galaxy redshifts with the Visible Multi-Object Spectrograph at the Very Large Telescope (VIMOS-VLT) overlap two CFHTLS Deep fields. The VIMOS-VLT Deep Survey (VVDS) covers approximately half of D1 with a redshift accuracy of 276 km s^{-1}, and their "First Epoch" catalog is publicly available (LeFèvre et al. 2005). Galaxies in the Cosmic Evolution Survey (COSMOS) field which overlaps D2 have also been spectroscopically observed with VIMOS-VLT by the zCOSMOS-bright survey, with a better redshift accuracy of 110 km s^{-1}. This data is also publicly available (Lilly et al. 2009).

Galaxies from C09 are matched to the VVDS and zCOSMOS-bright catalogs with a maximum separation of 2.0″ and maximum redshift offset of $\Delta z = 0.08$ ($\sim 3\sigma$ in the photometric redshift uncertainty). Of the 6792 VVDS catalog members, 3902 are matched to a C09 galaxy (57%); of the 6419 galaxies in L09, 3933 are matched to a C09 galaxy (61%). The majority of unmatched galaxies fall outside the C09 field or in masked regions. The completeness structure of these surveys, which varies spatially and with redshift, will be described in later sections when it is relevant to attempt a correction.

3.3 VLA Radio Sources

Here we describe our processing of the publicly available 1.4 GHz source catalogs from the Very Large Array (VLA). The VLA-VIRMOS 1.4 GHz Deep survey[4] covers D1 to a $S_{1.4GHz}$ flux of 80 μJy, with a mean rms noise $\sigma \simeq 17$ μJy, and 75% completeness at fluxes $S_{1.4GHz}$ =80–180 μJy (Bondi et al. 2003). The VLA-COSMOS 1.4 GHz Large Project[5] covers D2 to $S_{1.4GHz} \sim 45\,\mu$Jy with a mean rms noise of $\sigma \sim 15\,\mu$Jy (Schinnerer et al. 2007). For both radio source catalogs, optical counterparts are identified as the closest galaxy within 2″ (maximum VLA positional error). Away from the galaxy catalog's masked regions around foreground stars our optical counterpart match fraction is $\sim$ 60%, similar to Ciliegi et al. (2005). In total we find 662 radio galaxies in D1 and 1253 in D2.

Radio luminosities are derived from photometric redshifts of galaxy counterparts, include a $(1 + z)^{-1}$ bandpass correction (Hogg et al. 2002), and are plotted in Figure 3.3. A galaxy is radio-loud if $L_{1.4\,GHz} > 10^{29}$ ergs s^{-1} Hz^{-1}, the faint-end limit of the radio luminosity function. We use the same convention as DV05, but note that exact limits for radio-loud, -faint, and -quiet galaxies are not universal (Zamfir et al. 2008). Ledlow & Owen (1996)

[4]http://virmos.bo.astro.it/ virmos/radio/

[5]http://irsa.ipac.caltech.edu/data/COSMOS/images/vla/

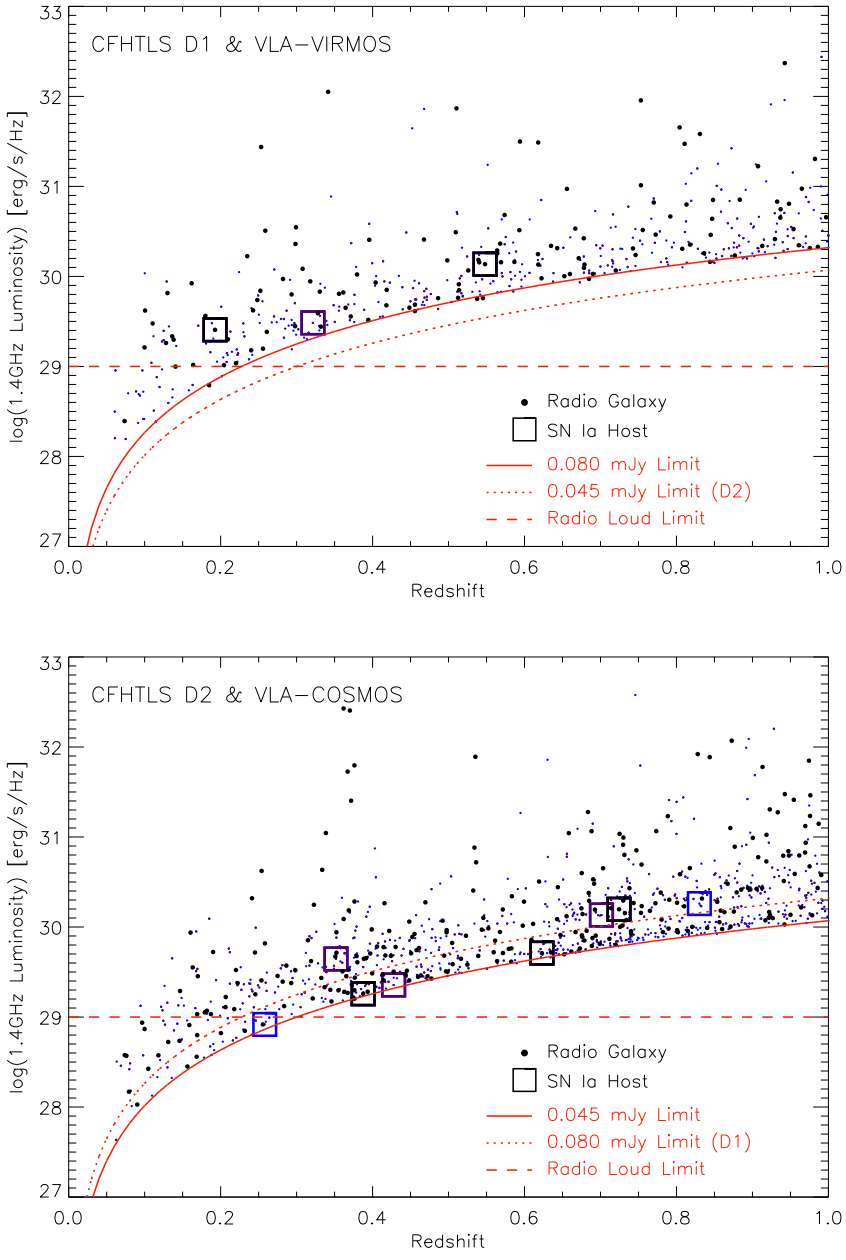

Figure 3.3 $L_{1.4\ GHz}$ versus photometric redshift for galaxies in D1 with VLA-VIRMOS (top) and D2 with VLA-COSMOS (bottom) counterparts. Filled circles are galaxies of SED type E/S0 (black), Sbc (purple), and later types (blue); squares are SN Ia hosts. Solid red line marks survey $S_{1.4GHz}$ flux detection limit (dotted red for limit of other field), dashed red line for radio-loud limit.

find 14% (±2.4%) of elliptical galaxies with absolute R magnitude $M_R \lesssim -20.5$ are radio-loud, and among C99 elliptical galaxies DV05 find 12% (±2%) are radio-loud. In our sample of SED type E/S0 galaxies with $z < 0.6$ we find 4–8% of galaxies with $M_V \lesssim -20$ are radio-loud, suggesting we can identify half of the radio-loud population among optically bright galaxies. The fact that we cannot identify more is due to our higher minimum radio flux limit.

A possible bimodality of VLA-COSMOS (D2) radio fluxes is apparent in Figure 3.3: there is a deficit of fluxes (coincidentally) at the VLA-VIRMOS (D1) lower flux limit. This apparent bimodality is a result of combining the integrated fluxes of resolved and unresolved sources. The flux of this bimodality "valley" corresponds to the lower limit of integrated fluxes for resolved sources, $S_{1.4GHz} \sim 0.08$ mJy, as shown in the right-hand plot of Figure 17 from Schinnerer et al. (2007). This may indicate VLA-VIRMOS and VLA-COSMOS sample slightly different radio source populations, with more faint, unresolved sources in D2. We consider any influence of this on our results in Chapter 4.

3.4 Spitzer Infrared Sources

Here we describe our processing of the publicly available infrared source catalogs generated with the Infrared Array Camera (IRAC) and Multi-band Imaging Photometer (MIPS) instruments on the Spitzer space telescope. The Spitzer Wide-area Infrared Extragalactic (SWIRE) survey covers D1 to a flux of $S_{3.6\mu m} \sim 6.6\ \mu$Jy (subscript denotes wavelength), and to $S_{24\mu m} \sim 300\ \mu$Jy (Lonsdale et al. 2003). SWIRE objects with $S_{3.6\mu m} > 200\ \mu$Jy and stellarity > 0.9 are most likely stars or QSOs and rejected from the catalog[6]. The Spitzer Cosmic Evolution Survey (S-COSMOS) covers D2 to $S_{3.6\mu m} \sim 0.8\ \mu$Jy and $S_{24\mu m} \sim 300\ \mu$Jy after required aperture corrections (Sanders et al. 2007). Objects flagged as likely compromised by nearby bright sources are rejected[7]. Both catalogs are available via the NASA Infrared Space Archive[8]. We reject foreground objects and QSOs, and identify optical counterparts as in § 3.3; the percentage of galaxies detected at 3.6μm is ∼ 20% and ∼ 70% in D1 and D2 respectively.

For both fields' catalogs, the fraction of galaxies detected in the MIPS 24μm band is $\sim 2-3\%$. Galaxies with $z \leq 0.6$ are plotted on infrared flux color-color diagrams in Figure 3.4, which also show the boundaries of AGN-dominated infrared sources. These bound-

[6] http://irsa.ipac.caltech.edu/data/SPITZER/SWIRE/docs/delivery_doc_r2_v2.pdf, page 43
[7] http://irsa.ipac.caltech.edu/data/COSMOS/gator_docs/scosmos_irac_colDescriptions.html
[8] http://irsa.ipac.caltech.edu

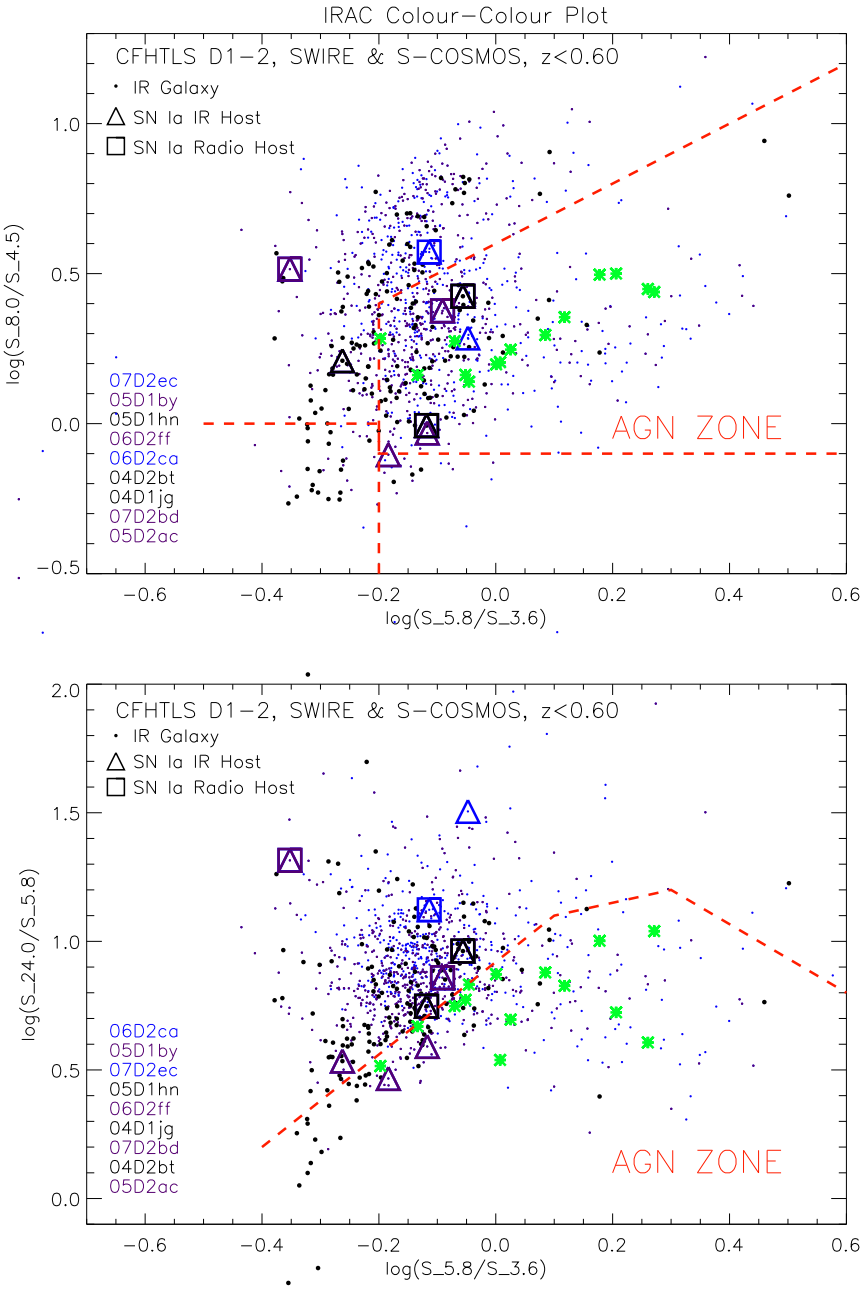

Figure 3.4 IR color-color diagrams for z ≤ 0.6 galaxies with IRAC counterparts only (top) and IRAC+MIPS counterparts (bottom), for D1 and D2 combined. Axes are infrared colors, the logged ratios of fluxes in two bands (i.e. S_3.6 is the flux at 3.6 μm, or $S_{3.6\mu m}$). Filled circles are galaxies of SED type E/S0 (black), Sbc (purple), and later types (blue). Triangles are SN Ia host galaxies, with squares for radio hosts. Red dashed lines mark AGN boundaries as in Figure 10 of Sajina et al. (2005) and Figure 2 of Lacy et al. (2004). Asterisks mark E/S0 galaxies in *both* AGN zones.

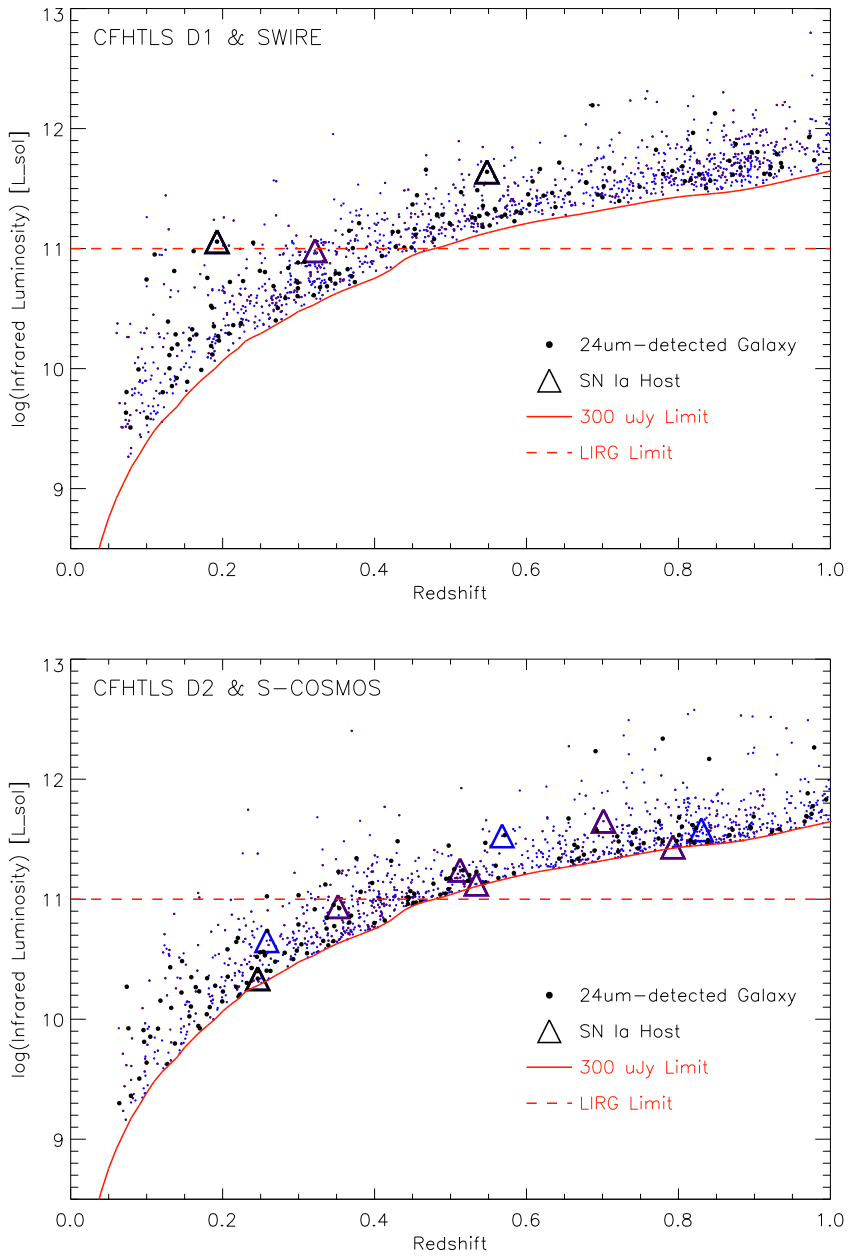

Figure 3.5 L_{IR} versus photometric redshift for Spitzer MIPS-detected galaxies in D1 (top) and D2 (bottom). Filled circles are galaxies of SED type E/S0 (black), Sbc (purple), and later types (blue); triangles are SN Ia hosts. Solid red line marks survey $S_{24\mu m}$ flux detection limit, dashed red line for LIRG limit.

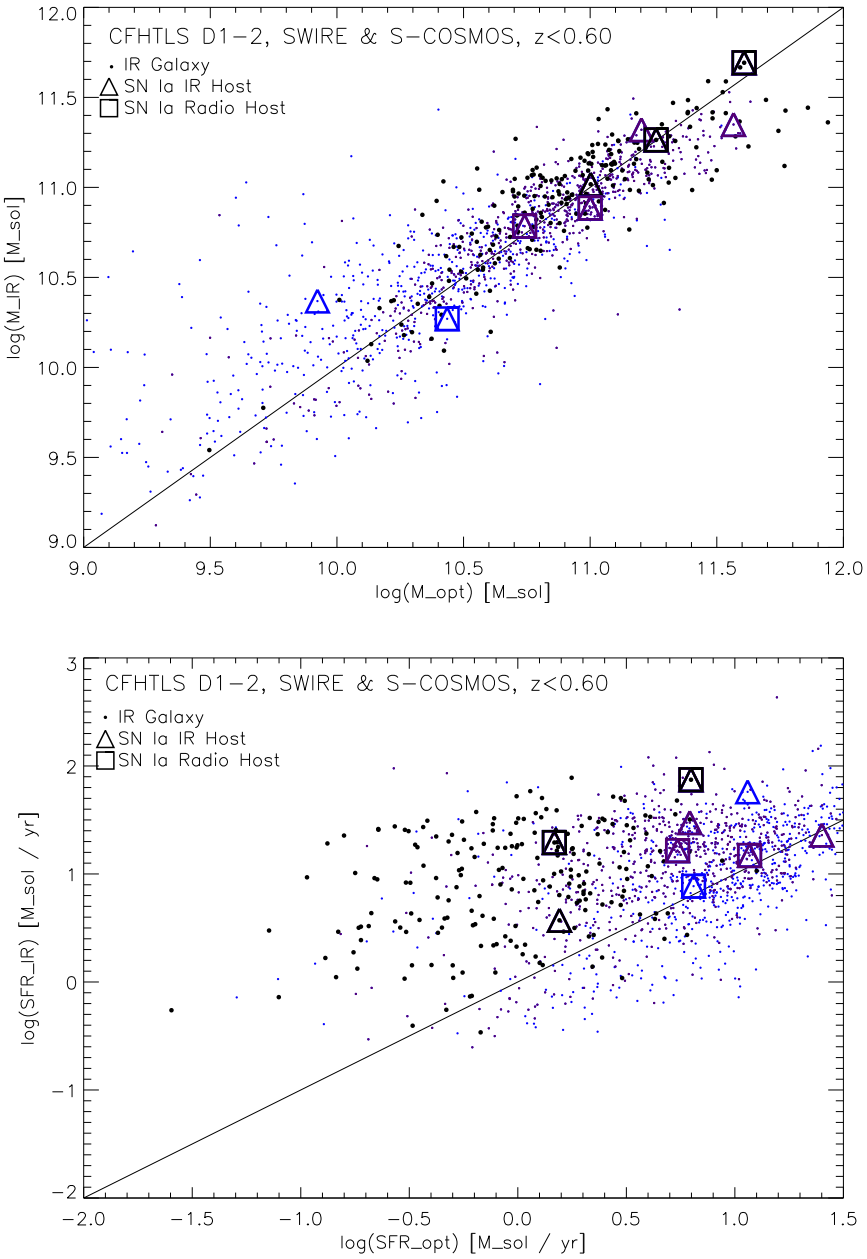

Figure 3.6 IR versus optical mass (top) and SFR (bottom) for z ≤ 0.6 galaxies IRAC+MIPS counterparts, for D1 and D2 combined. Filled circles are galaxies of SED type E/S0 (black), Sbc (purple), and later types (blue). Triangles are SN Ia host galaxies, with squares for radio hosts. Solid lines of slope equal to one are there to guide the eye.

aries are derived from Spitzer First Look Survey data of comparable flux-density limits ($S_{3.6\mu m} \sim 7$ μJy and $S_{24\mu m} \sim 300$ μJy) and redshifts ($z \lesssim 0.7$) (Lacy et al. 2004). Sajina et al. (2005) show the region on the IRAC color-color plot (top) is actually appropriate for AGN-dominated systems of redshifts 0–2. It should be noted that not all galaxies in these regions are AGN-dominated at IR wavelengths, but all AGN-dominated systems will be in the AGN zones. For part of the analysis in Chapter 4, all radio-loud galaxies with early-type SEDs which fall into *both* AGN zones are plotted as green asterisks.

We convert the IRAC $S_{3.6\mu m}$ to K-band stellar mass via Balogh et al. (2007), and $S_{24\mu m}$ to bolometric infrared luminosity, L_{IR}, and infrared star formation rate, SFR_{IR}, with publicly available templates and codes[9] (Chary & Elbaz 2001). Plots of L_{IR} versus redshift in Figure 3.5 show our sample of Luminous Infrared Galaxies (LIRG, $L_{IR} > 10^{11}$ $L_{\odot}$) is complete to $z \sim 0.5$. The conversion of L_{IR} to SFR_{IR} is appropriate for starburst-dominated infrared emission, but IR color-color diagrams in Figure 3.4 show some IR sources may be AGN-dominated; uncertainties introduced by applying this conversion to potentially AGN-dominated sources are discussed in Chapter 4. Figure 3.6 shows the optical and infrared masses agree very well, but SFR_{opt} is 3–10 times lower than SFR_{IR}. Having sampled the brightest infrared galaxies which are most likely to have obscured star formation, this factor is and should be higher than the usual $SFR_{IR} \sim 2 \times SFR_{opt}$ (Takeuchi et al. 2005).

For galaxies with infrared star formation rates, we can substitute SFR_{IR} for optical SFR in the two-component "A+B" model SN Ia rate, R_{Ia}, of Equation 3.1 in § 3.2. Doing this can account for contributions from dust-obscured star formation to the "prompt" component. When substituting SFR_{IR} into Equation 3.1, we must alter the "B" value. It was derived by Sullivan et al. (2006) based on *optical* star formation rates, but typically $SFR_{IR} \approx 2\ SFR_{opt}$, as dicussed above. Although Figure 3.6 shows $SFR_{IR} \sim 3\text{–}10 \times SFR_{opt}$, this is for the extreme fraction of brightest infrared galaxies. Had SFR_{IR} been used for all regular galaxies, the derived B value would be $B_{IR} \sim B_{opt}/2$. Thus, to incorporate IR SFR into the prompt component we instead use $0.5 \times B \times SFR_{IR}$. This will be done in Chapter 4.

3.5 Catalogs from Cappellaro et al. (1999)

In Chapter 2 we discussed, as part of our work's motivation, how the enhanced SN Ia rate in radio-loud early-type galaxies reported by DV05 is based on the SN Ia catalog of Cappellaro et al. (1999, hereafter C99). In Chapter 4, our tests for an enhanced SN Ia rate in radio-loud early-type galaxies in the SNLS sample are slightly different from DV05. For

[9] http://david.elbaz3.free.fr/astro_codes/chary_elbaz.html

Table 3.4 Properties of C99 Elliptical Host Galaxies.

SN Ia Name (and Type)	Galaxy Name	Hubble Type	Radio Luminosity [10^{29} erg s^{-1} Hz^{-1}]	NED Galaxy Type	Optical sSFR [10^{-10} y^{-1}]	Infrared Luminosity [10^{10} $L_{\odot}$]	Infrared sSFR [y^{-1}]
1961H (Ia)	NGC 4564	-4.9	<0.008 (<0.010)	E6	0.00	...	...
1968A (I)	NGC 1275	-1.6	720.0 (1462)	cD; pec; NLRG	0.26	17.5	0.63
1970J (Ia)	NGC 7619	-5.0	0.540 (0.590)	E	0.00	...	...
1972J (I)	NGC 7634	-2.0	<0.040 (<0.050)	SB0	0.27	...	...
1980I (Ia)	NGC 4374	-4.7	20.00 (31.18)	E1; LINER; Sy2	0.00	0.2	0.02
1980N (Ia)	NGC 1316	-1.9	1000. (1.752)	SAB; LINER	0.25	0.7	0.03
1981D (Ia)	NGC 1316	-1.9	1000. (1.752)	SAB; LINER	0.25	0.7	0.03
1981G (Ia)	NGC 4874	-4.0	24.00 (27.98)	cD	0.03	...	...
1983G (Ia)	NGC 4753	-2.2	0.530 (<0.015)	I0	0.26	0.6	0.08
1983J (?)	NGC 3106	-1.9	0.920 (0.692)	S0	0.26	1.7	0.13
1986G (Ia)	NGC 5128	-2.2	18.00 (52.39)	S0; pec; Sy2	0.25	1.6	0.20
1990M (Ia)	NGC 5493	-2.1	<0.040 (<0.051)	S0; pec	0.25	...	...
1991Q (?)	NGC 4926A	-1.6	0.310 (0.325)	S0; pec?; Sbrst	0.24	6.2	2.86
1991bg (Ia)	NGC 4374	-4.7	20.00 (31.18)	E1; LINER; Sy2	0.00	0.2	0.02
1991bi (Ia)	NGC 5127	-4.9	8.700 (9.843)	E; pec	0.00	...	...
1992A (Ia)	NGC 1380	-1.9	<0.020 (<0.018)	SA0	0.25	0.4	0.06
1992bo (Ia)	E352-G57	-1.5	<0.160 (<0.175)	SB; pec	0.27	...	...
1993C (Ia)	NGC 2954	-4.9	<0.080 (<0.105)	E	0.00	...	...
1993ah (Ia)	E471-G27	-2.0	41.00 (44.77)	SBb	0.26	...	...
1994D (Ia)	NGC 4526	-2.0	0.042 (0.047)	SAB	0.26	0.7	0.15
1996X (Ia)	NGC 5061	-5.0	<0.030 (<0.033)	E0	0.00	...	...

consistency we perform our analysis also on the C99 data set. In this section we describe the C99 sample, generously provided for our use by Enrico Cappellaro.

The C99 catalog is a combination of visual and photographic searches from Cappellaro et al. (1993) and Evans et al. (1989). These searches targeted nearby galaxies out to $z \leq 0.1$. The SN catalog data includes name, type (mostly classified spectroscopically, but some photometrically), and host name; galaxy catalog includes Hubble type, recession velocity, B-band luminosity and control time (the time during which an exploding SN would be detectable).

For radio counterparts we use the same methods, matching criteria, flux limits, and radio source catalogs as DV05: the NRAO VLA Sky Survey (Condon et al. 1998), the Parkes-MIT-NRAO survey (Griffith & Wright 1993), and the GB6 survey
(Gregory et al. 1996). We convert these radio fluxes to luminosities as described in § 3.3. In Table 3.4, column 4 contains the radio luminosities derived by DV05, and in brackets the radio luminosities derived by us. We do not recover precisely the same radio luminosities as DV05, but we do classify the same hosts as radio-loud with one exception. The host of SN 1983J is classified by DV05 as "borderline" radio-loud, so they add 0.5 SNe Ia to the number of radio-loud hosts. We find a lower radio power and do not do this.

For the C99 sample of early-type SN Ia hosts used by DV05 (their Table 2), we look up detailed galaxy classifications from the NASA Extragalactic Database[10] (NED). These are listed in column 5 of Table 3.4, where E: elliptical; cD: supergiant in cluster; I: irregular; LINER: low-ionization nuclear emission-line region; NLRG: narrow line radio galaxy; pec: peculiar; S: lenticular, A (unbarred), B (barred); Sbrst: starburst; Sy: Seyfert. These additional classifications show that some of these radio-loud early-type SN Ia hosts are peculiar (possibly merging) and/or have emission lines.

We derive mass and star formation rate from morphology and optical magnitude as in § 3.2, and K-band stellar masses from the 2 Micron All-Sky Survey (Skrutskie et al. 2006) as in § 3.4. We compile infrared data from two Infrared Science Archive [11] catalogs, the IRAS Faint Source Catalog (Moshir et al. 1992) and the IRAS Cataloged Galaxies and Quasars (Fullmer & Lonsdale 1989), and convert to infrared luminosity as described by Sanders & Mirabel (1996). We also calculate the expected number of SNe Ia for each galaxy from the two-component "A+B" model as described in 3.2, and use the given galaxy control times to account for SN detection efficiency (Cappellaro et al. 1997). Since these additional host properties require first converting the morphological Hubble Types into

[10] http://nedwww.ipac.caltech.edu
[11] http://irsa.ipac.caltech.edu

Gwyn SED types, the resulting type distribution is discontinuous, and the final optical properties have an uncertainty greater than the 40–50% quoted in § 3.2.

The properties of early-type C99 SN Ia hosts presented in Table 3.4 suggest they may not all be simply quiescent ellipticals, perhaps containing more SN Ia progenitors (of the 'prompt' or 'B' component variety) than previously expected. For example, NGC 1275 is a LIRG, and likely contains dust-obscured star formation and a young stellar component despite being morphologically early-type. These aspects of the C99 catalog galaxies are discussed more in Chapter 4.

3.6 Galaxy Groups and Pairs

Based on the zCOSMOS-bright sample of galaxy spectroscopic redshifts which covers CFHTLS Deep field D2 (Lilly et al. 2009), Knobel et al. (2009, hereafter K09) generate a catalog of galaxy groups and their members. They use a combination of both the Friends-of-Friends and Voronoi-Delaunay methods for group identification, which they verify as robust by comparisons with a realistic mock galaxy catalog. Their catalog of galaxy groups and pairs out to z = 1.0 is publicly available.

We match the K09 galaxies to the C09 catalog using a maximum separation of $\sim 1.8''$ and $\Delta z_{\rm phot} = 0.08$ ($\sim 3\sigma_{\rm D1}$ from § 3.2). Of the 800 K09 groups, $\sim$ 410 have *all* their member galaxies matched to C09. In total, 1585 of 2310 K09 member galaxies have a match in the C09 catalog. Of the 725 K09 member galaxies without C09 matches, 359 are outside of D2 (COSMOS covers 2 square degrees), and most of the rest are in regions masked by C09, with about $\sim$ 170 matched to galaxies rejected from the restricted C09 catalog due to poor photometric redshift fits. As discussed more in the following section, a small set of C09 galaxies are associated with both a K09 group and an Olsen catalog cluster; this amounts to $\sim$ 5% of the total mass in K09 groups.

For a sense of the relative completeness of the SNLS SNe Ia, Coupon galaxies, and Knobel group catalogs, we plot the fraction of each sample (out of the total with $z \leq 1.0$) in redshift bins from 0 to 1 in Figure 3.7. For the purposes of this plot, only groups with *all* of their members matched to the C09 catalog are included. Figure 3.7 shows the fraction of galaxies in groups fluctuates over redshift, and is not always consistent with the fraction of galaxies in each bin. This is a combined effect of completeness in the spectroscopic redshift catalog, and the formation and evolution of groups over redshift. We will assess any impact of this on our SN Ia rate per unit mass in groups in § 5.2.2.

The K09 group catalog is based on the VLT ZCOSMOS spectroscopic redshift catalog,

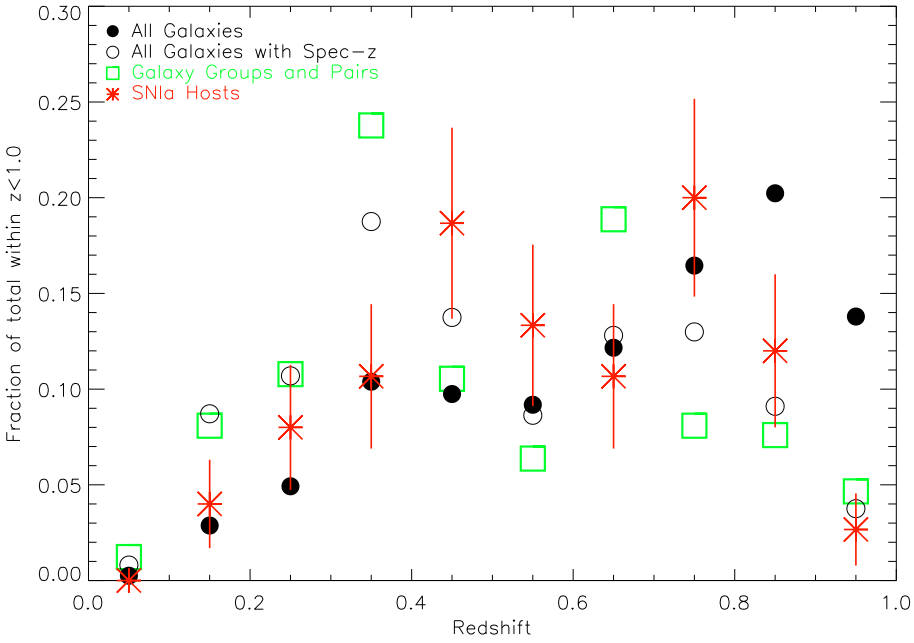

Figure 3.7 Normalized redshift distributions for SNLS SNe Ia (red asterisks), Coupon galaxies (black circles), and Knobel groups (green squares) within $z \leq 1.0$; redshift bin size ±0.05.

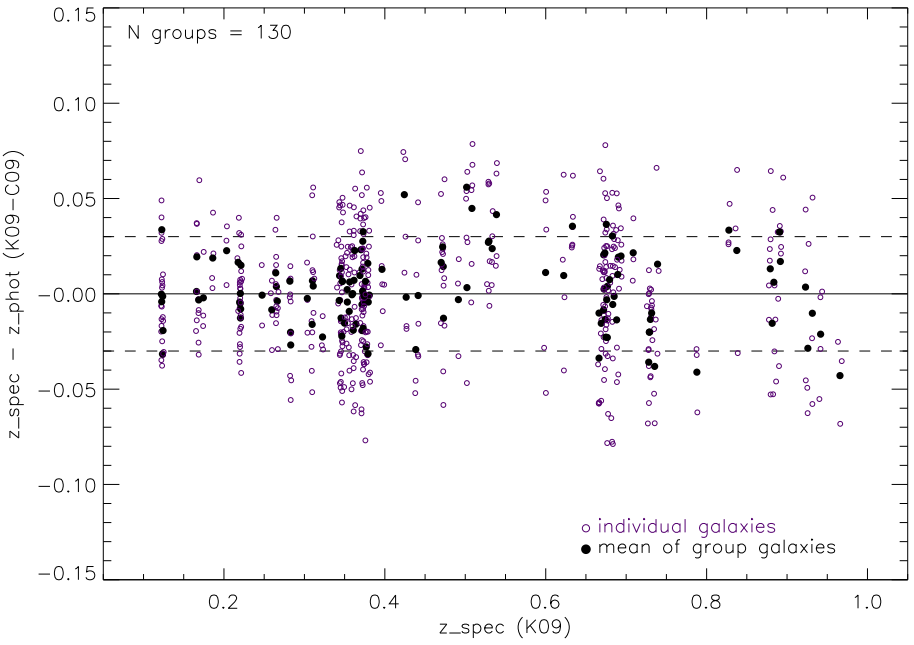

Figure 3.8 Dispersions between spectroscopic and photometric redshifts for K09 galaxy group members. Open circles show the difference between spectroscopic, z_{K09}, and photometric, z_{C09}, redshifts for individual galaxies, as a function of z_{K09}. Filled circles show the differences in the averages of these over all group members: $\overline{z_{K09}} - \overline{z_{C09}}$ versus $\overline{z_{K09}}$. Dashed lines mark the $\sim 1\sigma = 0.03$ uncertainties for photometric redshifts.

but the C09 photometric redshift catalog is more complete – can we identify additional group members from the C09 galaxy catalog? To illustrate the difficulty of group galaxy identification with photometric redshift, in Figure 3.8 we plot the dispersion between spectroscopic and photometric redshifts for known group members (open symbols). We also plot the difference between the *average* spectroscopic and photometric redshifts of galaxies in each of the 130 groups with 3 or more members (filled symbols). Figure 3.8 shows the difficulty of recovering missing group members among the C09 galaxies using photometric redshifts. In Chapter 5, we carefully attempt this only as a last resort to correct for group incompleteness.

3.7 Galaxy Clusters

Based on the CFHTLS Deep field galaxy catalog released by Terapix in August 2005 (T0002), Olsen et al. (2007) identify a catalog of galaxy clusters using a matched filter algorithm. This routine identifies regions of galaxy over-densities with luminosity functions and radial distribution profiles resembling an assumed cluster template. The Olsen catalog includes photometric redshifts and an optical grade (A–D). We use only clusters of grade A, meaning a concentration of similarly colored galaxies is visible; this leaves 19, 17, 16, and 10 clusters in D1–4. This optical cluster catalog was chosen over those of other selection techniques as it provides consistent completeness for all four SNLS Deep field areas.

Olsen et al. (2007) find their cluster redshifts are slightly overestimated for $z < 0.6$, and underestimated for $z > 0.7$, with a standard deviation of ~ 0.1 (Olsen et al. 2007). For the cluster redshift we instead use the peak of the galaxy photometric redshift distribution along the cluster's line of sight. We include all E/S0 and Sbc type galaxies within a physical radius $R_p \leq 0.5$ Mpc, converted to angular radius using the cluster's original redshift. For distributions which plateau instead of peak, the plateau's central redshift is used. In fields D1 and D2 which have VLT spectroscopy as described in § 3.2, peaks in the spectroscopic redshift distribution are used to adjust the cluster redshifts. Five clusters had no discernible peak and cannot be used. We are left with 56 clusters with $z \leq 1.0$ and 29 with $z \leq 0.6$ to use for this experiment. To evaluate corrected cluster redshift precision we compare the dispersion in spectroscopic redshift for those D1 and D2 cluster member galaxies which have VLT spectroscopic redshifts from VVDS or zCOSMOS (as described in § 3.2). The differences between spectroscopic redshifts and the new photometric redshifts for Olsen clusters have a standard deviation of $\sigma_{\Delta z/(1+z_{VVDS})}$ =0.03–0.04, indicating a good agreement.

As mentioned in the previous section, a small set of C09 galaxies are associated with both a K09 group and an Olsen catalog cluster; this amounts to ~ 10% of the total mass in Olsen clusters in CFHTLS Deep field 2. To be more specific, 68 galaxies from 8 unique Olsen clusters are associated with 23 unique K09 groups. Of the 23 groups, 10 are galaxy pairs, 10 are groups of between 3 and 10 members, and only 3 have more than 10 members; the 8 Olsen clusters have a mean number of members ~ 80.

In optimizing their group finding method using mock galaxy catalogs, Knobel et al. (2009) attempted to minimize over-merging (identifying multiple smaller groups as a single large group) and fragmentation (erroneously subdividing a single group into smaller parts). Despite such measures, in at least one case with the real data a manual intervention was required to subdivide a super-group of nearly-merging groups. As the matched-filter algorithm of Olsen et al. (2007) is tailored to avoid fragmentation, and we use photometric redshifts to identify cluster members, it is not surprising to find Knobel group galaxies within Olsen clusters. Some of these galaxies will be interlopers from nearby groups of comparable redshift. However, as structure in the Universe is likely formed by hierarchical clustering (in which large clusters are built up by the merger and acquisition of smaller groups), some of the K09 groups and pairs in or around Olsen clusters are likely to be physically related (e.g. in-falling) systems. In these cases, it is not entirely inappropriate to include them as part of the cluster. Ultimately, that 10% of the mass in Olsen clusters may be in groups and pairs is not a problematic issue for the experiments in Chapter 6.

3.8 Summary

This thesis relies entirely on data taken by other astronomers, but the collection and integration of these data sets has not been a trivial endeavor. Each catalog has its own unique completeness levels, both in two dimensions on the sky, and in the third dimension of distance or redshift. Every effort is made in the following chapters to assess any biases in the results stemming from incongruous completeness levels between catalogs; this often entails restricting one or more catalogs to only certain areas, or placing limits on redshift or other galaxy properties. At times this will make for a seemingly repetitive analysis, but since the cohesion of these data sets has resulted in the most comprehensive multi-wavelength study of intermediate redshift SN Ia hosts yet presented, we ultimately believe the extra efforts are necessary.

Chapter 4

Radio and Infrared Hosts

The correlation between a galaxy's SN Ia rate per unit mass and its star formation rate (SFR) was established by Mannucci et al. (2005), and expressed as the two-component "A+B" rate model by Scannapieco & Bildsten (2005). During this time, Della Valle et al. (2005, hereafter DV05) published their discovery of a $\sim 3\times$ SN Ia rate enhancement in early-type galaxies which are radio-loud ($L_{1.4\,GHz} > 10^{29}$ ergs s^{-1} Hz^{-1}). This relation was subsequently shown to be consistent with half of all SNe Ia belonging to a "prompt" population which explode within 10^8 years of star formation – a controversial postulate about the nature of SNe Ia, as discussed in Chapter 2.

In this chapter, we combine the SNLS SN Ia data set with the C09 photometric redshift galaxy catalogs and 1.4 GHz VLA radio catalogs. We calculate the SNLS SN Ia rate in radio-loud early-type galaxies at intermediate redshifts, and assess the likelihood of a $\sim 3\times$ enhancement over all early-type galaxies. DV05 suggested galaxy interactions and/or mergers as the root cause of both radio activity and enhanced SN Ia rate, either through the capture of a younger stellar population and/or induced star formation. With the latter, any rate enhancement should still agree with predictions of the two-component "A+B" model, so we test this with our observations. The blue light of young stars from which SFR is derived is susceptible to obscuration by dust; some is absorbed and re-emitted at infrared wavelengths, joining the infrared light which passes through dust. For a more accurate "A+B" model prediction, we incorporate Spitzer infrared luminosities into the SFR used for the B-component of the "A+B" model.

Dust extinction in starburst galaxies also hinders SN detection: only one SN Ia has been detected, and the SN Ia rate remains unconstrained in starburst galaxies (Mannucci et al. 2003; Mannucci et al. 2007). We use the infrared catalogs to calculate the SN Ia rate in Bright and Luminous Infrared Galaxies (BIRGs and LIRGs), of $L_{IR} > 10^{10}$ and $> 10^{11}$ $L_\odot$ respectively.

These galaxies are known to experience bursts of star formation up to $100 - 1000\ M_{\odot}\ y^{-1}$. We also compare the number of SNe Ia observed in B/LIRGs to predictions of the two-component "A+B" model. As will be explained in the following sections, our analysis methods differ from those DV05 applied to the low-redshift SN Ia data set of Cappellaro et al. (1999, hereafter C99). To properly compare our results, we perform an identical analysis on the C99 catalog. This catalog was described in § 3.5.

All of the data catalogs used in this chapter were presented in Chapter 3. In § 4.1 we present the radio and infrared properties of SNLS and C99 SN Ia early-type host galaxies. We derive the SN Ia rate in radio and infrared galaxies in § 4.2, compare to expectations of the two-component "A+B" model in § 4.3, and reanalyze with relaxed data constraints in § 4.4. In § 4.5 we juxtapose the properties of the SNe Ia in radio and infrared host galaxies with known correlations between SN Ia properties and stellar populations. We discuss the implications of our results and conclude in § 4.6 and 4.7.

Most of this chapter has already been published as Graham et al. (2010). For the thesis we have substituted the recent catalog of photometric redshifts from Coupon et al. (2009) for its predecessor, Ilbert et al. (2006). We have also used updated SN Ia stretch values from Guy et al. (2010). These updates have changed some of the details and rates, but not general conclusions, from those of Graham et al. (2010).

4.1 Properties of SN Ia and their Parent Galaxies

We find 16 SNLS SN Ia host galaxies with radio and/or infrared counterparts, 3 in D1 and 13 in D2 where the radio and infrared catalogs are deeper. The properties of these SNe Ia and their hosts are given in Table 4.1. We also plot the hosts as triangles and squares in the relevant plots of Chapter 3: radio luminosity versus redshift (Figure 3.3); IR color-color diagrams (Figure 3.4); IR luminosity versus redshift (Figure 3.5); and IR versus optical mass and SFR (Figure 3.6).

Light curve stretch and color values are from Guy et al. (2010). Image stamps centered on SN Ia coordinates are shown in Figure 4.1. In total, of these 16 SNe Ia hosts we find 10 are radio-loud, 12 are BIRG, and 8 are LIRG. In these same categories, 5, 3, and 2 respectively have early-type SEDs, and are also known as E/S0 or elliptical galaxies.

Galaxies which are bright at mid-infrared wavelengths (MIR, for example 24μm) are described as being starburst- or AGN-dominated, meaning they contain dust which absorbs high-energy photons from either young stars or AGN, and re-emits them in the MIR. The infrared-emitting, radio-loud SN Ia host galaxies fit with early-type SEDs are not necessar-

Table 4.1 Properties of SNLS SNe Ia and their Host Galaxies.

SN Ia SNLS ID	SN Ia z_{spec}	SN Ia Color	SN Ia Stretch SiFTO	Host SED	Host M_V	Host Mass [10^{10} $M_\odot$]	Host SFR [$M_\odot$ y^{-1}]	Host Radio Luminosity [10^{29} erg s^{-1} Hz^{-1}]	Host IR Luminosity [10^{10} $L_\odot$]	Host IR SFR [$M_\odot$ y^{-1}]
05D1hn	0.149	0.34 ± 0.03	1.06 ± 0.02	E/S0	-22.0	18.21	1.47	2.55	11.43	19.54
04D2bt	0.220	0.16 ± 0.03	0.99 ± 0.01	E/S0	-21.4	10.05	1.56	...	2.18	3.72
06D2je	0.418	...	...	E/S0	-19.9	2.28	0.58	1.81	...	...
06D2ck	0.555	−0.00 ± 0.04	1.02 ± 0.05	E/S0	-22.5	31.44	0.97	5.13	...	...
04D1jg	0.584	−0.08 ± 0.03	1.03 ± 0.02	E/S0	-22.9	40.56	6.28	13.68	43.60	74.55
07D2kh	0.731	...	...	E/S0	-23.0	45.62	7.06	15.73	...	...
05D1by	0.299	0.77 ± 0.03	1.02 ± 0.03	Sbc	-21.3	5.51	5.44	3.05	9.61	16.43
06D2ff	0.345	0.26 ± 0.04	1.03 ± 0.04	Sbc	-22.0	10.00	11.68	4.41	8.67	14.83
05D2ac	0.479	−0.01 ± 0.03	1.11 ± 0.02	Sbc	-23.2	36.82	25.16	...	13.40	22.91
07D2ae	0.501	...	...	Sbc	-20.2	2.92	1.14	2.27	...	...
07D2bd	0.572	...	...	Sbc	-22.0	15.94	6.20	...	17.47	29.87
08D2iq	0.709	...	...	Sbc	-21.6	6.14	8.55	13.58	44.71	76.45
04D2ca	0.835	0.06 ± 0.10	1.16 ± 0.27	Sbc	-20.8	5.00	2.36	...	27.27	46.63
07D2ec	0.270	...	...	Scd	-21.1	2.72	6.45	0.83	4.51	7.71
06D2ca	0.531	0.08 ± 0.03	1.13 ± 0.04	Scd	-21.1	0.84	11.45	...	33.66	57.56
08D2id	0.833	...	...	Scd	-21.5	2.11	12.41	18.19	37.86	64.73

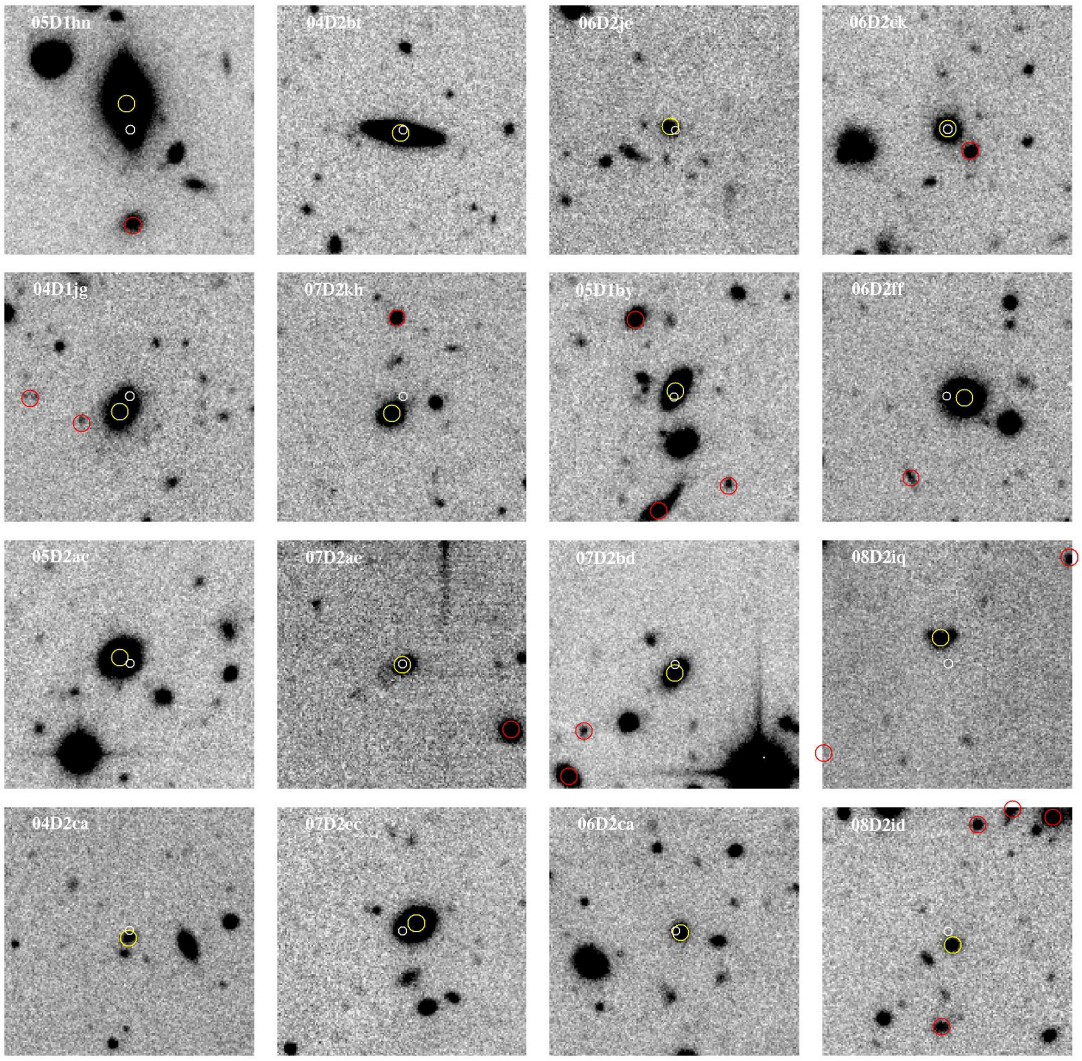

Figure 4.1 Image stamps in i_{Mega}, 30x30 arcseconds, centered on SNe Ia in host galaxies detected in radio and/or infrared source catalogs, labeled with SNLS IDs. Small white circles mark SNe Ia; yellow circles mark the host and red circles mark nearby galaxies within $\Delta z \leq 0.06$ (i.e. $\sim 2\sigma_{\Delta z/(1+z)}$).

ily AGN-dominated, despite the fact that an E/S0 SED type normally indicates a quiescent galaxy with no star formation. There are several reasons why this can be the case. First, the radio-loud E/S0 hosts with IR emission (05D1hn, 04D1jg) do not clearly lie along the "AGN plume" of the IRAC color-color plot (although 04D1jg is in its "AGN zone"), and are outside the "AGN zone" of the IRAC+MIPS color-color plot as shown in Figure 3.4. Second, AGN-dominated infrared emission originates from a hot dusty torus tens of parsecs across (Tristram et al. 2009) and would be unresolved, but the infrared sources associated with these two galaxies are not flagged as point-like. Third, a visual inspection of radio and infrared SN Ia hosts in u_M and GALEX (D2 only) images[1] show that all but the late-type hosts of 06D2ff and 07D2ec are quite faint or invisible in the ultraviolet, consistent with star formation obscured by dust. Fourth, although our radio-loud early-type SN Ia hosts appear morphologically elliptical or lenticular (Figure 4.1), and many starburst galaxies appear morphologically irregular, this is not a strict rule (e.g. Figure 4.68 of Binney & Merrifield 1998, in which a profoundly disturbed galaxy appears as an elliptical in a shallow exposure). We therefore accept the conversion of L_{IR} into SFR_{IR} for these radio-loud E/S0 SN Ia host galaxies as discussed in § 3.4, and in general find the properties of radio and infrared SN Ia hosts are not inconsistent with those of dusty starburst galaxies.

4.2 SN Ia Rates

Here we present SNLS and C99 SN Ia rates in galaxies which are radio-loud, radio-loudest ($L_{1.4\,GHz} > 10^{30}$ ergs s^{-1} Hz^{-1}), BIRG, and LIRG. As in Graham et al. (2010), we restrict the samples for our primary analysis in several ways. First, we limit ourselves to SNLS SNe Ia detected prior to 2006 December 31, because up to this date the SNLS spectroscopic analysis and typing is complete. Second, we limit our redshifts to $z \leq 0.6$, to which the SNLS SN Ia sample is nearly complete (Neill et al. 2006), and to which the radio and infrared catalogs are more complete. Third, we limit our host types to early-type (also known as E/S0 or elliptical) galaxies only in order to make direct comparisons to the results of DV05. We consider the results of extending these limitations in § 4.4.

The number of SNLS SNe Ia observed in D1–2 prior to 2006 Dec 21 for each subset, N_{obs}, is shown in Table 4.2. Also shown in brackets is the corrected SN Ia frequency, $\sum_{i=1}^{i=N_{obs}} 1/C_i$, in SN y^{-1} (the numerator for Equation 3.3). Recall that C is the correction factor which accounts for SNLS detection efficiencies and observing seasons, and that the corrected SN Ia frequency is the number of SNe Ia which explode per year of SNLS ob-

[1] http://www.cadc.hia.nrc.gc.ca/community/CFHTLS-SG/docs/cfhtls.html

Table 4.2 Number of SNe Ia in Early-Type Galaxies

Sample	SNLS[a]	C99
All	22 ($17.68^{+4.6}_{-3.7}$)	$21^{+5.7}_{-4.5}$
Radio-loud	4 ($3.21^{+2.5}_{-1.5}$)	$9.5^{+4.2}_{-3.0}$
Radio-loudest	1 ($0.77^{+1.8}_{-0.6}$)	$8^{+3.9}_{-2.8}$
BIRG	3 ($2.37^{+2.3}_{-1.3}$)	$4^{+3.2}_{-1.9}$
LIRG	2 ($1.53^{+2.0}_{-1.0}$)	$1^{+2.3}_{-0.8}$

[a]Brackets contain number of SNe Ia corrected for SNLS detection efficiencies to be the number which exploded per year of SNLS observations, as in § 3.2.

servations (i.e. years in observer's frame). Also quoted are Poisson uncertainties on N_{obs} at the 0.84 (1σ) confidence level from Gehrels (1986), propagated to uncertainties on the corrected SN Ia frequency.

The amount of mass in, and number of, galaxies in each subset is given in Table 4.3. We calculate the SN Ia rate per unit mass in each galaxy subset, $sSNR_{Ia}$ from Equation 3.3, and display them in Table 4.4 in the commonly used "supernovae unit" SNuM, which is equal to one supernova per century per 10^{10} $M_{\odot}$. Ratios of SN Ia rates in radio and IR subsets over all E/S0 galaxies are given in Table 4.5. The uncertainties quoted on rates and ratios are statistical, propagated from those in Table 4.2, and do not include the uncertainty from galaxy mass ($\sim$ 40%). These tables also contain equivalent values for the C99 SN Ia and galaxy catalogs. As described in § 3.5, we find slightly different radio luminosities for the C99 galaxies. We initially use radio luminosities from DV05 to classify SN Ia hosts in order to make a direct comparison with their results. We revise our results with our own luminosities and discuss in § 4.2.1.

4.2.1 Radio-Loud Galaxies

With SNLS data, we find the specific SN Ia rate in radio-loud early-type galaxies to be $0.091^{+0.072}_{-0.044}$ SNuM, in good agreement with the C99 result in Table 4.4. VLA radio catalog incompleteness means we can identify only half of the radio-loud population (§ 3.3) and cannot isolate a radio-quiet set for the SNLS (see Figure 3.3). This is in contrast to DV05, who quote a $\sim$ 4 times SN Ia rate enhancement in radio-loud over radio-*quiet* early-type galaxies. In lieu of comparing with a radio-quiet set, we consider the ratio between radio-

Table 4.3 Mass[a] in Early-Type Galaxies

Sample	SNLS	C99
All	42385.8 (4184)	23315.0 (2079)
Radio-loud	4787.6 (191)	7724.5 (314)
Radio-loudest	1935.9 (51)	2825.5 (92)
BIRG	2263.3 (4184)	1805.7 (166)
LIRG	692.0 (69)	469.2 (22)

[a]Mass units are 10^{10} $M_{\odot}$; brackets contain number of galaxies in sample.

Table 4.4 SN Ia Rates in Early-Type Galaxies

Sample	SNLS [SNuM[b]]	C99 [SNuM[b]]
All	$0.058^{+0.015}_{-0.012}$	$0.044^{+0.012}_{-0.010}$
Radio-loud	$0.091^{+0.072}_{-0.044}$	$0.101^{+0.045}_{-0.032}$
Radio-loudest	$0.056^{+0.128}_{-0.046}$	$0.197^{+0.097}_{-0.068}$
BIRG	$0.137^{+0.133}_{-0.074}$	$0.166^{+0.131}_{-0.079}$
LIRG	$0.324^{+0.426}_{-0.209}$	$0.213^{+0.488}_{-0.177}$

[b]SNuM = SN $(100\ \mathrm{yr})^{-1}$ $(10^{10}\ M_{\odot})^{-1}$

loud and *all* early-types as a lower limit. We find the SNLS result is consistent with C99 at the 1σ level, but that the SNLS and C99 ratios are also consistent with no enhancement at the 1σ and 2σ levels respectively, as shown in Table 4.5.

Can we correct our radio incompleteness? While we could use radio-loud galaxy mass functions to estimate the mass missing from our radio-loud sample, we could not know how many SNe Ia this mass hosted, so cannot correct the SN Ia rates for radio incompleteness. Instead, we simply use the limited mass in radio-loud galaxies we *do* find, and the limited sample of SNe Ia hosted by it, as representative. Any SN Ia rate enhancement in radio-loud galaxies would also appear in this limited sample, assuming it is not proportional to $L_{1.4\,\mathrm{GHz}}$ (i.e. AGN power). The SN Ia rate is not expected to be proportional to $L_{1.4\,\mathrm{GHz}}$ because AGN activity is not suspected of directly influencing the probability of a SN Ia explosion,

Table 4.5 Ratios of SN Ia Rates in Radio and IR Early-Types to All Early-Type Galaxies

Sample	SNLS	C99
Radio-loud	$1.6^{+1.3}_{-0.8}$	$2.3^{+1.2}_{-0.9}$
Radio-loudest	$1.0^{+2.2}_{-0.8}$	$4.4^{+2.5}_{-1.8}$
BIRG	$2.4^{+2.4}_{-1.4}$	$3.7^{+3.1}_{-2.0}$
LIRG	$5.6^{+7.5}_{-3.8}$	$4.8^{+11.1}_{-4.1}$

as discussed in § 2; any evolution in the physical properties of AGN is not expected to influence our results either. Our radio incompleteness thus still produces a sample which makes a suitable comparison to C99.

Unlike the radio-loud limit, the radio-loudest sample from the SNLS catalogs is complete to z = 0.6, as shown in Figure 3.5. As an extra test, we present the specific SN Ia rates among the radio-loudest early-type galaxies in Table 4.4, and their ratio over all early-types in Table 4.5. While the SNLS SN Ia rate in the radio-loudest early-type galaxies shows no increase over the rate in all early-types, the C99 catalog shows a $\sim 4\times$ enhancement – twice the enhancement for the radio-loud sample. However, this is still within 2σ of a null result, and additional factors may artificially inflate this rate, as discussed below.

Although we do not recover precisely the same radio luminosities for C99 early-type hosts as DV05, we have initially used their classifications in order to directly compare with their results. As shown in Table 3.4, we would place NGC 1316 in the radio-loud subset but not the radio-loudest, and would not classify NGC 3106 as "borderline" radio-loud. Also, SN 1968A in NGC 1275 is listed as type-I, not type-Ia. Although rare, core-collapse supernovae have been observed in early-type galaxies; this is often due to misclassification of late-types as early-type, especially for galaxies with HI and radio emission (Hakobyan et al. 2008; Bazin et al. 2009). NGC 1275 is a known star forming early-type galaxy, has the highest L_{IR} of all C99 early-type hosts (Table 3.4), and is precisely the sort of galaxy to potentially host a CC SN. Considering these speculative misclassifications, the C99 sample would have instead 5, 8, and 20 SN Ia hosts in the radio-loudest, radio-loud, and all early-type samples. This lowers their rates to $0.123^{+0.083}_{-0.053}$, $0.085^{+0.042}_{-0.030}$, and $0.042^{+0.012}_{-0.009}$ SNuM respectively. Ratios for the radio-loudest and radio-loud categories drop to $2.9^{+2.1}_{-1.4}$ and $2.0^{+1.1}_{-0.8}$, keeping the null result within 2σ. We note that these misclassifications are speculative, and that the discrepancies could also simply be due to small number statistics.

4.2.2 Bright and Luminous Infrared Galaxies

With SNLS data, we find the specific SN Ia rate in early-type BIRG and LIRG to be $0.137^{+0.133}_{-0.074}$ and $0.324^{+0.426}_{-0.209}$ SNuM respectively. As presented in Table 4.4, the C99 BIRG and LIRG rates are consistent with the SNLS results to within 1σ. Again we consider the ratios between B/LIRG and *all* early-types as a lower limit on any possible enhancement, as given in Table 4.5. It appears the SN Ia rate is a factor of ~ 2 (1σ) and ~ 5 (2σ) times higher in BIRGs and LIRGs respectively. While we could have isolated all non-LIRG early-type galaxies for a ratio, the LIRG fraction is small enough that this would not be significantly different from the all early-types sample. So we instead stick to a consistent method.

Regarding the C99 SN Ia rates in infrared galaxies, as discussed in § 4.2.1, SN 1968A in early-type LIRG NGC 1275 may not have been a type Ia. Also, SN 1983J and SN 1991Q do not have a definitive classification. The scenario that these three are not Type Ia drops the rate in C99 BIRG early-type galaxies to $0.041^{+0.095}_{-0.034}$ SNuM, consistent with the SN Ia rate in all early-type galaxies.

4.3 Comparison to Predictions of the "A+B" Model

So far we have found the specific SN Ia rates in subsets of radio and infrared early-type host galaxies are $\sim$ 1–5 times the rate in all early-type galaxies, and all enhancements have low significance (2σ at most). In this section we test whether these rates are also consistent with the two-component "A+B" model; whether the potential enhancements might simply be due to star formation providing additional SN Ia progenitors. To do this, we statistically compare the observed number of SNe Ia in radio and infrared early-type galaxies, N_{obs}, to that predicted by the two-component "A+B" model, N_{A+B}, as explained in § 3.2.

We calculate summed Poisson probabilities for the same SNLS and C99 radio and infrared galaxy subsets described in § 4.2. Where *optical* masses and star formation rates are used in the "A+B" model, we refer to the total expected number of SNe Ia as $N_{A+B,opt}$ and the associated summed probability as P_{opt}. We also derive $N_{A+B,IR}$ and P_{IR} using infrared SFR if a galaxy has a MIPS counterpart (using optical SFR if not); this accounts for contributions from dust-obscured star formation to the "prompt" component. As discussed in § 3.4, when substituting SFR_{IR} into the "A+B" model in Equation 3.1, we use $0.5 \times B \times SFR_{IR}$.

Table 4.6 Statistical Comparison to "A+B" SN Ia Rate Model

Sample		N_{obs}	$N_{A+B,opt}$	P_{opt}	$N_{A+B,IR}$	P_{IR}
Radio-loud	SNLS	4	2.45	0.23	2.63	0.27
	C99	9.5	4.84	0.04	5.10	0.05
Radio-loudest	SNLS	1	0.96	0.62	1.02	0.73
	C99	8	2.35	0.003[a]	2.39	0.003[b]
BIRG	SNLS	3	1.26	0.13	1.64	0.23
	C99	4	1.39	0.05	1.77	0.10
LIRG	SNLS	2	0.35	0.05	0.66	0.14
	C99	1	0.26	0.23	0.43	0.35

[a]Further considerations raise $P_P \gtrsim 0.1$ in § 4.3.1.

4.3.1 Radio-Loud Galaxies

Summed Poisson probabilities comparing the number of SNLS SNe Ia in radio-loud and radio-loudest early-type galaxies to predictions of the "A+B" model are given in Table 4.6. For the SNLS, all values are $P_{SUM} > 0.05$, indicating no significant deviation between observations and "A+B" model predictions. As discussed in § 4.2.1, it is unlikely the SNLS results are affected by our radio incompleteness. Although for radio-loud early-type galaxies $N_{A+B,opt}$ and $N_{A+B,IR}$ are quite similar, the fraction of expected SNe Ia contributed by the B-component changes from $\sim$ 5% to $\sim$ 20% when SFR_{IR} is used. However this is also the case for all early-type galaxies in general, not just those with radio emission. Thus, $\sim$ 20% from the B-component should just be considered a baseline effect of using SFR_{IR}.

However, results for the C99 samples suggest significant to *very* significant deviations in the samples of radio-loud and radio-loudest early-type galaxies. These results are unchanged with the consideration of infrared SFR. Could this be due to a variation between derived B values from different surveys (Greggio et al. 2008)? For example, for the C99 radio-loud sample, using 5×B yields $N_{A+B,opt} = 5.9$ and $P_{opt} = 0.11$. However, for the C99 radio-loudest sample, a 20×B is necessary to raise $N_{A+B,opt} \sim 4$ and $P_{opt} \gtrsim 0.05$; an inappropriate B value cannot wholly explain this under-estimate. As discussed in § 4.2.1, the actual number of SNe Ia in the radio-loud and -loudest subsets of C99 may be 8 and 5 respectively. This would increase P_{opt} and P_{IR} to $\gtrsim 0.1$ for both subsets, which we do not consider significant. It appears the more likely explanation is the misclassification of some

C99 supernovae.

4.3.2 Bright and Luminous Infrared Galaxies

Summed Poisson probabilities in Table 4.6 for SNLS BIRG and LIRG early-type samples shows a possible excess of SNe Ia over optical "A+B" model predictions, especially in LIRG, but the inclusion of SFR_{IR} raises $N_{A+B,IR}$ and P_{IR} to statistically acceptable values. The same can be said for C99 BIRG, though as discussed in § 4.2.1 the number of C99 SNe Ia in BIRGs may be just 1, in good agreement with $N_{A+B,opt}$. In general we find the number of SNe Ia in BIRG and LIRG is consistent with predictions of the "A+B" model.

As noted in the previous section, the fraction of expected SNe Ia contributed by the B-component is about $\sim 20\%$ when SFR_{IR} is considered. This fraction increases to $\sim 30\%$ and $\sim 45\%$ for BIRGs and LIRGs respectively, which is further evidence that dust-obscured star formation is the root cause of the potential SN Ia rate enhancements in B/LIRG early-type galaxies.

We note in § 3.4 that infrared emission of potentially AGN-dominated galaxies has been converted to SFR_{IR} using a starburst-dominated template, thereby artificially inflating $N_{exp,IR}$. We identify E/S0 radio-loud galaxies which lay along the "AGN plume" (top plot, plume between $-0.1 \lesssim \log(S_{5.8}/S_{3.6}) \lesssim 0.5$) and in the "AGN Zone" (bottom plot) of Figure 3.4 as the most likely to be AGN (green asterisks). This population contributes 20–40% *of the additional* SNe Ia predicted when SFR_{IR} is included (i.e. 20–40% of $N_{A+B,IR} - N_{A+B,opt}$).

4.4 Altering the Data Constraints

To consider whether altering the constraints on SNLS data affects our results, we try: extending our sample to the full five-year SNLS survey (SNLS-2008), extending our redshift range to $z = 1.0$, including galaxies with SED type Sbc, and different combination methods for our radio catalogs.

To begin we extend to SNLS-2008 but there are no additional SNLS SNe Ia in $z \leq 0.6$ early-type galaxies with radio or infrared emission after 2006 December 31, so the results do not change. Next we extend to $z \leq 1.0$, but there are no SNLS-2006 early-type SN Ia hosts which are radio-loud, BIRG, or LIRG at $z > 0.6$, so this has the net effect of lowering all rates and ratios, and increasing all summed Poisson probabilities, to be (even more) consistent with the null result of no enhancements. The same general effect is found if we include SNLS-2008 *and* $z \leq 1.0$. This is not surprising as our radio and infrared catalogs

are very incomplete at z > 0.6.

We originally limit our host types to early-type (also known as E/S0 or elliptical) galaxies only in order to make direct comparisons to the results of DV05. However, their galaxies were *morphologically* classified as early-type, which is not equivalent to our SED types. Mannucci et al. (2007) estimate increased star formation during radio-loud epochs leads to 3–5% of the galaxy's mass in new stars (after the 10 bursts of 10^8 years, each 10^9 years apart). As E/S0 galaxy masses are around 10^{11} $M_\odot$, $0.05 \times 10^{11} = 5 \times 10^9$ $M_\odot$ of new stars over $10 \times 10^8 = 10^9$ years is an average star formation rate of of ~ 5 $M_\odot$ y^{-1}. Our SED models and SFR calculations classify such galaxies as Sbc; so we redo our analysis including Sbc type galaxies.

In the SNLS-2006 z $\leq$ 0.6 sample, 05D1by and 06D2ff have radio-loud Sbc-type hosts, and 05D2ac is an Sbc-type LIRG. Including Sbc-type adds a lot of mass to the galaxy sample, which has the net effect of lowering all rates and ratios. This also increases all summed Poisson probabilities to be (even more) consistent with the null result of no enhancements. If we take these data constraints to maximum relaxation and include all types of SNLS-2008 SN Ia hosts out to z $\leq$ 1.0, all rate ratios are $\leq$ 1.0.

The deeper flux limit of the VLA-COSMOS in D2 may result in slightly different radio source populations between D1 and D2. To investigate whether this affects our results, we first restrict VLA-COSMOS to the same flux limit as VLA-VIRMOS, $S_{1.4GHz} > 0.08$ mJy, and then consider the results from only the deeper radio catalog in D2. In both cases these experiments simply degrade the sample, and the rates in the radio-loud subset remain consistent with no enhancement.

4.5 Properties of SNe Ia in Radio and IR Hosts

It is well established that SN Ia light curve shape and peak luminosity are correlated: more slowly-declining light curves reach a brighter peak luminosity. This relation was discussed in Chapter 2. Light curves are parametrized by Δm_{15}, the decrease in magnitude over the first 15 days after maximum light (Phillips 1993), or by stretch, s, the amount that a template (average) light curve must be "stretched" to fit the observations. For stretch, s > 1 is for brighter, slower declining SNe Ia and vice versa (Perlmutter et al. 1997). SN Ia peak luminosity depends on the mass of ^{56}Ni synthesized during the explosion (Arnett 1982); whether this mass is influenced more by the metallicity or age of the white dwarf progenitor star is under much debate (Timmes et al. 2003; Röpke & Hillebrandt 2004;
Gallagher et al. 2005; Gallagher et al. 2008; Howell et al. 2009).

SN Ia properties are also correlated with qualities of the host galaxies, where late-type star-forming galaxies host mostly bright, slowly declining SNe Ia, and early-type elliptical galaxies with little to no star-formation host faint, rapidly declining SNe Ia (Hamuy et al. 1996; Howell et al. 2001). Gallagher et al. (2005) compiled a database of 57 local SNe Ia and found the mean Δm_{15} in late-type (Sa to Peculiar) host galaxies is $\overline{\Delta m_{15}} \sim 1.1$, and in early-type (E/S0) hosts $\overline{\Delta m_{15}} \sim 1.45$. Sullivan et al. (2006) also show the median stretch of SNLS SNe Ia in late-type star-forming galaxies is greater than in early-types. This is supported by Howell et al. (2007) who use light curve fitting routine SiFTO (Conley et al. 2008) to constrain the stretch distribution of "B" (prompt) component SNe Ia (associated with young stellar populations) to be centered at s = 1.071 with $\sigma = 0.063$, and of "A" (delayed) component SNe Ia (associated with old stellar populations) to be centered at s = 0.945 with $\sigma = 0.077$.

If SNe Ia in radio-loud early-type hosts are associated with young stars, their stretch values should be consistent with the "B" component stretch distribution. Here we consider the stretch values for SNLS-2006 SNe Ia in radio-loud early-type galaxies with $z \leq 0.6$: 04D1jg, 05D1hn, and 06D2ck, as given in Table 4.1. SN Ia 06D2je was not included in the SNLS third-year results, but preliminary fits show its stretch is similar to 05D1hn. Stretches for SNe Ia 04D1jg, 05D1hn, and 06D2ck are most consistent with the "B" component distribution of Howell et al. (2007). Individually, 05D1hn and 06D2ck are also consistent with originating from the "A" component at the $\sim 1\sigma$ level. These three have a mean stretch of s = 1.04 with $\sigma = 0.02$, most consistent with the "B" component and indicative of association with a younger or intermediate-age stellar population. There probability that all three are associated with the "A" component is $\lesssim 2\%$.

Among C99 SNe Ia in radio-loud early-type hosts, five of eight have a Δm_{15} given in Table 2 of DV05, $\Delta m_{15} = \{1.28, 1.33, 1.73, 1.88, 1.30\}$. Their mean is $\overline{\Delta m_{15}} = 1.5$ with $\sigma_{\Delta m_{15}} = 0.25$ which is consistent with $\overline{\Delta m_{15}} \sim 1.45$ for SNe Ia in early-type hosts (Gallagher et al. 2005). DV05 find that this distribution of decline rates for SNe Ia in radio-loud early-type hosts is intermediate between that found for late-type and early-type hosts. They suggest this supports a *continuum* of SN Ia and host galaxy properties, from young progenitors in very active galaxies, intermediate age progenitors in active galaxies, and old progenitors in passive galaxies. This agrees with our finding for the stretch values of higher redshift SNLS SNe Ia in early-type radio-loud galaxies.

Aside from the SNLS SNe Ia in early-type hosts, two SNLS-2006 SNe Ia are found in $z \leq 0.6$ radio-loud *late*-type hosts: 05D1by and 06D2ff. They both have stretch values consistent with the "B" component distributions. Of the three SNLS-2006 SNe Ia in BIRG

and LIRG hosts which have stretch values, only the early-type host of 04D2bt has a stretch consistent with the "A" component.

Since we find the properties of radio and infrared SN Ia hosts to resemble dusty starburst galaxies (§ 4.1), we would expect their SN Ia light curves to be reddened and extinguished. SNLS analysis finds 05D1by, 05D1hn, 06D2ff, and 04D2bt are particularly red, indicating this is an unusually red, faint sample of SNe Ia. Also, the first three have large Hubble residuals. It is interesting that 04D1jg and 06D2ca are not particularly red or faint, because these two SNe Ia have the *brightest* infrared hosts. However, they need only have originated on the 'near' side of the galaxy and escaped dust extinction to explain this (neither have large host offsets, 2″ and 0.5″ respectively). Also, since the host of 06D2ca is SED type Scd, it likely has unobscured star forming regions.

As a final note, SN Ia 05D1by is also spectroscopically peculiar in that the 6150Å Silicon line is very broad, indicating fast ejecta velocities. It is similar to SN 2001ay (Nugent et al. 2001), which had an atypically slow light curve decline given its unremarkable peak magnitude, a very luminous near-IR magnitude at $\sim$ 10 days post maximum, and an early-type host (Phillips et al. 2003). Such peculiar spectra comprise $\sim$ 1% of all SNe Ia, but in this small sample it is impossible to comment on whether they are more or less common in active galaxies.

4.6 Discussion

With the C99 catalog we recover the SN Ia rate in radio-loud early-type galaxies of DV05, but this is not the case for the SNLS catalog. For the first time we calculate SN Ia rates in the radio-loudest, BIRG, and LIRG subsets of early-type galaxies. We find these rates are $\sim$ 1–5 times the rate in all early-type galaxies, and that where we do observe a potential enhancement, it is with $\lesssim 2\sigma$ confidence. For the first time, we have incorporated infrared star formation rates into the two-component "A+B" model. While it does slightly increase the number of SNe Ia predicted, more so in B/LIRG than in radio-loud(est) samples, ultimately *all* SNLS results are consistent with the two-component "A+B" model. The same cannot initially be said for all C99 results, but the observed number of C99 SNe Ia may be an upper limit due to SN Ia and/or host misclassifications.

The benefit of considering infrared host galaxy properties to account for possible dust obscured star formation is best shown in Figure 4.2, which plots the specific SN Ia rate as a function of mean specific star formation rate (sSFR) for each early-type galaxy subset. Blue symbols indicate where sSFR was derived from optical data only, and red symbols

where SFR_{IR} was substituted for all galaxies with counterparts in the Spitzer IR catalogs. Curved lines show the two-component "A+B" model from Sullivan et al. (2006). Although error bars are large and all rates are within 2σ of the optical "A+B" model, when plotted with $sSFR_{IR}$ the SNLS SN Ia rates in B/LIRG subsets do align more closely with "A+B". The same can be said for C99 B/LIRG, and the apparent discrepancy for the C99 radio-loud(est) subset may be due to misclassifications discussed in § 4.2.1. These results are not significant, but are included to demonstrate the utility of such an analysis for future SN Ia rates.

DV05 suggested the SN Ia rate enhancement in radio-loud early-type galaxies may be due to galaxy mergers triggering radio activity and providing extra SN Ia progenitors by induced star formation. Although we do not recover their rate enhancement in the SNLS catalog, some other aspects of the SNLS data are consistent with this scenario: the evidence for dust-obscured star formation in SN Ia radio hosts, the agreement between observations and "A+B" model predictions in SN Ia radio hosts, and the properties of SN Ia in radio hosts being similar to those associated with intermediate age stellar populations. However, the discrepancy between observations and "A+B" model predictions for C99 radio galaxies remains. In § 4.2.1 we discuss possible SN Ia and/or host misclassifications, but might it be the two-component model is simply inappropriate for radio galaxies? It is a linear approximation to a relation that is not necessarily linear, and uses current SFR as a measure of the SFR when the white dwarf progenitor star was born – the parameter actually related to the number of SN Ia progenitors. In regular spiral galaxies where the SFR remains constant for 10^9 to 10^{10} Gyr this is essentially true, but not necessarily for galaxies experiencing interactions and/or mergers, and perhaps episodic star formation (discussed below), on timescales of $\sim 10^8$ years (DV05). This is not a failure of the "A+B" model, merely a limitation of its application to individual galaxies with episodic SFH. In large samples this effect should approximately "average out".

With such a hypothetical episodic SFR, Mannucci et al. (2006) attempt to account for this problem. In doing so, they show the radio-loud SN Ia rate enhancement of DV05 (for C99) is best fit with a *bimodal* delay-time distribution (DTD) for SNe Ia in which $\sim 50\%$ of the prompt component explodes in $\lesssim 10^8$ years, and suggest two physically distinct populations of SN Ia progenitors. However, we find the SNLS SN Ia rate in radio galaxies agrees with the "A+B" model, which is consistent with *continuous* DTDs (Pritchet et al. 2008). We also find the properties of SNe Ia in radio hosts do not constrain them to very young stellar populations, similar to the results of DV05.

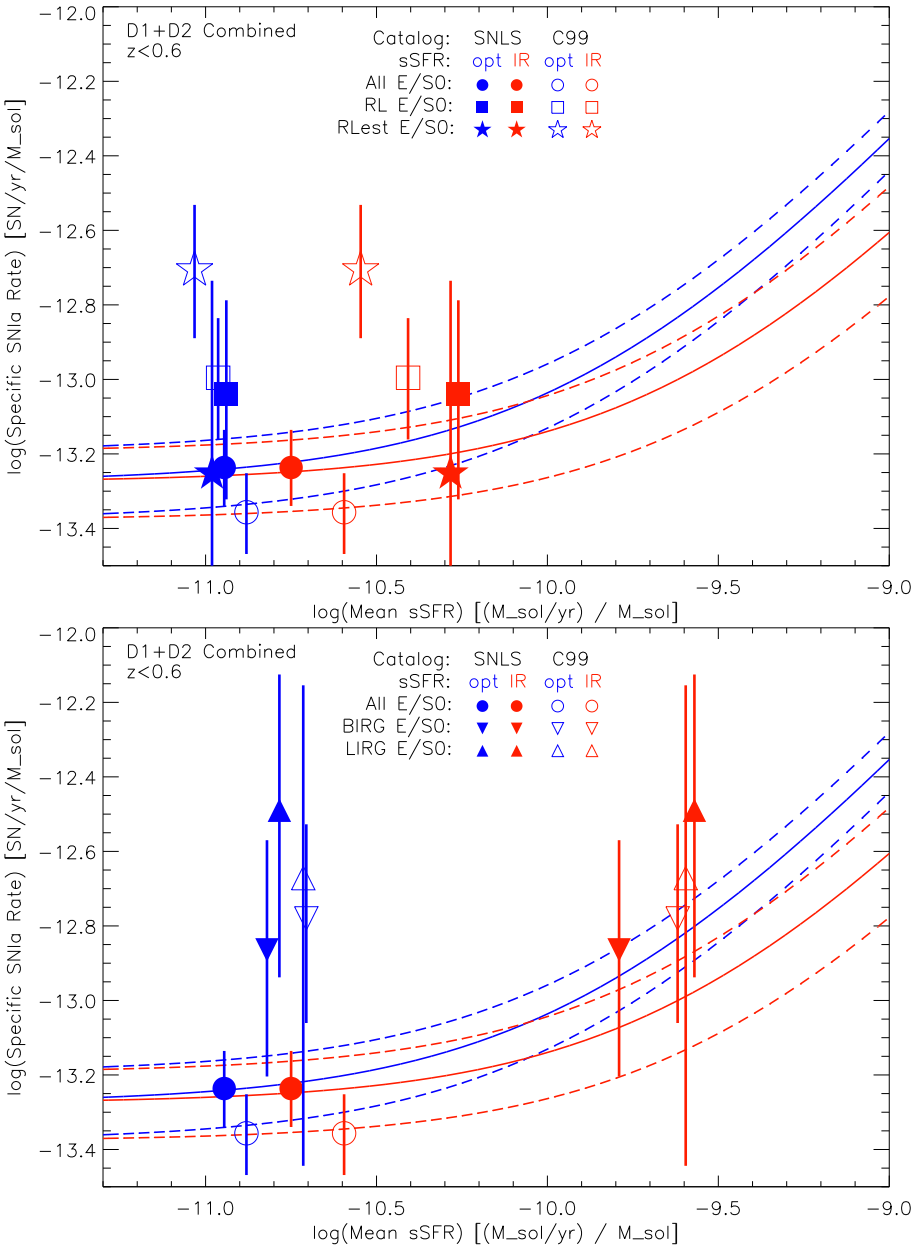

Figure 4.2 Specific SN Ia rates in SNLS (filled) and C99 (open) early-type galaxies (circles) from Table 4.4, versus mean sSFR of each sample. Top plot shows radio-loud (RL, square) and radio-loudest (RLest, star) samples; bottom plot shows BIRG (inverted triangle) and LIRG (triangle) samples. Symbol color indicates sSFR derived from optical data only (blue), or by incorporating infrared data when available (red). Also plotted is the two-component "A+B" model (solid) with uncertainties (dashed) from Sullivan et al. (2006) (blue lines), and the theoretical infrared "A+B" model (with $B_{IR} \sim B_{opt}/2$) (red lines) as discussed in § 3.2.

4.7 Summary

Based on the SNLS catalog, SN Ia rates in radio and infrared early-type galaxies are $\sim$ 1–5 times the rate in all early-type galaxies, but any enhancement we find is $\lesssim 2\sigma$. Rates in these subsets are consistent with predictions of the two component "A+B" SN Ia rate model. The infrared properties of SN Ia radio-loud early-type host galaxies suggest the presence of dust obscured star formation, and we have for the first time incorporated SFR_{IR} in the "A+B" model. In the C99 catalog, radio-loudest SN Ia hosts are consistent with the "A+B" model only if some SNe Ia and/or host galaxies have been misclassified. In general, we find the stretch values of SNe Ia in radio and infrared galaxies support a *continuum* of SN Ia and host galaxy properties, from young progenitors in very active galaxies to old progenitors in passive galaxies, as did DV05. Also these SNe Ia are fainter and redder than other SNe Ia, consistent with a dusty environment, and one was spectroscopically peculiar.

As a final note, the suggestion by DV05 that galaxy interactions and/or mergers cause both the radio activity and enhanced SN Ia rate is consistent with the documented correlation between clustered environments and radio galaxies (Magliocchetti et al. 2007). In Figure 4.1, we show image stamps of radio SN Ia host environments, and mark with red circles any neighbor galaxies within $\Delta z \leq 0.06$ (i.e. $\sim 2\sigma_{\Delta z/(1+z)}$). We find many radio-loud SN Ia hosts have nearby neighbors, as expected. Of particular note is the heart-shaped Sbc host of 08D2iq which, in deep stacks made by Stephen Gwyn and available on his website (see footnotes of § 4.1), is clearly one or more merging or recently merged galaxies. As reported in Graham et al. (2008), the host of 05D1by is located in the outskirts of a galaxy cluster. We also find the galaxy density within $r < 50$kpc of this host shows clustering over the background field galaxy distribution, as determined by a "significance parameter" (Graham et al. 2008). A full analysis of SNe Ia in small groups and pairs is presented in Chapter 5, including a test of whether the radio and infrared properties of SN Ia hosts and galaxies in groups are different from those in the field.

Chapter 5

Hosts in Pairs and Groups

In the previous chapter, we presented the SNLS SN Ia rate in radio and infrared host galaxies. This confirmed the SN Ia rate enhancement discovered in low redshift radio-loud early-type galaxies by DV05. They suggested their enhancement could be due to galaxy interactions and mergers, which are most likely to occur where galaxy density is high and relative velocity dispersion is low: in galaxy pairs and groups. At the end of Chapter 4 we commented that many radio hosts had nearby neighbors, and that the host of 08D2iq appears to be merging or a recent merger product. In this Chapter we continue by calculating the SNLS SN Ia rate in galaxy pairs and groups, and testing whether it is different from the field rate or expectations of the two-component "A+B" model.

To do this, we combine the SNLS supernova data set with the catalog of galaxy pairs and groups in CFHTLS Deep field 2 from Knobel et al. (2009, hereafter K09). The K09 catalog is derived from the zCOSMOS spectroscopic redshift survey of Lilly et al. (2009, hereafter L09). All of these data are described in Chapter 3. We present the properties of SNLS SNe and their host galaxies which we find to be associated with K09 groups in § 5.1. We calculate and analyze the specific SN Ia rate in pairs and groups, and compare with the rate among field galaxies, in § 5.2. In § 5.3 we assess whether the number of SNe Ia observed in groups is statistically consistent with expectations of the two-component "A+B" rate model. Finally, in § 5.4 we review our findings, and make a special assessment of our lack of hostless SNe Ia in groups.

5.1 SN Hosts in Groups and Pairs

Here we present the properties and host characteristics of SNLS SNe that we find to be associated with K09 groups in CFHTLS Deep field 2. As several catalogs have been com-

bined here, § 5.1.2 describes a classification scheme for our group-SN associations. In § 5.1.3 we examine whether the group hosts show any differences from field hosts in properties such as brightness or SED type, and in § 5.1.3 we present several SNLS SNe II we find in K09 groups.

5.1.1 Properties of SN and their Parent Galaxies

Table 5.1 lists the detailed properties of all SNe Ia we find to be associated with K09 pairs and groups. Columns 1–3 list the SNLS ID name, spectroscopic redshift and SiFTO stretch value (Guy et al. 2010). Columns 4–9 list properties relating to the host galaxy: best fitting SED type, SN offset, host redshift, absolute V-band magnitude, stellar mass, and specific star formation rate (derived from optical data and described in § 3.2). Column 10, the group class, is described below. Column 11 contains the number, N, of K09 galaxies in the group associated with that supernova. In brackets we list how many of these are *not* matched to a C09 galaxy, N_{nm}. Column 12 lists the spectroscopic redshift of the K09 group, and column 13 gives the SNe Ia offset from the group center normalized to R_{group}, the distance between K09 group center and its furthest member.

Figure 5.1 contains image stamps centered on K09 groups hosting SNe Ia, which are marked with white circles. The K09 member galaxies are also marked – red if matched to a C09 galaxy, and yellow otherwise. The SN Ia name, group class, and length of image side in arcseconds is marked on every stamp.

5.1.2 SN Ia Group Class

In Table 5.1 we list the SNe Ia associated with Knobel groups. The characteristics of that association are categorized by what we call the group class, in column 10. As several catalogs have been combined for this work, there are different levels of certainty in the associations we make between them. In § 5.2 we will analyze the SN Ia rates in individual and combinations of these group classes. Table 5.2 contains a chart showing how these group classes A–E are defined, as explained more fully below. The prefix P denotes that the group is a pair.

Classes A and B are the most likely real associations between SNe Ia and K09 groups, as both the SN Ia C09 hosts are matched to a K09 group member galaxy, and the SNLS SNe Ia spectroscopic redshift is consistent with the K09 group's z_{spec}. The only difference is that for class B, the K09 groups have one or more members not matched to a C09 galaxy ($N_{nm} \geq 1$). In total, there are 8 SNe Ia in classes A and B (two of which are in pairs); these

Table 5.1 Properties of SNLS SNe in Galaxy Groups.

(1) SN SNLS ID	(2) SN z_{spec}	(3) SN Ia stretch [SiFTO]	(4) Host SED	(5) Host Offset [″]	(6) Host z_{phot} (z_{spec})	(7) Host M_V	(8) Host Mass [10^{10} $M_\odot$]	(9) Host sSFR [10^{-10} y^{-1}]	(10) Group Class	(11) Group N (N_{nm})	(12) Group z_{spec}	(13) Group Offset [R_{group}]
Type Ia Supernovae:												
07D2ec	0.270	...	Scd	1.94	0.26 (0.267)	-21.10	2.72	2.37	PA	2 (0)	0.268	0.91
08D2iq	0.709	...	Sbc	3.21	0.70 (0.708)	-21.61	6.14	1.39	A	3 (0)	0.709	0.94
04D2mc	0.348	0.81 ± 0.02	E/S0	0.86	0.37 (0.347)	-21.93	18.93	0.03	A	5 (0)	0.345	0.37
04D2bt	0.220	0.99 ± 0.01	E/S0	0.52	0.25 (0.220)	-21.40	10.05	0.15	A	4 (0)	0.220	0.30
08D2ad	0.554	...	Scd	1.02	0.48 (0.555)	-20.91	0.73	13.67	PB	2 (1)	0.555	0.90
06D2fb	0.124	0.96 ± 0.01	Sbc	1.55	0.10 (0.125)	-19.06	0.78	0.82	B	14 (1)	0.124	0.26
05D2ie	0.348	0.98 ± 0.02	Scd	0.46	0.37 (0.349)	-19.59	0.32	7.29	B	4 (1)	0.348	0.75
05D2ci	0.630	0.88 ± 0.03	E/S0	1.19	0.59 (0.630)	-22.08	17.71	0.25	B	7 (1)	0.630	0.96
08D2id	0.833	...	Scd	1.70	0.83 (...)	-21.51	2.11	5.89	C	5 (2)	0.836	0.64
05D2mp	0.354	1.14 ± 0.03	Scd	0.15	0.40 (...)	-18.10	0.08	7.29	C	12 (1)	0.354	1.06
05D2ay	0.920	0.98 ± 0.08	Scd	2.75	0.87 (0.839)	-21.69	2.85	4.90	D	3 (0)	0.838	0.76
07D2ag	0.250	...	...	...	...(...)	...	...	...	PE	2 (2)	0.251	1.02
Type II Supernovae:												
04D2dc	0.185	...	Sbc	0.46	0.15 (0.186)	-19.24	1.00	0.68	B	9 (2)	0.187	0.20
08D2jh	0.220	...	Scd	3.71	0.36 (...)	-17.94	0.04	16.6	C	4 (0)	0.220	0.36
07D2ke	0.114	...	Scd	2.56	0.13 (0.114)	-19.08	0.12	16.6	PD	2 (0)	0.114	...

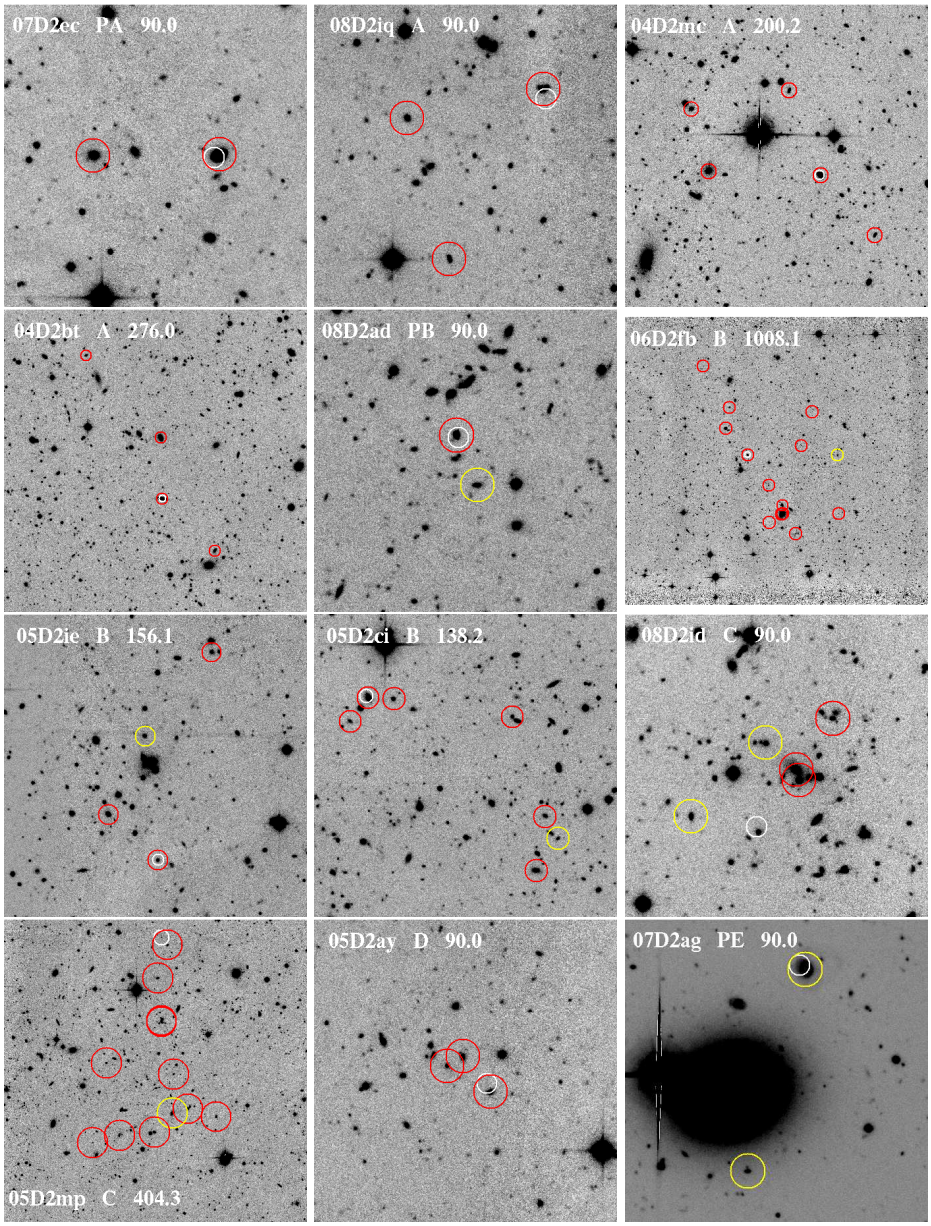

Figure 5.1 Image stamps in r_{Mega} centered on Knobel groups containing SN Ia host galaxies. SNLS SN Ia ID, group class, and image size (box length) in top left. Circles mark positions of SNe Ia (white) and K09 group members (red if matched to C09 galaxy, yellow otherwise; 3″ and 5″ unless image size > 400″, then 10″ and 20″ are used for clarity).

Table 5.2 Characteristics of Group Class.

	A	B	C	D	E
1. SN Ia hosted by C09 galaxy	✓	✓	✓	✓	
2. SN Ia matched to K09 group	✓	✓	✓		✓
3. SN Ia host matched to K09 group galaxy	✓	✓		✓	
4. All K09 group galaxies matched to C09	✓				

will form the basis of our primary analysis.

Classes C, D, and E are all defined by how the SNe Ia are associated with the group, and do not involve group properties. Class C contains two SNe Ia whose C09 host galaxies are not matched to K09 group members. These SNe Ia associated with group based on their spectroscopic redshift and group offset. Neither of these C09 host galaxies have VLT z_{spec}, a requirement for K09 group membership. SN Ia 08D2id is also associated with an Olsen galaxy cluster, as discussed more in Chapter 6.

Class D contains the interesting case of 05D2ay. Its C09 host galaxy is matched to a K09 member galaxy. However, the spectroscopic redshift of 05D2ay is discrepant, and its host offset is large. This could conceivably be a background SN Ia with a misidentified host. Furthermore, the SNLS spectral typing fit for 05D2ay remains uncertain; it could possibly have been a SN Ic.

Class E contains one SN Ia which does not have a C09 host, 07D2ag. As with class C, this SN Ia is associated with a K09 group based on its spectroscopic redshift and group offset. SN Ia 07D2ag is not hostless, but falls in a masked region near a foreground star. This is also why neither K09 pair member has a C09 match (N=2, N_{nm}=2). In fact, we find no hostless SNe Ia associated with Knobel groups; this fact is discussed further in § 5.4.

5.1.3 SN Ia Host Properties

Since DV05 suggest galaxy interactions and mergers as the root cause of the radio-loudness of their SNe Ia hosts, and galaxy interactions are most common in pairs and groups, here we examine the properties of SNLS SN Ia parent galaxies in group environments. We examine whether they are different from other hosts in field environments, and/or different from other galaxies in pairs and groups. We do consider radio and infrared emission, but first we examine the absolute magnitude, SED type, stellar mass, and SFR of these galaxy samples. We also examine whether SNe Ia are distributed proportionally to the radial distribution

of light in their hosts, or show a preference for large offsets indicating association with harassed or stripped stellar populations.

Host Magnitude, Type, Mass, and SFR

We compare the normalized, cumulative distributions of V-band absolute magnitude, Gwyn type, stellar mass, and SFR for galaxies and SN Ia hosts in group and field environments in Figures 5.2 and 5.3. Our sample of field galaxies includes all those *not* associated with a Knobel group, but this does not necessarily mean that they are isolated galaxies. Our sample of group galaxies includes all pairs and groups, regardless of how many of their members were matched to C09 galaxies.

Since galaxies in groups are from the zCOSMOS-bright component of the zCOSMOS spectroscopic survey, the field galaxies plotted in these figures are only those with spectroscopic redshifts. All field galaxies from C09 are also plotted as dotted lines to show the selection effect in the zCOSMOS-bright sample. Since brighter galaxies are more massive, of earlier SED types, and have lower star formation rate, this effect appears for every property plotted in these figures. We do not require the SN Ia host galaxies be covered by zCOSMOS-bright for inclusion in the distribution of field hosts. This is appropriate because we also include class C and D SNe Ia in the distribution of group hosts – which were not directly associated with a K09 member galaxy and do not have spectroscopic redshifts from zCOSMOS-bright.

We use the Kolmogorov-Smirnov test to assess the probability that SN Ia hosts in groups are consistent with being drawn from the population of SN Ia hosts in the field, and from the population of galaxies in groups. We show the KS test statistics D and P on every plot, and find all are $P > 0.05$, indicating consistency between the samples. This is consistent with the general conclusions of Navasardyan et al. (2001); they also find the blue luminosity of SN Ia hosts in isolated pairs is higher than in isolated galaxies and galaxy groups. Although we cannot make a similar comparison with our sample, we find that the two SN Ia hosts in pairs, 07D2ec and 08D2ad, are both in blue, late-type (Scd) hosts. Also, the host of 08D2ad has the highest SFR of all by a factor of two. However with only two SNe Ia in pairs, we cannot draw any definitive conclusions.

Host Radio and IR Emission

In Chapter 4 we discussed radio and infrared properties of SNLS SN Ia hosts, and considered the postulate of Della Valle et al. (2005) that galaxy mergers and interactions could be

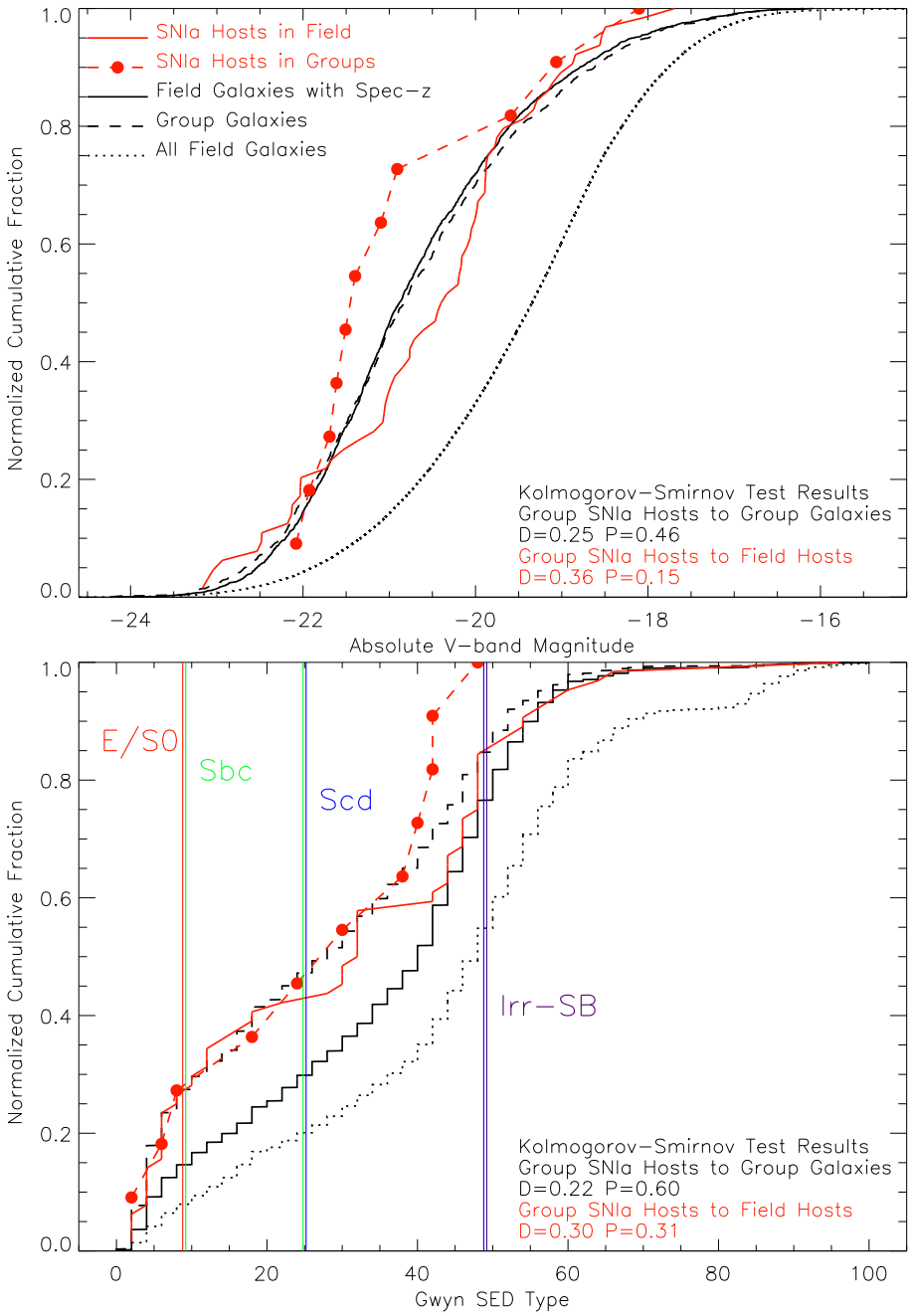

Figure 5.2 Normalized cumulative distributions of V-band absolute magnitude and Gwyn SED type five galaxy samples: all field galaxies (black dotted), all field galaxies with spectroscopic redshifts (black solid), group galaxies (black dashed), field SN Ia hosts (red solid), and group SN Ia hosts (red dashed with filled circles). All for $z \leq 1.0$.

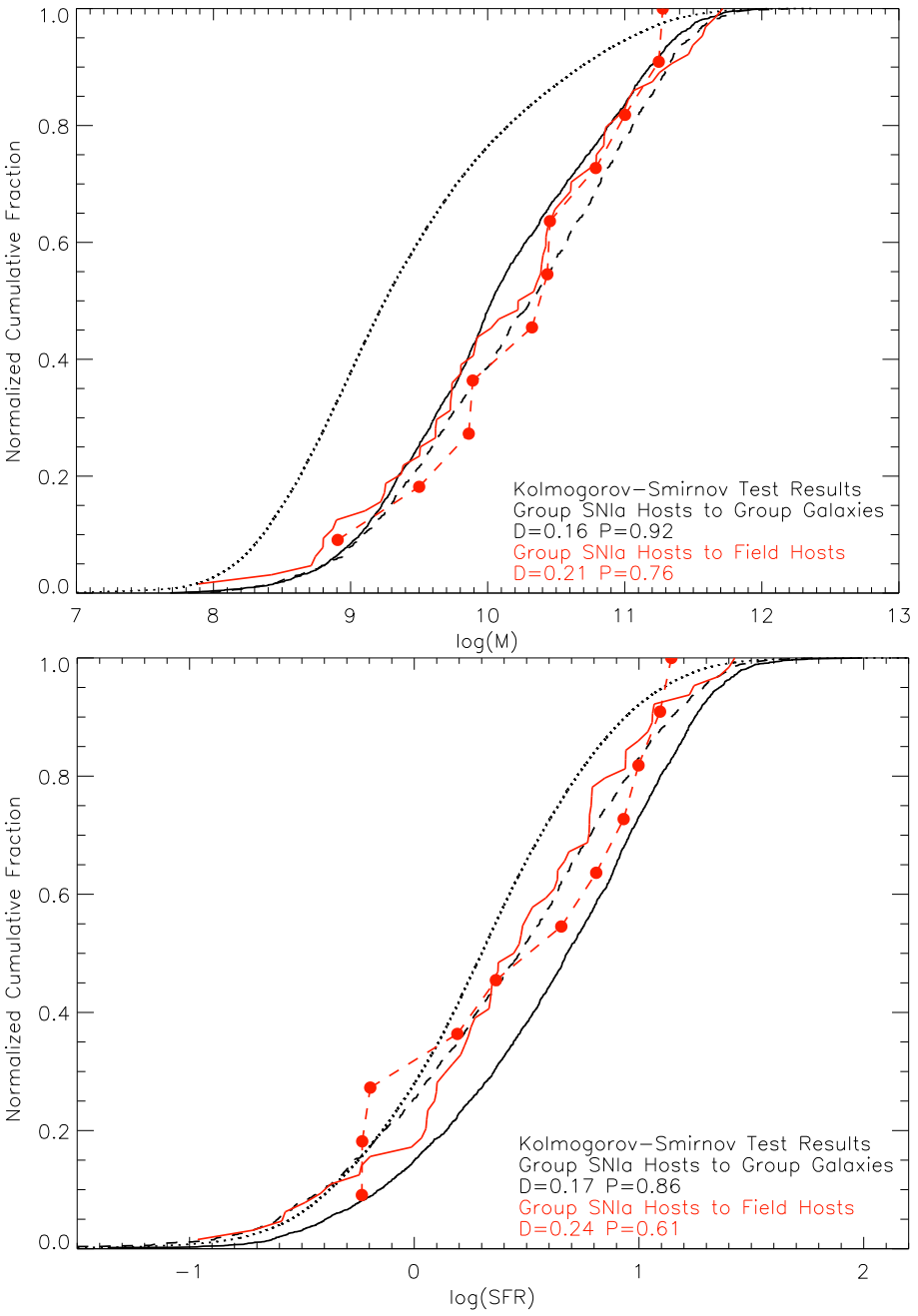

Figure 5.3 Normalized cumulative distributions of stellar mass and star formation rate for the same five galaxy samples as Figure 5.2.

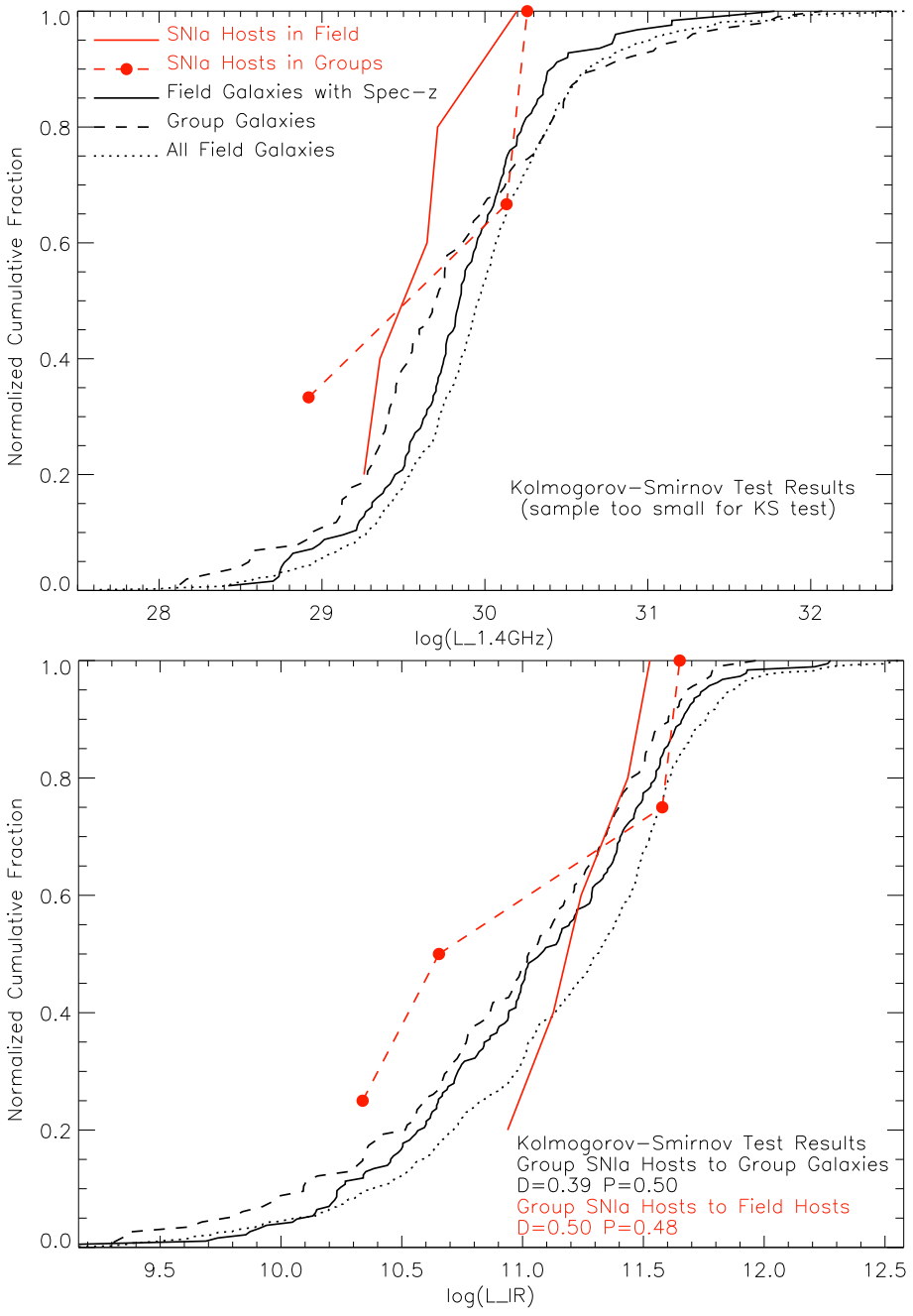

Figure 5.4 Normalized cumulative distribution of radio and infrared luminosity for galaxies and SNLS SNe Ia in the field and in groups, as in Figure 5.2.

Table 5.3 Percentage of Galaxies with Radio and/or IR Emission

Sample		Percent[a] Detected Radio	Infrared
Galaxies	Groups	6 ± 1	8 ± 1
	Field	5 ± 1	8 ± 1
SN Ia Hosts	Groups	14 ± 14	29 ± 20
	Field	50 ± 35	25 ± 25

[a]Uncertainties are simply $\pm\sqrt{N}$ in the numerator.

the root cause of the radio emission in radio-loud SN Ia hosts. First, we check whether a higher fraction of Knobel group members have radio and/or IR emission than field galaxies. For this comparison, we limit the samples to $z \leq 0.6$ for better completeness of the radio catalog, and to galaxies and SN Ia hosts with spectroscopic redshifts only (the set from which all group members are drawn). We find the fractions of galaxies with radio and infrared emission is the same in field and group environments, as shown in Table 5.3.

Is this true also for the fractions of SN Ia hosts with radio and IR emission? We find that of the nine $z \leq 0.6$ SN Ia hosts in D2 with radio and/or IR, four are in galaxy groups: 07D2ec, 08D2iq, 04D2bt, and 08D2id (see Table 4.1). We find the fraction of SN Ia hosts with IR emission is the same in both field and group environments, as shown in Table 5.3. From the results in this table, it appears that SN Ia hosts are not more likely to show radio emission in group environments, as the two fractions actually agree to within 1σ. However, this is based on very few supernovae. If we consider only pairs, we find the fraction of SN Ia hosts with radio emission is equivalent in pair and field environments, though still with large uncertainties. Based on these data, group membership does not appear to make a galaxy, whether it hosts a SN Ia or not, more likely to show radio and/or infrared emission.

These data in Table 5.3 do clearly show that the fraction of SN Ia hosts with radio or IR emission is significantly higher than for the general population of galaxies. This may simply be because SNe Ia follow mass, and so does radio and IR emission. The next logical step is to test whether the radio and IR luminosity distributions for SN Ia host galaxies are similar to those of the general population of galaxies. To do this, we extend our sample of galaxies to $z \leq 1.0$, and plot these distributions in Figure 5.4. Small number statistics dominate. We can only apply the KS test to the IR distribution, and conclude that the dis-

tributions of radio and IR luminosities for SN Ia hosts in both group and field environments are consistent with the general population of galaxies.

Host Offset

Since SN Ia rates are, to first order, proportional to mass, the radial distribution of SNe Ia should be the same as the radial distribution of host light. For example, half of all SNe Ia should occur within the "half-light" or "effective" radius R_e, the radius encompassing half of a galaxy's total light. Since the C09 catalog contains galaxy R_e, and we know the host offset for each SNLS SN Ia R_{SN}, we can calculate the relative host offset R_{SN}/R_e. Although we do not take galaxy inclination into account, since *both* the SN Ia host offset and galaxy effective radius are in projection, this is still a useful comparison.

Figure 5.5 compares the distribution of relative host offsets for SNe Ia in field and group galaxies. We can see that $\sim$ 50% of SNe Ia do occur within $\sim$ 1 R_e. If SNe Ia in a given population show a preference for large offsets, it could indicate an association with harassed or stripped stellar populations. Although the distribution of relative offsets for SN Ia hosts in groups in Figure 5.5 is *suggestive* of such a trend, the Kolmogorov-Smirnov test results cannot rule out the null hypothesis that they are drawn from the same distribution. This is similar to the findings of Navasardyan et al. (2001).

5.1.4 SNe II in Groups

Although spectroscopic follow-up for the SNLS was carefully designed to prioritize supernovae likely to be of Type Ia, some type II SNe were spectroscopically confirmed. Of the 15 in D2, we match 11 with a host from the C09 galaxy catalog (using the matching procedure described in § 3.2). Of the 11, three are associated with Knobel galaxy groups. Image stamps for these SN II are given in Figure 5.6, and they are included at the bottom of Table 5.1.

As SNe II are fainter than SNe Ia, the three SNe II are all within $z \leq 0.4$. Also, as SNe II are associated with young stellar populations, their hosts are quite different from those of SNe Ia. All three SNe II are from bright late-type galaxies, two of which have quite high specific star formation rates. No SN II host is associated with a radio or IR source. It is very rare for core collapse SNe to be observed in early-type galaxies, but *if* we had seen a SN II in an early-type group member, this would be indicative of low levels of star formation in an otherwise quiescent-looking galaxy.

The rate ratio between SNe II and SNe Ia has been determined to be $\sim$ 4.5 by several

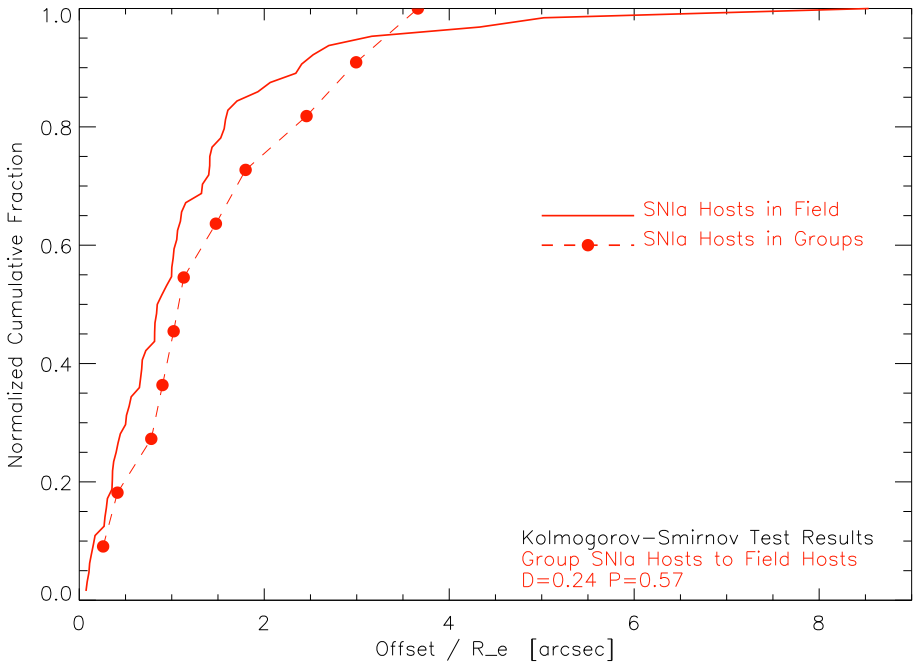

Figure 5.5 Normalized cumulative distribution of relative host offset, the radial distance from host center to SN divided by the host's effective radius R_e (radius containing half the light). For SNLS SNe Ia in field galaxies (solid) and in groups (dashed). All for $z \leq 1.0$.

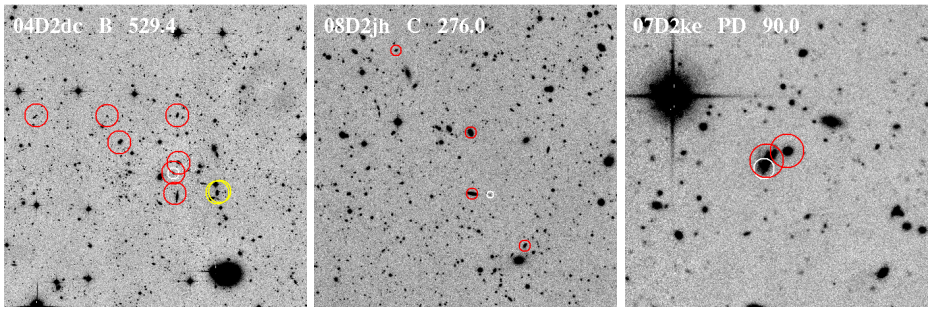

Figure 5.6 Image stamps in r_{Mega} centered on Knobel groups containing SN II host galaxies. SNLS SN Ia ID, group class, and image size (box length) in top left. Circles mark positions of SNe II (white) and K09 group members (red if matched to C09 galaxy, yellow otherwise; 3″and 5″unless image size >400″, then 10″and 20″for clarity).

Table 5.4 Observed Number Ratio of SN Ia to SN II in Group and Field (for $z \leq 0.4$).

Sample	N_{Ia}/N_{II} Ratio[a]
Group	$4/3 = 1.3 \pm 1.0$
Field	$8/8 = 1.0 \pm 0.5$
With spec-z galaxies only:	
Group	$3/3 = 1.0 \pm 0.8$
Field	$2/3 = 0.7 \pm 0.6$

[a]With $\pm \sqrt{N}$ uncertainties.

experiments (Mannucci et al. 2005; Bazin et al. 2009). We can use this to make an estimation of how many SNe II we expect in groups, based on the number of SNe Ia. We see six SNe Ia with $z \leq 0.4$ in groups and pairs; four of these are in late-type galaxies. Thus we would expect to see $\sim$ 18–27 SNe II in Knobel groups of $z \leq 0.4$. This discrepancy exists because SNLS did a very good job at only using spectroscopic time to follow up on likely SNe Ia (Sullivan et al. 2006b). It is also why Bazin et al. (2009) performed a "deferred" search for SNe II in the CFHTLS Deep exposures, independent of the SNLS.

Since this SNLS sample of SNe II is very spectroscopically incomplete, we cannot include them in the rates analysis of the follow sections. If we assume that detection efficiencies are equivalent in both group and field environments – a reasonable assumption – we can test whether the number ratio of SNe Ia to SNe II, N_{Ia}/N_{II}, is the same in group and field environments. These number ratios are given in Table 5.4. We find the N_{Ia}/N_{II} ratio

appears to be higher in groups than in the field. This is also the case when we limit both samples to only galaxies with spectroscopic redshifts, which is a more appropriate comparison because K09 is derived from the spectroscopic redshift survey. While this *suggests* there *may* be a factor other than SFR affecting the supernova rate in group environments, all uncertainties are ±50% or higher and the group and field ratios remain within 1σ.

As previously mentioned, only a lucky few SNe II are spectroscopically confirmed during SNLS follow-up. However, the SNLS database contains every detected transient, with unofficial photometric classifications. SNe II are the most common type of supernova, so most of the transients classified as "likely to be supernovae" – but rejected for follow-up – are SNe II. Some will also be SNe Ib/c, and an small number will be missed SNe Ia. As a final test we derive the N_{Ia}/N_{II} ratio treating all SNLS transients which look like SN, but lack spectroscopic follow-up, as if they are SN II. We associate these SN with a host galaxy as in § 3.2, and then impose $z_{host} \leq 0.4$. We only associate a few with groups, one of which (the only "SN Ib/c?" type) is a very tenuous association: it is in Group Class E (no host identified) and has the maximum $R_{group} = 1.10$. These new "SNe II" lower the group N_{Ia}/N_{II} to ~ 0.8. The remainder of these SNe II are in field galaxies, which lowers the field N_{Ia}/N_{II} ratio by a factor of ~ 8 to ~ 0.12. If we limit to the sample of galaxies with spectroscopic redshifts only, very similar ratios are recovered. This supports a higher N_{Ia}/N_{II} ratio in groups than in the field, as we find with the spectroscopically classified SNe II. However, since the group N_{Ia}/N_{II} ratio uncertainty is large, these field ratios are still within $\sim 1\sigma$ of the group ratio.

5.2 SN Ia Rates

Here we consider the SN Ia rates in K09 galaxy groups, and assess whether any evidence for an enhancement in pairs or groups is found in the SNLS sample. In the previous and next chapter, we limit the sample for primary analysis to $z \leq 0.6$, SNLS-2006, and galaxies of SED type E/S0. Since we are limited here to a single CFHTLS Deep field, we relax these constraints and consider $z \leq 1.0$, SNLS-2008, and galaxies of all SED types. We then consider the limiting scenario in § 5.2.2. We attempt to correct for incompleteness in the sample of group galaxies from the C09 photometric catalog in § 5.2.3. We also consider the rates in the densest and most massive groups, and among radio galaxies in groups, in § 5.2.4 and 5.2.5. In § 5.2.6 we provide a summary of our SN Ia group rates.

Table 5.5 SN Ia Rates in Knobel Galaxy Groups

(1) Class	(2) # SN Ia[a,b]	(3) Mass (Number)[c]	(4) $sSNR_{Ia}$[a,d]	(5) Ratio[a,e]
PA	$1\ (0.64^{+1.46}_{-0.53})$	3314 (545)	$0.031^{+0.071}_{-0.026}$	$0.282^{+0.646}_{-0.236}$
PA & PB	$2\ (1.27^{+1.67}_{-0.82})$	3903 (628)	$0.053^{+0.070}_{-0.034}$	$0.482^{+0.637}_{-0.316}$
A	$3\ (2.46^{+2.38}_{-1.33})$	3806 (517)	$0.101^{+0.098}_{-0.055}$	$0.916^{+0.897}_{-0.510}$
A & B	$6\ (4.37^{+2.60}_{-1.73})$	7157 (928)	$0.095^{+0.056}_{-0.038}$	$0.857^{+0.525}_{-0.356}$
PA, PB, A, & B	$8\ (5.64^{+2.78}_{-1.95})$	11060 (1556)	$0.081^{+0.040}_{-0.028}$	$0.729^{+0.374}_{-0.268}$
Field	$64\ (79.08^{+11.17}_{-9.86})$	122116 (57489)	$0.111^{+0.016}_{-0.014}$	...

[a] Uncertainties are derived from Poisson errors at the 1σ confidence level, as in Gehrels (1986).

[b] Brackets contain number of SNe Ia corrected for SNLS detection efficiencies as in § 3.2 to be the number which exploded per year of SNLS observations.

[c] Mass units are 10^{10} $M_\odot$; brackets contain number of galaxies in class sample.

[d] SNuM = SN $(100\ \mathrm{yr})^{-1}$ $(10^{10}\ M_\odot)^{-1}$

[e] Ratio between rates in group and field.

5.2.1 SN Ia Rates in the General Sample

We use the same method for calculating SN Ia rate in group samples as presented for radio and IR galaxies in Chapter 4, the relevant equations and variable definitions for which were given in § 3.2. In Table 5.5 we present the relevant data for each group class, or combination of group classes, and for the field sample (all galaxies not associated with a K09 group). Column 2 contains the number of SNe Ia observed, N_{obs}, and in brackets the corrected SN Ia frequency (after the application of the correction factor C as detailed in § 3.2), quoted with Poisson uncertainties at the 1σ confidence level from Gehrels (1986).

Column 3 contains the amount of mass in each sample, and in brackets the number of galaxies. Column 4 contains the SN Ia rate calculated from Equation 3.3 of Chapter 3, in the commonly used "supernovae unit" SNuM, equal to one supernova per century per 10^{10} $M_\odot$. Poisson uncertainties on the rates are propagated as in Chapter 3, and do not include uncertainty in galaxy masses. Column 5 contains the ratio of the rate in a given class over the rate in field galaxies, also with Poisson uncertainties propagated from column 4.

The SN Ia rate per unit mass in pairs (group class PA, and PA & PB) appears to be a factor of 3–5 lower than the rate in field galaxies; however, with such small number

statistics, this is within 1σ of a ratio equal to one. Navasardyan et al. (2001) find the rate in pairs to be ~ 1.45 higher than the SNe Ia rate per unit mass from C99 (but within 1σ) . Due to small number statistics, our rate ratio between pairs and field galaxies of ~ 0.5 is also within 2σ of Navasardyan's ~ 1.45 enhancement. This means their results for the rate of SNe Ia in pairs could be hiding in our small number statistics.

The SN Ia rate per unit mass in groups (group class A, and A & B) is consistent with the rate in field galaxies, as is the combination of pairs and groups together (PA, PB, A,& B). Navasardyan et al. also find the rate in groups to be statistically equivalent to the SN Ia rate from C99.

Recall there are two SNe Ia in group class C: 08D2id and 05D2mp. If we add these to the 6 SNe Ia in group class A & B, the resulting specific SN Ia rate is $0.124^{+0.061}_{-0.043}$ SNuM, a ratio of $1.122^{+0.575}_{-0.412}$ over the field rate and within 1σ of a null result. Recall, however, that group C contains SNe Ia hosted by C09 galaxies which were not matched to a K09 group member. Due in part to incompleteness in the Lilly et al. (2009) spectroscopic catalog, this set of galaxies in groups is not complete. In § 5.2.3 below we attempt to compile a more complete sample.

Finally, adding in class D SN Ia 05D2ay at z = 0.92 results in a specific SN Ia rate of $0.177^{+0.081}_{-0.058}$ SNuM, and a rate ratio of $1.598^{+0.763}_{-0.558}$ which is only slightly $> 1\sigma$ from a ratio of 1. This result is actually even less significant that that, because since $C_{D2}(z > 0.8) = 0.3$, 05D2ay has effectively contributed 3 SNe Ia to that rate. Also, as mentioned in § 5.1.2, 05D2ay might be a background SN Ia with a misidentified host, or might be a SN Ic.

5.2.2 Rates in Conservative Samples

For our SN Ia group rates in the preceding section, we have relaxed the catalog limitations we impose in other chapters. In this section, we limit the catalogs in a variety of ways, to account for various incompleteness and detection efficiencies of the combined data catalogs.

First, we consider the fact that all group members are chosen from the sample of galaxies with spectroscopic redshifts, but in the above analysis our field sample included *all* galaxies. We instead derive the field rate based only on galaxies with spectroscopic redshifts. We present the SN Ia rate ratio between groups and the limited field sample for a representative set of group classes in Table 5.6. We find the SN Ia rate per unit mass in field galaxies with spectroscopic redshifts is lower than, but within 1σ of, the previously derived field rate in Table 5.5. Although this increases the SN Ia rate ratios, all remain consistent with the null result.

Table 5.6 Limiting Field Sample to Galaxies with Spectroscopic Redshifts

Group Class	# SNe Ia[a]	$sSNR_{Ia}$[a]	Ratio[a]
PA & PB	2 ($1.27^{+1.67}_{-0.82}$)	$0.053^{+0.070}_{-0.034}$	$0.705^{+1.001}_{-0.523}$
A & B	6 ($4.37^{+2.60}_{-1.73}$)	$0.095^{+0.056}_{-0.038}$	$1.253^{+1.006}_{-0.677}$
Field	7 ($6.10^{+3.28}_{-2.25}$)	$0.076^{+0.041}_{-0.028}$	...

[a] As in Table 5.5.

Now we consider the results if, as in other chapters, we limit our analysis to SNLS-2006 and $z \leq 0.6$ where the detection efficiencies are more uniform (thereby reducing our reliance on the correction factor), and to galaxies of certain SED types. We will do this for our largest sample of SNe Ia in groups, classes A & B combined. Limiting the A & B sample to SNLS-2006 yields nearly identical results. Limiting to $z \leq 0.6$ increases the rate ratio slightly to $1.241^{+0.876}_{-0.576}$, and imposing both limitations increases it to $1.638^{+1.175}_{-0.777}$. Both are suggestive of an enhancement, but actually within 1σ of a null result.

Limiting to all early-type (E/S0) galaxies drops the field rate only by ~half (consistent with the rate in all early-type galaxies from Chapter 4). For our original sample of SNLS-2008 and $z \leq 1.0$, the rate in early-type group galaxies is nearly identical to the field rate. Imposing the limitations of SNLS-2006 and $z \leq 0.6$ appears to show an enhanced rate in groups of $\sim 2.5\times$, but all ratios remain within 1σ of the null result. In general, we find that by tightening our constraints on the sample, our main conclusions are not altered.

The redshift distributions of SNLS SNe Ia, Coupon galaxies, and Knobel groups were compared in Figure 3.7 of § 3.6. There, we noted that the C09 galaxies and the K09 groups have different redshift distributions, and that this is a combined effect of completeness and the formation and evolution of groups over redshift. In light of this incompleteness, our SN Ia rates in groups are still valid because they are rates *per unit mass*. Any missing groups, and their SNe Ia, will simply be included in the field. Of course this affects our field rate, but since the field is a much bigger sample, the effect is small. (We address the issue of individual group galaxies missing from the Knobel catalog due to spectroscopic redshift incompleteness in the next section).

To ensure a possible change in group completeness over redshift is not a problem, we have recalculated the SN Ia rate per unit mass with SNLS-2008 for three redshift ranges: low $0.1 < z < 0.3$, intermediate $0.4 < z < 0.6$, and high $0.7 < z < 0.9$. These are reported

Table 5.7 Redshift Binned SN Ia Rates in Knobel Galaxy Groups

Redshift Bin	Group Class	# SNe Ia[a]	$sSNR_{Ia}$[a]	Ratio[a]
$0.1 < z < 0.3$	PA & PB	$1\ (0.64^{+1.46}_{-0.53})$	$0.317^{+0.726}_{-0.263}$	$3.030^{+7.161}_{-2.782}$
	A & B	$2\ (1.27^{+1.67}_{-0.82})$	$0.179^{+0.236}_{-0.116}$	$1.714^{+2.473}_{-1.296}$
	Field	$6\ (3.82^{+2.28}_{-1.51})$	$0.105^{+0.062}_{-0.041}$	...
$0.4 < z < 0.6$	PA & PB	$1\ (0.64^{+1.46}_{-0.53})$	$0.156^{+0.357}_{-0.129}$	$1.335^{+3.074}_{-1.143}$
	A & B	$1\ (0.64^{+1.46}_{-0.53})$	$0.073^{+0.166}_{-0.060}$	$0.623^{+1.434}_{-0.533}$
	Field	$21\ (13.36^{+3.60}_{-2.89})$	$0.117^{+0.031}_{-0.025}$	...
$0.7 < z < 0.9$	PA & PB	$0\ (0.00^{+0.00}_{-0.00})$	$0.000^{+0.000}_{-0.000}$	$0.000^{+0.000}_{-0.000}$
	A & B	$1\ (1.19^{+2.71}_{-0.98})$	$0.100^{+0.228}_{-0.083}$	$0.614^{+1.413}_{-0.525}$
	Field	$21\ (42.34^{+11.39}_{-9.16})$	$0.162^{+0.044}_{-0.035}$	...

[a] As in Table 5.5.

for pairs and groups in Table 5.7. In such small redshift bins, the uncertainties are large and, although we see a trend of rate enhancement to deficit with increasing redshift, this is not statistically significant. At low redshifts, smaller groups are more easily found; an enhanced SN Ia rate in small groups may fit with the postulate of enhanced SN Ia rates in merging systems (as discussed in Chapter 4). Small group radial velocities are lower, and their galaxies are more likely to be undergoing mergers.

5.2.3 Rates with Improved Completeness

Knobel et al. (2009) apply their methods to mock catalogs and find their group sample to have remarkably high levels of completeness and purity: around $\sim 80\%$ for both. However, since based on the sample of galaxies with spectroscopic redshifts, they cannot escape from the spectroscopic sampling and redshift success rates that vary across the zCOSMOS field (Lilly et al. 2009). Some of the mass in groups is surely missing from our rates calculations. In the last section, we attempted to avoid the effects of catalog incompleteness on our rates by limiting our samples to regions of constant completeness levels.

In this section, we attempt to identify the undetected galaxies in groups so we can include them in our analysis. We find that, unfortunately, none of the other group parameters such as number of members, dynamical mass, or velocity dispersion correspond well enough with optical (stellar) mass to be used as a proxy. We considered using the mean group mass as a function of group richness, but this has far too much scatter to be useful.

However, these methods would only have added mass to the groups, not specific galaxies, and thus not added any more SNe Ia which may have exploded in that mass. Instead we attempt to improve completeness in two ways: limiting to the region of highest spectroscopic completeness of the zCOSMOS survey, and associating additional galaxies with groups using C09 photometric redshifts.

First we consider only groups within the area bounded by $\alpha = 150^\circ \pm 0.4^\circ$ and $\delta = 2.15^\circ \pm 0.4^\circ$, the region containing maximum spectroscopic completeness (Lilly et al. 2009; Knobel et al. 2009). This lowers the number of SNe Ia in all group classes, and although it also lowers the rates slightly, all ratios remain within 1σ of the null result (true also for all limitations to samples described in § 5.2.2).

Second, and as a last resort for recovering galaxies, we turn to the C09 photometric redshift catalog and include any galaxy within $\Delta z_{phot} = 0.03$ ($\sim 1\sigma$ from § 3.2), and with a separation $\leq 0.9\ R_{group}$. The separation limit is slightly generous considering beyond $\leq 0.8\ R_{group}$, the relation between the number of galaxies added per unit area (i.e. $N_g \times R^{-2}$) and R_{group} starts to flatten out (indicating most added galaxies actually belong to the field). Although this will increase our completeness of galaxies in groups, it comes at the expense of group sample purity because it introduces interlopers.

This method increases the total mass in groups by $\sim 1.5\times$. To the sample including group classes A, B, & C, it adds 2 additional SNe Ia hosted by galaxies which were not originally associated with Knobel groups: 05D2dw and 04D2mj. This yields a SN Ia rate in groups of $0.149^{+0.064}_{-0.046}$ SNuM, a ratio of $1.350^{+0.606}_{-0.451}$ over the field rate. Note that we have not removed these additional group galaxies from the field, and use the same field rate from Table 5.5 for all ratios. This remains consistent with the null result at the 1σ level. This is true also for all limitations described in § 5.2.2, except for SNLS-2006 with $z \leq 1.0$, in which the ratio increases to almost two but remains within 2σ of the null result.

5.2.4 Rates in Extreme Group Environments

In this section, we identify samples of the most massive and densest groups, and test whether any influence on the SN Ia rate per unit mass is detectable in these extreme group environments. For this we use two different qualifiers. First, we use an approximation to the group mass density, D_M. This is the total mass in group members divided by an approximation of physical group volume: $V_p = \frac{4}{3}\pi R_p^3$, where R_p is the physical distance to the furthest member. Second, we use the group dynamical mass from Knobel et al. (2009), M_{dyn}, to identify the most massive groups. M_{dyn} equals the dynamical mass they call M_{Fudge}, which they derive from velocity dispersion and group radius, and calibrated to mock catalogs. As

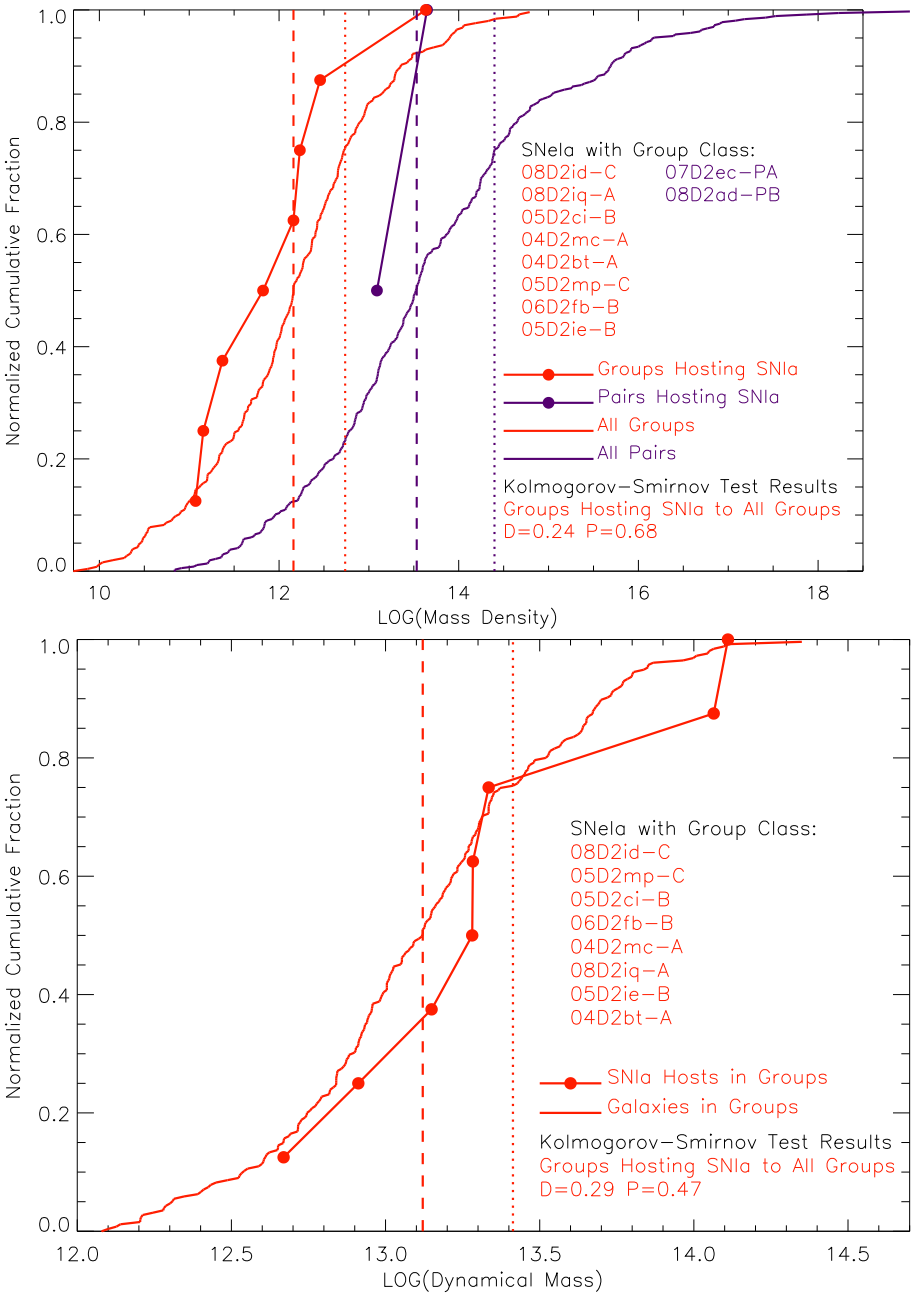

Figure 5.7 Normalized cumulative distribution of group mass density D_M (top) and dynamical mass M_{dyn} (bottom) for galaxies in groups (red) and pairs (purple). Distributions for SN Ia hosts have filled circles. Dotted and dashed lines mark the 50% and 25% most dense/massive groups and pairs. SN Ia names and group classes are listed in descending order. KS-test results displayed at lower right corner.

we are only interested in the most massive groups, for our experiments with M_{dyn} we omit the pairs.

The normalized cumulative distributions of D_M and M_{dyn} for groups and pairs of galaxies are given in Figure 5.7. The distributions of groups and pairs hosting SNe Ia are shown with solid circles. Although the distribution offsets for D_M suggest SNe Ia prefer groups and pairs of lower mass density, the KS test results (in plot legends) show this is statistically insignificant. This is true also for M_{dyn}.

The dashed and dotted lines of Figure 5.7 confine the top 50% and top 25% most dense and most massive groups respectively. If we constrain our sample to the group class A & B, or the PA, PB, A, & B sets, we find the specific SN Ia rates in these extreme, limited samples are slightly lower than, but still consistent with, the field rate. Since the SNe Ia in groups in the top 25% bin have a group class of C, we also derive a rate including them, and find it is slightly higher, but again, consistent with the field rate.

Recall that group class C means their hosts belong to the population of galaxies which can only be associated with groups through their photometric redshift (but the SNe Ia are associated through their spectroscopic redshifts). As discussed previously, rates including SNe Ia in group class C should include the mass of this population *and* any SNe Ia hosted by that population, because of the inclusion of interloping galaxies. If we add these galaxies to the sample (which adds no new SNe Ia to the top 50% and 25% bins), we find the SN Ia rates in the densest and most massive groups are $\sim 1.5\times$ the field rate, but within 1σ of it also. This is due mainly to the small number of SNe Ia in extreme group environments.

5.2.5 Rates in Radio and IR Group Members

In § 5.1.3 we presented the 4 SN Ia group hosts with radio and/or infrared emission. We found the fraction of galaxies showing radio and/or infrared emission was the same in both group and field environments, and that this was also true for SN Ia hosts. Here we test whether the SN Ia rate per unit mass in radio and infrared galaxies is the same in both the group and field environments.

To do this, we limit our experiment to galaxies showing radio or infrared emission (of any strength, without limiting to radio-loud as in Chapter 4), and calculate the SN Ia rate per unit mass in group and field environments. Results for two representative group classes (PA & PB, and A & B) are shown in Table 5.8. These radio and infrared field rates are not equivalent to those quoted in Chapter 4 because the catalog limitations are much less restrictive here ($z \leq 1.0$, SNLS-2008, and galaxies of all SED types).

Although the SN Ia rates in radio group members appear $\gtrsim 2\times$ the rate in radio field

Table 5.8 SN Ia Rates in Radio and IR Members of Knobel Galaxy Groups

Sample	Group Class	# SNe Ia[a]	$sSNR_{Ia}$[a]	Ratio[a]
Radio	PA & PB	$1\ (0.64^{+1.46}_{-0.53})$	$0.167^{+0.383}_{-0.139}$	$2.866^{+6.834}_{-2.676}$
	A & B	$1\ (1.19^{+2.71}_{-0.98})$	$0.164^{+0.376}_{-0.136}$	$2.816^{+6.715}_{-2.630}$
	Field	$5\ (3.73^{+2.52}_{-1.61})$	$0.058^{+0.039}_{-0.025}$	...
Infrared	PA & PB	$1\ (0.64^{+1.46}_{-0.53})$	$0.235^{+0.537}_{-0.194}$	$3.362^{+8.018}_{-3.148}$
	A & B	$2\ (1.82^{+2.39}_{-1.17})$	$0.432^{+0.567}_{-0.278}$	$6.183^{+9.131}_{-4.790}$
	Field	$5\ (3.73^{+2.52}_{-1.61})$	$0.070^{+0.047}_{-0.030}$	...

[a] As in Table 5.5.

galaxies, they are within 1σ of it, and also within 1σ of the original SN Ia group rates in Table 5.5. This is true whether or not we limit to the radio-loud galaxies or simply use all radio galaxies. The SN Ia rates in IR group members appear $\gtrsim 3\times$ the rate in IR field galaxies. For pairs (PA & PB) this is consistent with the null result at the 1σ level, and for groups (A & B) at the 2σ level.

In § 5.2.2 we limited the field sample to galaxies with spectroscopic redshifts, since the Knobel group catalog was built from them. We do this again now. The SN Ia rate in field radio galaxies increases to $0.209^{+0.203}_{-0.113}$ SNuM, and drops the group-to-field ratio to ~ 0.8. The rate in field IR galaxies drops slightly to $0.061^{+0.140}_{-0.051}$ SNuM, increasing the ratios slightly. These experiments suggest the correlation between SN Ia rate and IR emission may be enhanced by group membership, but that any correlation between SN Ia rate and radio emission may not be affected by group environments. However, due to large uncertainties from very small numbers, these results remain statistically inconclusive.

5.2.6 Rates Summary

In Chapter 4, we found the SNe Ia in early-type radio-loud galaxies have stretch values which indicate a likely association with a young or intermediate age stellar population. In Table 5.1 we list the stretch values of SNLS SNe Ia in groups. All but SN Ia 05D2mp (host SED type Scd) have a stretch value within 1σ of the distribution established for the "delayed" component, indicating a likely association with an older stellar populations (Howell et al. 2007). This is true for SNe Ia in early- and late-type hosts in group, and is not surprising because both types have old stellar populations. Unlike in Chapter 4, for

SNe Ia in galaxy groups the stretch values are completely consistent with expectations.

In general the SN Ia rate per unit mass in pairs and groups appears to be consistent with the field rate, albeit with large uncertainties from small number statistics. How large a possible effect could be hiding in our data? At the 3σ confidence level, in pairs and groups we can rule out 3× rate enhancements if we use our largest samples including SNLS-2008, $z \leq 1.0$, and all SED types of galaxies. If we combine pairs and groups in group class PA, PB, A, & B, we can rule out a 2× enhancement at the 3σ confidence level. In all such cases, a rate ratio of 0 is consistent at the $\leq 3\sigma$ level, so we cannot constrain any possible rate deficits with this sample. If we limit to more conservative samples of SNLS-2006 and $z \leq 1.0$ for group class PA, PB, A, & B, we can only rule out a 4× enhancement at the 3σ confidence level.

5.3 Comparison to Predictions of the "A+B" Model

As a final test of whether the SN Ia rate in galaxy groups is influenced solely by progenitor evolution, and not by other environmental effects, we statistically compare the observed number of SNe Ia in galaxy groups to predictions of the two-component "A+B" model. The method of determining the summed Poisson probability, P_{SUM}, is explained in Chapter 3. The values derived for this statistical assessment are given in Table 5.9. Column 2 lists the number of SNe Ia observed in each group class, N_{obs}. Column 3 lists the number of SNe Ia, N_{A+B}, predicted by "A+B" over the survey's duration, in each group class. In column 4 we list P_{SUM}, the probability of having observed N_{obs} SNe Ia given N_{A+B} were predicted by the "A+B" model. For this test we consider values of $P_{SUM} \leq 0.05$ as statistically significant.

In all cases, the "A+B" model predictions are completely consistent with observations of SNe Ia in galaxy pairs and groups, as shown in Table 5.9, where all values of P_{SUM} are greater than 0.05. As in Graham et al. (2010), we repeated this experiment including infrared-derived star formation rates instead of optical. This assesses the contribution of dust-obscured SFR to the "B" component of the predicted number of SNe Ia. However, we found an insufficient number of group members have IR luminosities large enough to alter the results.

5.4 Summary

We make one final analysis prior to concluding. McGee & Balogh (2010) find that, of their 59 SNe Ia in low redshift ($0.1 < z < 0.2$) groups from the Sloan Digital Sky Survey, 19 have

Table 5.9 SNe Ia in Knobel Galaxy Groups and the "A+B" Model

(1) Class	(2) # SNe Ia[a,b]	(3) N_{A+B}[c]	(4) P_{SUM}[d]
PA	1	1.90	0.43
PA & PB	2	2.16	0.63
A	3	2.11	0.35
A & B	6	3.97	0.21
PA, PB, A, & B	8	6.13	0.27
Field	64	66.47	0.41

[a]Uncertainties are derived from Poisson errors at the 1σ confidence level, as in Gehrels (1986).

[b]Brackets contain number of SNe Ia corrected for SNLS detection efficiencies as in § 3.2 to be the number which exploded per year of SNLS observations.

[c]Number of SNe Ia expected in group class from "A+B" rate model.

[d]Summed Poisson probability as described in § 3.2.

no apparent host. We, on the other hand, have found no hostless SNe Ia in groups. Is this surprising? Based on the fraction of hostless SNe Ia from McGee & Balogh, and the fact that we found 12 hosted SNe Ia in Knobel groups, we should have found 3.86 additional hostless SNe Ia. The probability of finding zero is very low, P $\sim$ 0.02. Since they were working with SDSS at lower redshift, their galaxy catalog is more complete ($\sim$ 95% at $M_R \sim$ -15 to -16), and 3.86 is probably a lower limit to the number of SNe Ia we should expect to find apparently hostless. However, for their analysis McGee & Balogh (2010) actually only used groups of halo mass $M > 10^{13}$. Making the same cut leaves us with just 6 SNe Ia in similarly massive groups, as shown in Figure 5.7, and so we would expect an additional 1.9 hostless SNe Ia in such groups. The fact that we see none has a probability of P $\sim$ 0.15, which is low, but not statistically significant.

In summary, we draw three main conclusions from the preceding experiment. One, the properties of SN Ia hosts in groups are not significantly different from those of the field hosts. Two, the specific rates of SNe Ia in groups are statistically consistent with the rates in the field, and that this is true for a wide variety of host and group characteristics. Three, the number of SNe Ia observed to be associated with groups is statistically consistent with expectations of the two-component "A+B" SN Ia rate model. The biggest drawback of this experiment is that the Knobel group catalog covers only CFHTLS D2. Small numbers of SNe Ia associated with groups results in large statistical uncertainties. In Chapter 7, we

parametrize clustering strength in the environments of SNe Ia to better assess the influence of small scale clustering – such as galaxy groups – on SN Ia rates.

Chapter 6

Hosts in Galaxy Clusters

The volumetric SN Ia rate in rich galaxy clusters is higher than in the field due to the concentration of stellar mass, which makes galaxy clusters a useful target for high redshift supernova studies (Dawson et al. 2009). Galaxy clusters are well known to contain a high fraction of elliptical galaxies; this phenomenon is referred to as the morphology-density relation (Postman & Geller 1984). Elliptical galaxies are quiescent and have little to no star formation. In combination with the two-component "A+B" SN Ia rate model, this indicates the SN Ia rate per unit mass should be lower in galaxy members than in field galaxies. Despite this prediction, Mannucci et al. (2008) found a $\sim 3\times$ enhancement of the SN Ia rate in cluster over field ellipticals.

In this chapter, we combine the SNLS SN Ia data with the catalog of rich galaxy clusters in the CFHTLS Deep fields published by Olsen et al. (2007). We look to confirm or deny the presence of a SN Ia rate enhancement in intermediate redshift galaxy clusters. Mannucci et al. (2008) suggest star formation in their morphologically elliptical galaxies as the source of the rate increase. We use the star formation rates for our SED-typed galaxies, and the "A+B" model empirical rate relation, to predict how many SNe Ia we expect in clusters and statistically compare this with our observations.

The data catalogs used for this experiment were presented in Chapter 3. In § 6.1 we present the SNLS SNe Ia discovered in Olsen clusters. In § 6.2 we derive the SN Ia rate in galaxy clusters, and in § 6.3 we consider the effects of altering our data constraints. Finally in § 6.4 we make a statistical comparison of our observations to predictions of the two-component "A+B" model.

Much of this chapter was published as Graham et al. (2008). Improvements made for this thesis include the use of the updated Coupon et al. (2009) catalog of photometric redshifts, and a short analysis of the stretch values of cluster SNe Ia. In § 6.5 we provide a

summary of this chapter, and also discuss the current status of cluster SN Ia rates based on relevant papers published by other astronomers over the past two years.

6.1 SNLS SN Ia Hosts and Galaxies in Clusters

Here we explain how we identify SNLS SNe Ia and C09 galaxies in grade "A" Olsen clusters, and present the properties of cluster SNLS SNe Ia and their hosts. Galaxies and SNe Ia in clusters are identified as those within $\leq R_p$ Mpc and $\Delta z \leq 2\sigma \times (1 + z_C)$, where z_C is the cluster photometric redshift. We use $\sigma = 0.03$ as the photometric redshift uncertainty, as discussed in § 3.7. In our limited sample there are 56 clusters in D1–4.

Since the cluster filter used by Olsen et al. (2007) has a profile with core radius $r_c = 0.133h_{75}^{-1}$ Mpc and cut off radius of $r_{co} = 1.33h_{75}^{-1}$ Mpc, results for $R_p = 0.2$, 0.5, and 1.0 Mpc will be presented as representative. Olsen et al. (2007) and Coupon et al. (2009) use different Terapix data releases (T0002 and T0004 respectively), but the catalogs are very similar. Although Olsen et al. extend the bright star masks of T0002 and as a result have an effective area of 3.112 square degrees, this is actually slightly less than the C09 effective area of 3.23 square degrees. This difference in effective areas is $< 4\%$, so a reasonable estimate is that there are just ~ 2 Olsen-like clusters in the C09 galaxy catalog whose member galaxies we will include as part of the field population.

Table 6.1 presents the 15 SNLS SNe Ia we find associated with Olsen clusters. Image stamps of the 12 clusters hosting these 12 SNe Ia are given in Figure 6.1. As with the radio and infrared hosts, we limit our main analysis to SNe Ia discovered up to and including SNLS-2006 with $z \leq 0.6$ (top of Table 6.1), and in § 6.3 include a discussion of relaxing these restrictions (and the limit to Olsen clusters of grade 'A' only).

What is the probability of these SNe Ia residing in interloper galaxies? Considering here the $z \leq 0.6$ sample, the 3 SNe Ia with cluster offsets of $R_p \leq 0.5$ Mpc are probably physically associated with the clusters. This is less certain for the 6 SNe Ia between 0.5 and 1.0 Mpc. From the total number of SNe Ia with $z \leq 0.6$, we predict ~ 1.9 SN Ia would randomly appear between $R_P \geq 0.5$ and $R_p \leq 1.0$Mpc, and $\pm 2\sigma_{\Delta z/(1+z_{VVDS})}$. The probability that all 6 are interlopers is only $\sim 1\%$, but the probability that they are all real associations and no interlopers are observed is just $\sim 15\%$. As the most likely scenario is that two are interlopers and that 4 are real associations we include all of them in our results, but note this will contribute to our uncertainties. Furthermore, the spectroscopic redshift of 05D3hh is $\Delta z > 2\sigma \times (1 + z)$, and would not be associated with a cluster on its own, but is through its host whose z_{phot} makes it a cluster member galaxy. Though likely to be an interloper, as

Table 6.1 Properties of Cluster SNLS SNe Ia and their Host Galaxies.

SN Ia SNLS ID	SN Ia z_{spec}	SN Ia Stretch SiFTO	Host SED	Host M_V	Host Offset [″]	Cluster z_{phot}	Cluster Offset [Mpc]
03D1ax	0.496	0.93 ± 0.01	E/S0	-23.5	1.99	0.47	0.064
05D3mq	0.246	0.91 ± 0.03	E/S0	-21.6	4.64	0.27	0.081
06D1kg	0.320	...	Sbc	-20.7	1.82	0.27	0.195
05D1by	0.299	1.02 ± 0.03	Sbc	-21.3	0.73	0.27	0.574
04D1pg	0.515	1.10 ± 0.02	Sbc	-19.7	0.22	0.50	0.520
06D4bo	0.552	1.09 ± 0.02	Scd	-20.4	1.37	0.56	0.912
06D1kf	0.561	...	Scd	-17.7	0.69	0.50	0.886
04D2mj	0.513	1.15 ± 0.03	Scd	-20.2	0.23	0.49	0.802
05D3lb	0.647	1.04 ± 0.02	Irr	-19.0	0.07	0.60	0.959
SNe Ia found post-2006 or in clusters with z > 0.6.							
05D3hh	0.766	1.06 ± 0.05	E/S0	-20.6	0.09	0.63	0.418
07D2kh	0.731	...	E/S0	-23.0	2.34	0.67	0.885
04D2al	0.836	0.87 ± 0.11	Sbc	-19.9	0.86	0.82	0.833
05D2ct	0.734	1.04 ± 0.05	Scd	-20.6	0.56	0.82	0.794
08D2id	0.833	...	Scd	-21.5	1.70	0.74	0.152
07D3af	0.356	...	Scd	-18.6	0.12	0.28	0.602

it is z > 0.6 it does not affect our main conclusions.

We also note that cluster SN Ia 08D2id (z > 0.6) is associated spectroscopically with a galaxy group, but that this does not necessarily mean it is an interloper also. As discussed in § 3.7, it could be in an in-falling group which will or is currently joining the cluster. Defining environments as groups, clusters, clustered groups, etc., is a gray area. This is why we include a very general analysis of clustering in the environments of SNe Ia in Chapter 7, which avoids any strict definitions such as “cluster” and “group”.

6.2 SN Ia Rates

Here we present our derived SN Ia rates in the field and in galaxy clusters for a variety of physical cluster radii: R_p = 0.2, 0.5, and 1.0 Mpc. We also identify a sample of field galaxies as those which are $R_p \geq$1.0 Mpc and $\Delta z \geq 0.1$ from any cluster. As in Graham et al. (2008) and Graham et al. (2010) we restrict our analysis sample in several ways. First, we limit ourselves to SNLS SNe Ia detected prior to 2006 December 31, because up to this date the SNLS spectroscopic analysis and typing is complete. Second, we limit our redshifts to

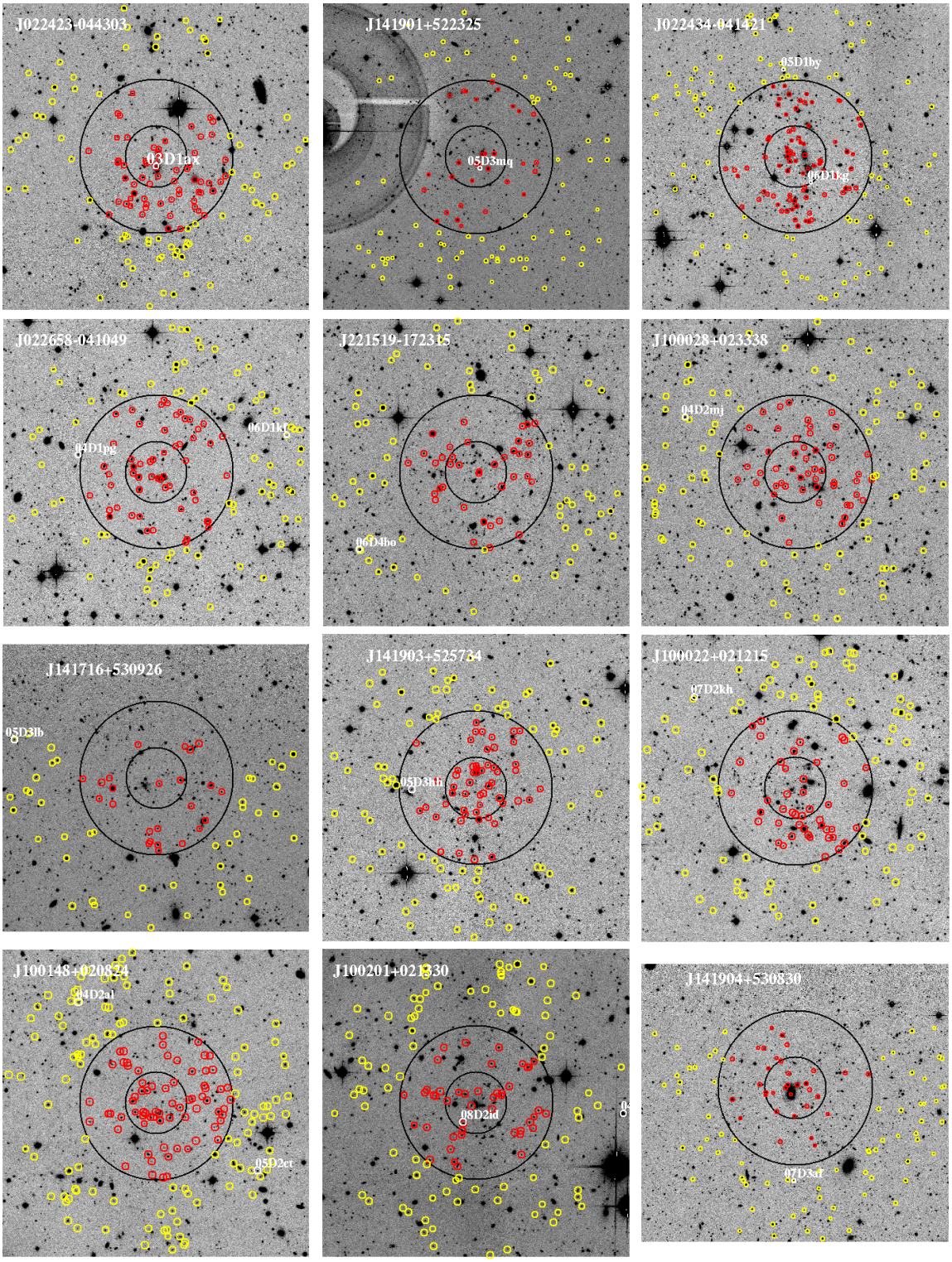

Figure 6.1 Image stamps in i_M, 2.0x2.0 Mpc, centered on clusters hosting SNe Ia and labeled with cluster coordinates for identification. Small (3″) circles mark SNe Ia (white), galaxy members within $R_p \leq 1.0$ Mpc (red) and within $R_p \leq 0.5$ Mpc (yellow). Black concentric rings mark $R_p = 0.2$ Mpc and $R_p = 0.5$ Mpc.

$z \leq 0.6$, to which redshift the SNLS SN Ia sample is nearly complete (Neill et al. 2006). We consider the effects of extending these limitations in § 6.3.

The number of SNLS SNe Ia observed in D1–4 prior to 2006 Dec 21 for each subset, N_{obs}, is shown in Table 6.2, and in brackets the corrected SN Ia frequency (after the application of the correction factor C as detailed in § 3.2), quoted with Poisson uncertainties at the 1σ confidence level from Gehrels (1986). The amount of mass in galaxies in each subset is also given in Table 6.2. We calculate the specific SN Ia rate in each galaxy subset, $sSNR_{Ia}$, via Equation 3.3. Specific SN Ia rates are given in Table 6.2 in the commonly used "supernovae unit" SNuM, which is equal to one supernova per century per 10^{10} $M_{\odot}$. Ratios of SN Ia rates in clusters over the rates in field galaxies are also given in Table 6.2.

With such small number statistics from the small sample of SNe Ia in clusters, statistical uncertainties dominate this calculation; systematics, mainly the error in galaxy mass calculations, are likely another $\sim$ 30%. Thus, our SN Ia rate in cluster galaxies of any SED type is consistent with both the rate in early-type galaxies, 0.053 ± 0.011SNuM (Sullivan et al. 2006a) and the low redshift cluster rate from WOOTS, $0.098^{+0.059}_{-0.039} \pm 0.009$ SNuM (Sharon et al. 2007).

There are two factors not considered which could affect SN Ia detection efficiencies in cluster galaxies. First, SN Ia detection efficiencies decrease in brighter hosts
(Neill et al. 2006), and the brightest galaxies are early-type. Second, the SN Ia detection efficiency decreases for fainter, lower stretch SNe Ia, and these faint SNe Ia occur preferentially in early-type hosts (Sullivan et al. 2006a). Since cluster galaxies are predominantly early-type, both of these effects dominate in clusters: the first effect decreases the number expected in clusters by $\sim$ 15%, but quantifying the second would require more detailed completeness simulations. Both effects would cause us to underestimate the rate of SNe Ia in clusters relative to the field.

6.2.1 SN Ia Rates in E/S0 Cluster Galaxies

To avoid these effects and the morphology-density relation, we limit the galaxy sample to two subsets: all early-type galaxies, and the brightest population of early-type galaxies (those with $M_V < -23.0$ like brightest cluster galaxies, BCG's). This has the added benefit of rejecting interlopers misidentified as cluster members. Two cluster SNe Ia have early-type hosts, and the host of 03D1ax is brighter than $M_V = -23.0$. Detection efficiency corrections are performed as described above, with the final results and rates presented in Table 6.2.

Although these samples are more sensitive to the two detection efficiency biases af-

fecting early-type galaxies as described in the previous section, limiting all galaxies to early-types minimizes differences between the clusters and the field and results in a more meaningful test. The results, although not statistically significant, are *suggestive* of the rate enhancement in cluster over field early-type galaxies established by Mannucci et al. (2008). An enhancement in BCG-like galaxies would be consistent with the findings of an enhanced SN Ia rate in radio-loud elliptical galaxies (Della Valle et al. 2005), as these are usually the brightest cluster galaxies.

In § 6.1, Table 6.1 lists the stretch values for SNe Ia associated with clusters. As in Chapters 4 and 5, we test whether they are consistent with known stretch distributions for the "prompt" and "delayed" components, associated with younger and older stellar populations respectively (Howell et al. 2007). The one SN Ia in a BCG-like early-type galaxy, 03D1ax, has a stretch value consistent with being drawn from the "delayed" component. This agrees with its host type, as do all the other cluster SNe Ia except for one. SN Ia 05D2hh has an early-type host, but a stretch value greater outside 1σ of the "delayed" distribution. However, given 3 SNe Ia are observed in cluster early-type galaxies, finding 1 outside of 1σ is not statistically significant. The probability that all three SNe Ia in cluster early-type galaxies are associated with the "delayed" component is high, ~ 0.4. SN Ia 04D2al has a low stretch value and a later-type host, but this is not remarkable as Sbc galaxies have an old population. In general we find no overwhelming evidence that cluster SNe Ia are associated with a younger or intermediate age stellar population, as would be expected if trace amounts of star formation were the root cause for the SN Ia rate enhancement of Mannucci et al. (2008).

6.3 Altering the Data Constraints

Here we consider whether altering the constraints on SNLS data affects our results. We try: extending our sample to the full five-year SNLS survey (SNLS-2008); extending our redshift range to $z \leq 1.0$; and including Olsen clusters with grade 'B'.

First, we extend our SN sample to SNLS-2008, and find only SN Ia 07D3af is added to the sample of SNe Ia in galaxy clusters for $R_p \leq 1.0$Mpc. The number of SNe Ia in the field sample also increases to 132 (30 early-type), though the field rates remain the same. The larger C values (Table 3.3) for SNLS-2008 decrease the rates in clusters slightly, and decreases all ratios by 0.1–0.2 (a small effect). Second, extending the SNLS-2006 sample to $z \leq 1.0$ adds SN Ia 05D3hh, 04D2al, and 05D2ct to the number of SNe Ia in clusters for $R_p \leq 1.0$Mpc. The sample of field SNe Ia increases to 208 (51 early-type, 4 early-type with

Table 6.2 SN Ia Rates in z ≤ 0.6 Early-Type Cluster Galaxies

Sample	# SNe Ia N_{obs}[a,b] [SNe] ([SNe y^{-1}])	Mass in Galaxies[c] [$10^{10}M_{\odot}$]	SN Ia Rate [SNuM][d]	Rate Ratio Over Field
Field	104 ($93.56^{+10.10}_{-9.16}$)	124805 (87786)	$0.106^{+0.011}_{-0.010}$	...
$R_p \leq 1.0$ Mpc	9 ($7.82^{+3.57}_{-2.55}$)	10044 (4257)	$0.104^{+0.047}_{-0.034}$	$1.0^{+0.5}_{-0.3}$
$R_p \leq 0.5$ Mpc	3 ($2.51^{+2.43}_{-1.36}$)	5986 (1629)	$0.056^{+0.054}_{-0.030}$	$0.5^{+0.5}_{-0.3}$
$R_p \leq 0.2$ Mpc	3 ($2.51^{+2.43}_{-1.36}$)	3548 (460)	$0.094^{+0.091}_{-0.051}$	$0.9^{+0.9}_{-0.5}$
For early-type galaxies only:				
Field	25 ($21.27^{+5.16}_{-4.22}$)	69594 (7087)	$0.043^{+0.010}_{-0.009}$	...
$R_p \leq 1.0$ Mpc	2 ($1.74^{+2.29}_{-1.12}$)	7390 (810)	$0.031^{+0.041}_{-0.020}$	$0.7^{+1.0}_{-0.5}$
$R_p \leq 0.5$ Mpc	2 ($1.74^{+2.29}_{-1.12}$)	4916 (461)	$0.047^{+0.062}_{-0.030}$	$1.1^{+1.5}_{-0.7}$
$R_p \leq 0.2$ Mpc	2 ($1.74^{+2.29}_{-1.12}$)	3160 (208)	$0.074^{+0.097}_{-0.047}$	$1.7^{+2.3}_{-1.2}$
For the brightest early-type galaxies only:				
Field	1 ($0.77^{+1.75}_{-0.63}$)	13122 (154)	$0.008^{+0.019}_{-0.007}$	...
$R_p \leq 1.0$ Mpc	1 ($0.77^{+1.75}_{-0.63}$)	1776 (23)	$0.058^{+0.133}_{-0.048}$	$7.0^{+22.7}_{-8.2}$
$R_p \leq 0.5$ Mpc	1 ($0.77^{+1.75}_{-0.63}$)	1701 (22)	$0.061^{+0.139}_{-0.050}$	$7.3^{+23.6}_{-8.6}$
$R_p \leq 0.2$ Mpc	1 ($0.77^{+1.75}_{-0.63}$)	1516 (19)	$0.068^{+0.155}_{-0.056}$	$8.1^{+26.3}_{-9.5}$

[a] Brackets contain number of SNe Ia corrected for SNLS detection efficiencies to be the number which exploded per year of SNLS observations, as in § 3.2.

[b] Uncertainties are derived from Poisson errors at the 1σ confidence level, as in Gehrels (1986).

[c] Brackets contain number of galaxies in sample.

[d] SNuM = SN $(100\ yr)^{-1}$ $(10^{10}\ M_{\odot})^{-1}$

$M_V < -23.5$), but the field rate does not change appreciably. The SN Ia rate ratios decrease for all galaxy types, early-types, and especially for the BCG-like (to ∼ 2–3), and remain consistent with the null result. The general trends in results from relaxing to SNLS-2008 or z ≤ 1.0 continue if both are done simultaneously.

Finally, we consider Olsen clusters with grade 'B', which adds one SN Ia to our sample for SNLS-2006, z ≤ 0.6, and a couple more when we extend to SNLS-2008 and/or z ≤ 1.0. The major difference is an increase in the amount of mass in clusters. The net result is that all cluster rates are either unchanged or lowered, and all ratios are lowered.

Table 6.3 Summed Poisson probabilities for cluster SNe Ia for D1–4.

Sample	N_{obs}	N_{A+B}	P_{SUM}
$R_p \leq 1.0$ Mpc	9	6.60	0.22
$R_p \leq 0.5$ Mpc	3	3.45	0.55
$R_p \leq 0.2$ Mpc	3	1.82	0.28
For early-type galaxies only:			
$R_p \leq 1.0$ Mpc	2	3.54	0.31
$R_p \leq 0.5$ Mpc	2	2.34	0.58
$R_p \leq 0.2$ Mpc	2	1.49	0.44

6.4 Comparison to Predictions of the "A+B" Model

Here we statistically compare the number of SNLS SNe Ia observed in clusters to the number predicted by the two-component "A+B" model. Table 6.3 presents the number of SNe Ia observed, N_{obs}, the number predicted by the two-component "A+B" model, N_{A+B}, and the summed Poisson probabilities, P_{SUM}. These variables were first presented and described in § 3.2.

This test is done for all galaxies, and for early-type galaxies, for each of our sample of cluster redshifts. In all cases we find observations are consistent with the two-component SN Ia rate model.

In fact, > 4 SNe Ia would have to have been observed in early-type galaxies within $R_p \leq 0.2$ Mpc of galaxy clusters (> 5 for $R_p \leq 0.5$ Mpc; > 7 for $R_p \leq 1.0$ Mpc) for $P_{SUM} < 0.05$. This constrains the SN Ia rate in clusters to agree with the two-component model to within a factor of two. In § 4.3 we incorporated SFR_{IR} into the "A+B" model and P_{SUM}, but we find an insufficient number of cluster members are infrared bright enough to have a similar effect. As a final note, we find that in early-type cluster galaxies, the fraction of expected SNe Ia contributed by the "B" component is $\sim 5\%$, which is normal for our conventions of SED types and their associated SFR.

6.5 Summary

Our results for the SNLS SN Ia rate in galaxy clusters at intermediate redshiftdo not show strong support for the rate enhancement in cluster over field early-type galaxies established by Mannucci et al. (2008). They are dominated by the statistical uncertainties in identifying only a small number of cluster SNe Ia. They are consistent with the SN Ia rate in early-type

field galaxies, and also with predictions of the two-component model. Based on our data we can, at best, constrain the SN Ia rate in clusters to agree with the two-component model to within a factor of two.

Since this work was published in 2008, there have been two cluster catalogs generated for the CFHTLS Deep fields based on more advanced optical cluster detection algorithms. Were we to fully repeat this experiment, we would use these instead. First, Thanjavur et al. (2009) published a list of galaxy clusters for the CFHTLS Wide fields, in which half the Deep fields are encompassed. They show their method results in a more complete catalog than Olsen et al. (2007), but the cluster catalogs generated from CFHTLS Deep field data were not ready for distribution in time (private communication). With only 2 of 4 fields from the Wide survey, we could not get better statistics than we already have with the Olsen catalog. Secondly, Milkeraitis et al. (2010) published a cluster catalog for CFHTLS Deep fields in which they find $\sim 4\times$ as many galaxy clusters per square degree as Olsen et al. (2007); unfortunately this appeared too late to incorporate it in this thesis.

Several notable attempts to characterize any relations between galaxy clustering and SNe Ia have been published since Graham et al. (2008). Carlberg et al. (2008) applied the cross-correlation technique to SNLS SN Ia host galaxies, and found they are significantly more clustered than field galaxies, but that the correlation signal is well matched to a sample of field galaxies weighted by mass and SFR (i.e. the "A+B" model). Cooper et al. (2009) found the local environments of red SN Ia hosts (i.e. cluster ellipticals) from the SDSS-II supernova survey do not show a preference for over-densities. However, Dilday et al. (2010) also use the SDSS-II SN survey data set, and found the SN Ia rate ratio between cluster and field early-type galaxies to be $\sim$ 2–3 at the $\sim 2\sigma$ level. They also found minimal evolution in the SN Ia cluster rate over redshift. Most recently, Barbary et al. (2010) presented preliminary results of the HST cluster survey (Dawson et al. 2009). They found the SN Ia rate in $z \geq 0.9$ clusters was marginally higher than at low redshift (at the $< 2\sigma$ level, private communication), and is currently consistent with several theoretical delay time distributions for SNe Ia.

Clearly the SN Ia rate in galaxy clusters remains a hot topic. Our involvement in this field has not ended with Graham et al. (2008). In Chapter 7 we use a statistical parametrization of environment density to test whether SN Ia hosts prefer clustered regions without relying on any catalogs using specific definitions of clusters and groups; a similar, less sophisticated version of this was also presented in Graham et al. (2008). In Appendix A we present the CFHT Multi-Epoch Nearby Cluster survey, the largest low redshift cluster survey for SNe Ia yet attempted, and discuss our role in that project.

Chapter 7

Parametrization of Clustering in Parent Galaxy Environments

In Chapters 5 and 6 we used CFHTLS Deep field group and cluster catalogs from the literature to assess whether the SN Ia rate per unit mass is influenced by clustering in the environment of parent galaxies. Here, instead of relying on these catalogs, we use two clustering-strength parameters to identify galaxies in over- and under-dense environments. The first is a measure of the excess, or deficit, of galaxies in a region compared to the background distribution. In § 7.1 we introduce and refine this parameter, and apply a variety of statistical tests to determine whether the specific SN Ia rate is different in clustered environments. In § 7.2 we use this parameter to test whether the specific SN Ia rate is different in under-dense and void environments. The second parameter measures, for any given galaxy, the summed probability that its on-sky neighbors are within 500 km/s, which is the typical velocity dispersion of galaxy groups and clusters. In § 7.3 we introduce this second parameter and apply it in a similar fashion to the first.

The advantage of these parametrizations is that a strict cluster definition is avoided, and any desired scale of clustering can be explored by altering the physical environment radius, R_p. We use them to explore a larger parameter space and look for environment differences, on many size scales, between SN Ia host galaxies and the general population. In principle, with some training and calibration, one could use these parameters to find groups and clusters. The disadvantage of using these parameters is that they are previously undocumented ways to measure clustering around a galaxy, and require detailed descriptions and a careful assessment of their value prior to their application. Given the importance and current relevance of constraining environmental effects on SNe Ia discussed in Chapter 6, we think it warranted.

7.1 Environment Significance

In this section we introduce the clustering parameter of environment significance, Σ, starting with the version used in Graham et al. (2008) in § 7.1.1. We refine this parameter to a probability-based significance Σ_P, verify it is appropriate for our tasks, and use it to assess the environments of SNe Ia in § 7.1.2–7.1.4.

7.1.1 Simple Environment Significance

The simple environment significance parameter, Σ, quantifies the statistical significance of finding N_E neighbor galaxies in the volume around a galaxy or SN Ia, given the number expected from the background distribution:

$$\Sigma = \frac{N_E - N_F(A_E/A_F)}{\sqrt{N_F(A_E/A_F)}}. \tag{7.1}$$

For our purposes, this volume around a galaxy is a cylinder centered on the galaxy or SN Ia of interest, with physical radius R_p in Mpc, and redshift depth $\pm\sigma_{\Delta z/(1+z)}$. The number expected from the background distribution is the total number of galaxies within $\pm\sigma_{\Delta z/(1+z)}$ in all fields, times the ratio of environment area to total field area: $N_F(A_E/A_F)$. Environment area is $A_E = \pi r^2$ square degrees, where r is the angular radius of the environment converted from R_p. The field area is $A_F = 3.23$ square degrees after accounting for foreground star masks (Coupon et al. 2009). Since N_F is computed at the same redshift as the object being studied, incompleteness at high redshift is automatically compensated for.

The advantage of this parametrization is that a strict cluster definition is avoided – any desired scale of clustering can be explored by altering the environment radius R_p. This parameter was used in Graham et al. (2008) to show that the parent galaxy environments of SNLS SNe Ia had the same distribution of Σ as the general population of galaxies. However, Σ has several flaws which can be improved.

First, the volume depth of $\pm\sigma_{\Delta z/(1+z)}$ represents the uncertainties in photometric redshifts, but can not capitalize on the relatively tiny spectroscopic redshift uncertainties provided by VLT coverage of D1 and D2. Second, if a galaxy has two neighbors within $\sigma_{\Delta z/(1+z)}$ and $0.1 \times \sigma_{\Delta z/(1+z)}$ respectively, each results in $N_E = N_E + 1$. Instead of adding 1, we would prefer to add some value proportional to the probability that the two galaxies are actually associated. We incorporate these qualities in a new, probabilistic version of environment significance presented in § 7.1.2.

One final drawback of such environmental parametrizations is that galaxies at the bound-

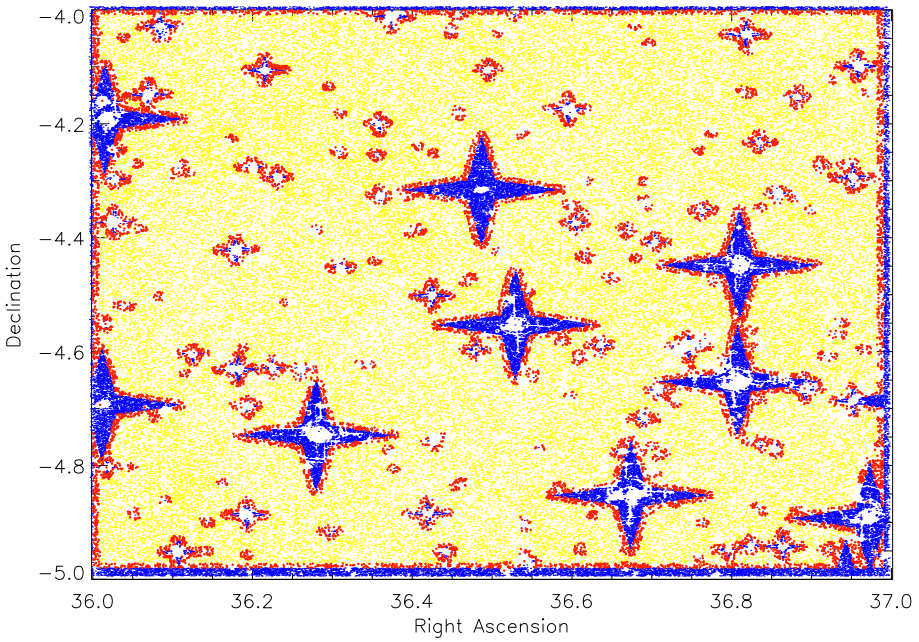

Figure 7.1 A map of D1 galaxies (yellow) showing the masked regions (blue) and galaxies identified at the boundaries (red). Both axes are in decimal degrees.

aries of the field, and near masked regions around foreground stars, will have an artificially low N_E. We fix this by identifying boundary galaxies as those within $\theta \leq 20''$ of a raw C09 catalog galaxy with Terapix flag=4, as shown in Figure 7.1 for D1 as an example. (The Terapix flag=4 indicates the source is on a masked region). We omit them from our galaxy samples throughout this chapter, for all parameters used, *but* still include them in the environments of their neighbors (otherwise, we would only have moved the boundaries).

7.1.2 Probabilistic Environment Significance, Σ_P

A redshift's uncertainty, $\pm\sigma_{\Delta z/(1+z)}$, is the standard deviation of its Gaussian probability distribution function (PDF). We want to use this to measure the probability that two galaxies along a sight-line are physically associated. One possibility is to use the area contained by the overlap of their PDFs, but this is problematic when combining spectroscopic and photometric redshifts of very different σ. Instead, we use the total area contained under each Gaussian PDF which overlaps the $\pm1\sigma$ region of the other. We refer to this area as $P_{SUM,1\sigma}$. This technique is best explained visually by the six case scenarios plotted in Figure 7.2.

For photometric redshifts we use $\pm\sigma_{\Delta z/(1+z)} = 0.03$ (Coupon et al. 2009). The spectroscopic redshift uncertainties are $\sigma_{\Delta z/(1+z)} \sim 0.0009$ in D1 (LeFèvre et al. 2005), and $\sigma_{\Delta z/(1+z)} \sim 0.00036$ in D2 (Lilly et al. 2009). However, these are smaller than typical velocity dispersions for groups and clusters, which range from $\sigma_{\Delta V} = 200$km s^{-1} in small groups to $\sigma_{\Delta V} \geq 800$km s^{-1} in rich clusters (Becker et al. 2007). To account for this, we actually use $\sigma_{\Delta V} = 500$km s^{-1} ($\sigma_{\Delta z} = 0.0017$) for all spectroscopic redshifts. (Note the factor of 1+z does not apply after this adjustment, as this is a $\sigma_{\Delta z}$ and no longer an uncertainty $\sigma_{\Delta z/(1+z)}$).

We use $P_{SUM,1\sigma}$ to calculate the probabilistic environment significance, Σ_P, as follows:

$$\Sigma_P = \frac{P_E - P_F(A_E/A_F)}{\sqrt{P_F(A_E/A_F)}} \tag{7.2}$$

For every C09 galaxy we calculate the $P_{SUM,1\sigma}$ value between it and each of its on-sky neighbors within a physical environment radius R_p. The total environment probability, P_E, is the sum of $P_{SUM,1\sigma}$ for all neighbors. The total field probability, P_F, is the sum of $P_{SUM,1\sigma}$ between the galaxy, and every other galaxy in the field. Environment area A_E and field area A_F are the same as in § 7.1.1.

Essentially, Σ_P is proportional to the *probability* that an environment contains clustering on the scale of radius R_P, normalized to the expected probability of finding field galaxies

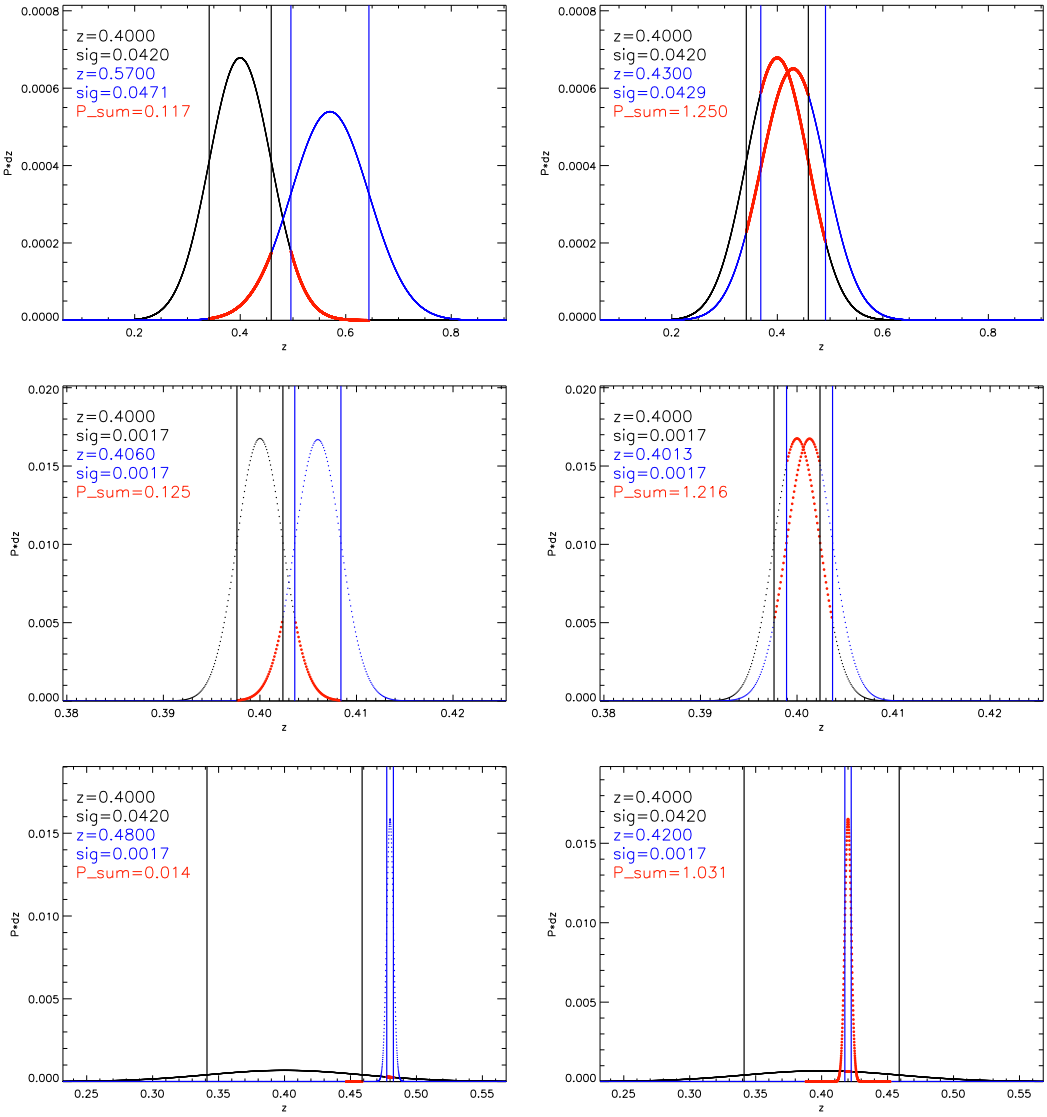

Figure 7.2 Gaussian redshift PDFs case scenarios illustrating the calculation of $P_{SUM,1\sigma}$. Left/right columns have PDF peak values outside/inside 1σ. Rows top to bottom show two photometric redshifts, two spectroscopic redshifts (note the different x-axis scale), and one of each. Black/blue lines indicate lower/higher PDF peak. Red highlights the regions within 1σ of the other which contribute to $P_{SUM,1\sigma}$, given as "Area P" at top left.

within the environment area. Figure 7.2 shows that neighbor galaxies contribute to the total P_E in a manner proportional to the actual probability of physical association. We calculate the Σ_P for galaxies in all four CFHTLS Deep fields. In a later section we will separately consider the results from only fields with VLT spectroscopic redshifts (D1 and D2).

7.1.3 Assessment of Σ_P

Before applying Σ_P to investigate clustering in the environments of SN Ia parent galaxies, we must verify its suitability as an environment clustering parameter. We plot the normalized distributions of Σ_P values for all galaxies in all four CFHTLS Deep fields in Figure 7.3. We omit from this sample the galaxies at the boundaries of the field, and near masked regions around foreground stars, as we do at all times, as described in § 7.1.1. Distributions of Σ_P values for samples limited to Olsen cluster and Knobel group galaxies only are plotted as blue and green lines. The two-sided Kolmogorov-Smirnov (KS) test results, displayed in plot legend, confirms the distributions for cluster and group members are both significantly different from the distribution for all galaxies. Though shown only for $R_p = 0.2$ Mpc, the KS test confirms this for all environment radii 0.05–1.0 Mpc. It is also true if we limit the sample to early-type galaxies only. We conclude that the Σ_P parameter is a successful measure of clustering in a galaxy's environment.

7.1.4 The Σ_P of SN Ia Environments

Here we use the KS test to say whether the distribution of Σ_P values for SN Ia parent galaxies shows any deviation from that of the general population. In the top plot of Figure 7.4 we present the normalized cumulative distributions for $R_p = 0.2$ Mpc. The KS test statistic P (in plot legend) shows only a 1% probability that SN Ia host environments are drawn randomly from the population of all galaxies. Is this a robust result? In the bottom graph of Figure 7.4 we plot the KS test probability as a function of environment radius with varying limitations on galaxy SED type and redshift. In nearly all cases – except for the one which happened to be our example – we find $KS_P > 0.05$. We must therefore conclude that this test does not show robust evidence that the environments of SN Ia parent galaxies have more or less clustering than the general galaxy population.

Identifying High Significance Environments (HSEs)

Although the distribution of Σ_P of SN Ia hosts is statistically similar to that of the general population of galaxies, there may still be an undetected influence on SN Ia rates in only

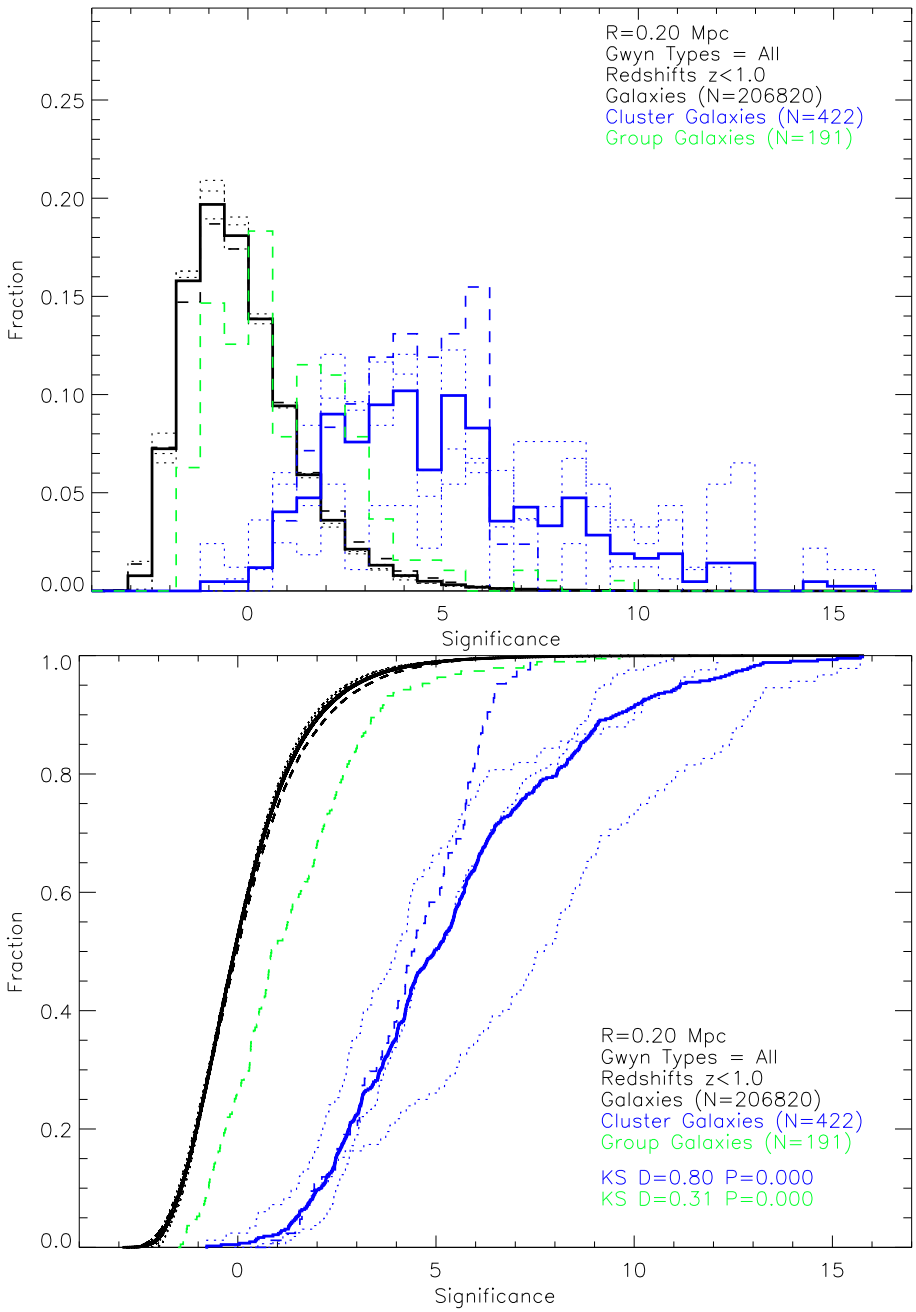

Figure 7.3 Normalized distributions of Σ_P, for all galaxies (black) and members of Olsen clusters (blue) and Knobel groups (green). Shown for environment radius R_p = 0.2 Mpc, for all Deep fields combined (thick solid lines). Distributions for individual CFHTLS Deep fields (dotted, dashed for D2) show field variation.

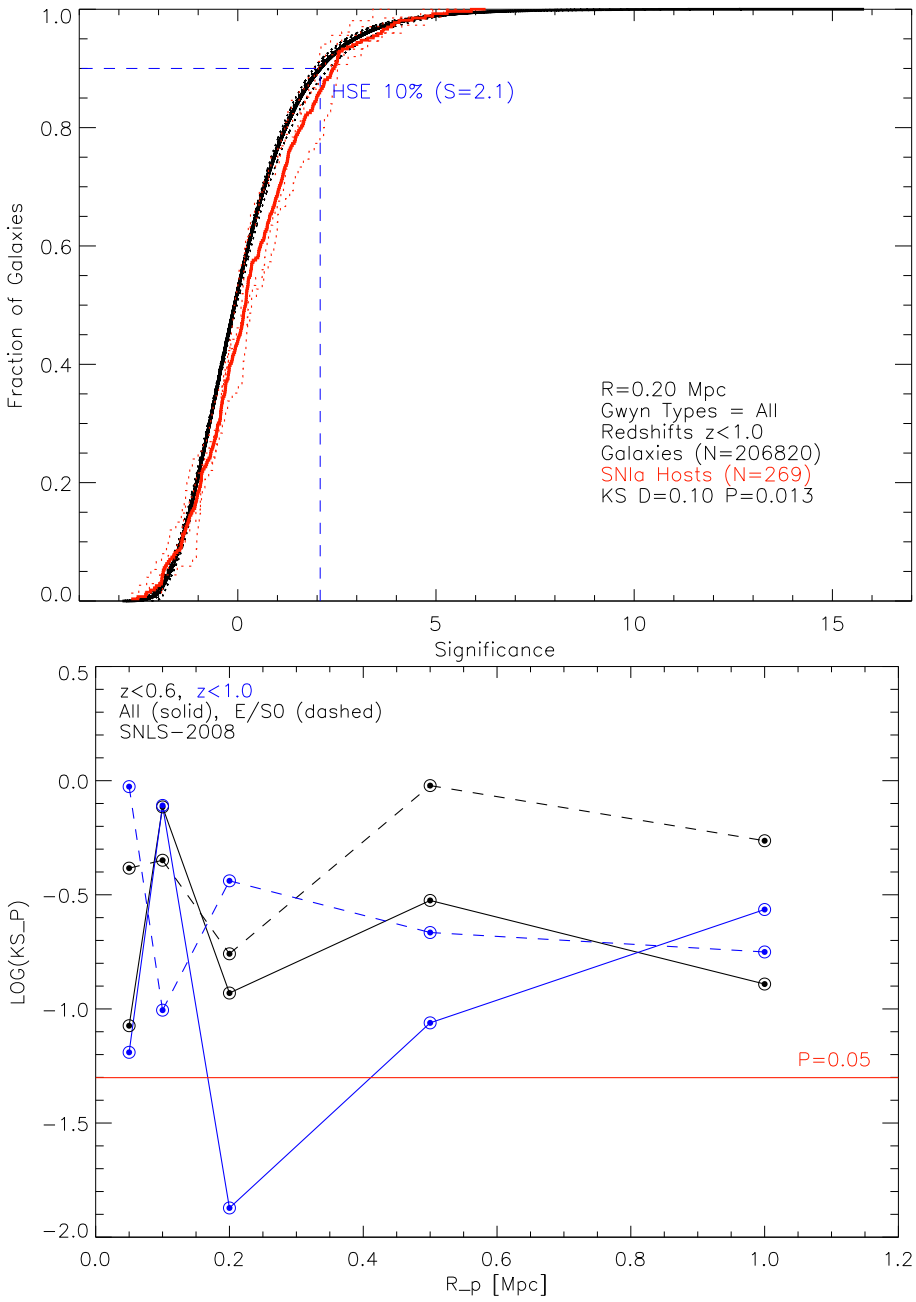

Figure 7.4 Top: Normalized cumulative distributions of Σ_P for all galaxies (black) and SN Ia hosts (red); line styles as in Figure 7.3. Bottom: The KS test probability, KS_P, between SN Ia hosts and all galaxies, as a function of environment radius R_p.

the *most* significant environments. Such an effect would be diluted by the presence of lower and intermediate significance environments in the previous experiment. To test this we identify samples of galaxies in the most clustered environments, calculate the rate in these samples, and compare it to the rate in the general population and to predictions of the two-component "A+B" model.

We refer to these samples of galaxies with the most clustered environments as the "high significance environments" or "the HSEs". Each HSE is comprised of all galaxies with environment significance $\geq \Sigma_{P,X\%}$, where $\Sigma_{P,X\%}$ is defined to enclose the X% most significant environments. For example, the boundary line of X=10% for R_p = 0.2 Mpc is shown on the cumulative distribution of Figure 7.4. The value of $\Sigma_{P,X\%}$ varies for different environment diameters. When we consider samples of galaxies, limited by their redshift or SED type, the value of $\Sigma_{P,X\%}$ is determined from the cumulative distribution containing that specific sample only. In this way, we always isolating the top X% most significant environments in the sample of interest. In § 7.3.2 we compare our two clustering parametrizations, and at that time present the fraction of known cluster and group members in the Σ_P HSEs.

SN Ia Rates in HSEs

In each HSE we calculate the specific SN Ia rate, and compare it to the rate in the general population and to predictions of the two-component "A+B" model. Figure 7.5 plots the specific SN Ia rate in each HSE as a function of $\Sigma_{P,X\%}$ for X=100, 50, 25, 10, 5, and 1%. In the top graph we include all galaxy SED types, but in the bottom limit to early-types only. Recall that the values of $\Sigma_{P,X\%}$ are different in each sample for a given X% because $\Sigma_{P,X\%}$ is calculated for each specific sample. In Figure 7.5, open squares are predicted SN Ia rates from the two-component "A+B" model. The expected decrease in the most clustered environments for all SED types is simply a combination of the morphology-density relation, and the "A+B" model's lower specific SN Ia rate in early-type galaxies. It is not seen if we limit to early-type galaxies only.

Filled circles are the observed SN Ia rates with 1σ error bars. The rate in the HSE defined by X=100% is the rate in *all* galaxies, and we extend a horizontal line there for comparison. For all SED types, the observed SN Ia rates follow the "A+B" model trend and are consistent to within 1σ of its predictions; this is true for our range of environment diameters R_p =0.05–1.0 Mpc. With the sample of early-type galaxies only, observed rates are consistent with both the rate in all early-type galaxies, and "A+B" predictions. Though Figure 7.5 shows this just for R_p = 0.2 Mpc, when all environment radii are considered we actually see a possible trend. The SN Ia rate appears enhanced by $\sim 2\times$ in the most signifi-

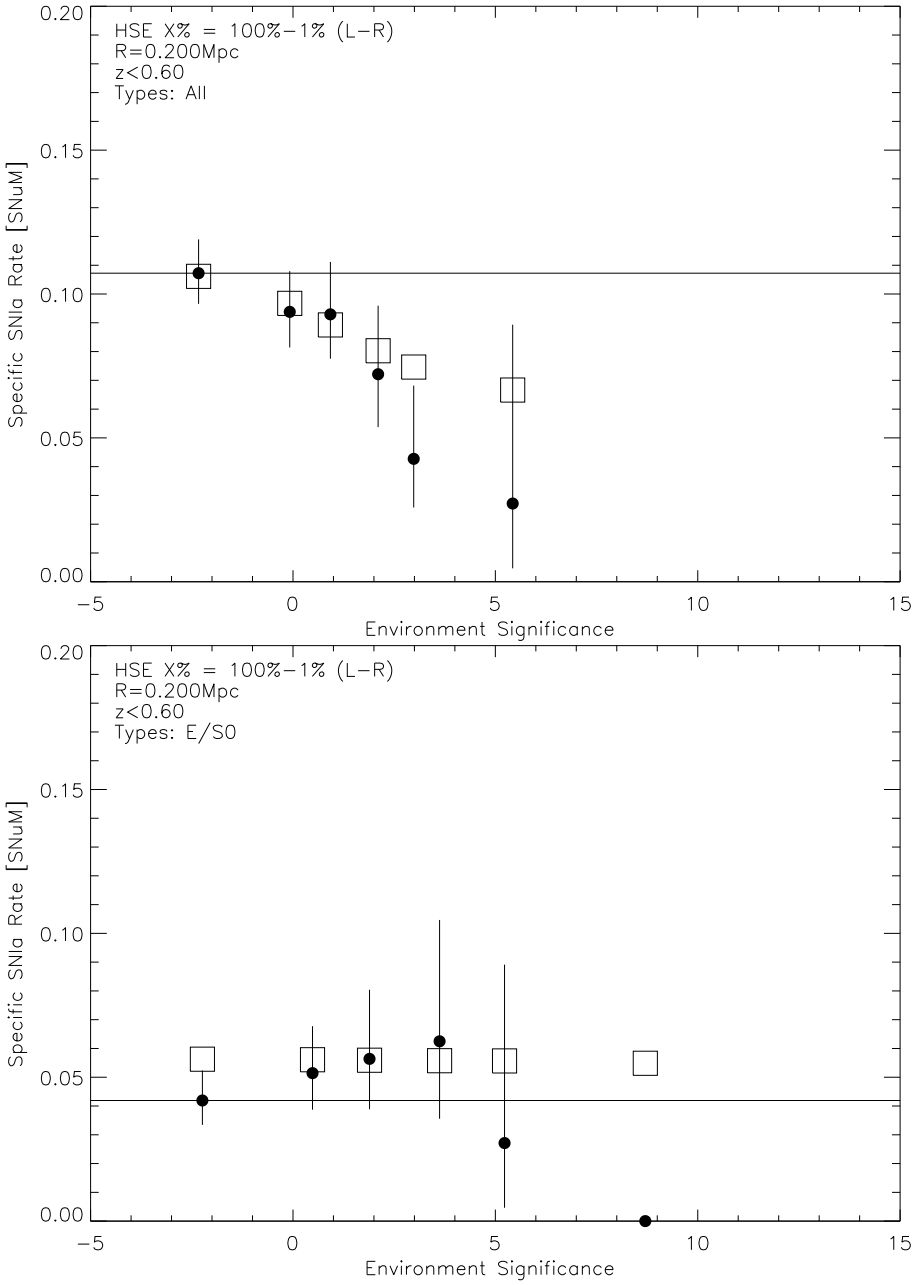

Figure 7.5 Specific SN Ia rates in HSEs for X=100, 50, 25, 10, 5, and 1% (points left to right). Rates based on observations and predictions of the "A+B" model (circles/squares). For galaxies of all SED types and early-type only (top/bottom), for SNe Ia from the SNLS-2006 sample. Environment radius R_p = 0.2 Mpc.

Table 7.1 SNe Ia Observed and Predicted in Σ_P HSE.

Radius	$\Sigma_{P,10\%}$			$\Sigma_{P,5\%}$			$\Sigma_{P,1\%}$		
(Mpc)	N_{obs}	N_{A+B}	P_{SUM}	N_{obs}	N_{A+B}	P_{SUM}	N_{obs}	N_{A+B}	P_{SUM}
0.05 Mpc	25	13.70	0.00	12	7.64	0.09	1	1.84	0.45
0.10 Mpc	16	15.18	0.45	10	8.35	0.33	2	2.45	0.56
0.20 Mpc	15	15.58	0.51	6	9.15	0.19	1	2.15	0.37
0.50 Mpc	10	14.68	0.14	4	8.01	0.10	1	1.95	0.42
1.00 Mpc	14	13.50	0.48	3	7.25	0.07	0	1.48	0.23
For early-type galaxies only:									
0.05 Mpc	6	3.60	0.16	2	1.90	0.57	0	0.44	0.64
0.10 Mpc	6	3.66	0.16	2	2.15	0.64	0	0.32	0.73
0.20 Mpc	5	3.95	0.36	1	1.79	0.47	0	0.32	0.73
0.50 Mpc	1	3.24	0.17	1	1.59	0.53	0	0.26	0.77
1.00 Mpc	1	3.37	0.15	0	1.51	0.22	0	0.32	0.73

cant environments of early-type galaxies when small environment radii, R_p, are considered, and repressed by $\lesssim 1/2\times$ in the most significant environments at large R_p. The statistical significance of this trend is only $\lesssim 2\sigma$, and is discussed more below.

SNe Ia and "A+B" Predictions in HSEs

Here we use summed Poisson probabilities to statistically compare the number of SNLS SNe Ia in each HSE, N_{obs}, to the number expected from the two-component "A+B" model, N_{A+B} (sum of the expected number of SNe Ia in each galaxy in the HSE). This statistical analysis method was described in § 3.2. In Table 7.1 we present results based on the sample of galaxies with $z \leq 0.6$, and SNe Ia from SNLS-2006.

We see the same general trend discussed above: the ratio of N_{obs} to N_{A+B} in the most significant environments moves from excess-to-deficit over small-to-large scale environments. In the case of HSE $\Sigma_{P,10\%}$ for $R_p = 0.05$ Mpc, this excess is extremely significant and almost $\sim 2\times$ more SNe Ia are observed than expected. The trend is less obvious with the small numbers for $\Sigma_{P,5\%}$ and $\Sigma_{P,1\%}$, and when limiting to early-type galaxies only. Can we really say this is a "trend"? If we exclude $P_{SUM} \leq 0.05$ as discrepant, this result looks less like a trend and all results remain consistent with predictions of the "A+B" model. However, since $P_{SUM} \leq 0.05$ is accepted as a statistically robust result, this deserves further exploration.

Could this "trend" be the manifestation of some bias in our data set? It is still de-

tectable when we limit to $0.3 < z < 0.6$, or to Deep fields 1 and 2, or 3 and 4, only. This suggests it is not the result of any biases related to redshift, or the mixing of photometric and spectroscopic redshifts, or a strange cosmic variance effect. For each X%, the number of galaxies in each R_p HSE is constant, and the total HSE mass does not vary much ($\sim$ 30%, randomly). The percentage of predicted SNe Ia contributed by the "B" component are not unusual; $\sim$ 20–40% for galaxies of all SED types ($\sim$ 40% for X=10%, $\sim$ 20% for X=1%, a likely reflection of the morphology-density relation), and $\sim$ 5% for early-type galaxies. Also, the mean galaxy mass in each HSE group does not appear to vary with R_p. Basically, we find no catalog bias to pin this apparent "trend" on.

Though it appears the environments of host galaxies may affect their SN Ia rates over and above the influence of the morphology-density relation, it might not be as straightforward as an increase in small, and a decrease in large clusters. With the Σ_P technique our results could also stem from an increase in the central regions of large clusters, and/or the outskirts of large clusters. In summary, since no *statistically significant* excess or deficit of SNe Ia is seen over multiple HSE, we cannot say with confidence that this trend is evidence that the Σ_P parametrization reveals an influence of clustering on SN Ia events.

If we extend our galaxy sample to $z \leq 1.0$, and the SN Ia sample to SNLS-2008, the same general trend is seen with the same level of statistical confidence. If we limit our sample to CFHTLS D1 and D2 (the fields with spectroscopy), we also find the results are similar. If we limit to only galaxies with spectroscopy, we find decreasing the sample size increases the statistical errors to the point where no conclusions can be drawn.

7.2 SN Ia Rates in Under-dense Environments with Σ_P

In this section we use the probabilistic environment significance Σ_P to investigate the SN Ia rate in environments of relatively *low* clustering. Navasardyan et al. (2001) found the SN Ia rate in isolated galaxies was less than – but statistically consistent with – the specific SN Ia rate in field galaxies. Studies of SDSS galaxies have shown a continuity in galaxy properties between voids and clusters, with void galaxies being less luminous and bluer, and cluster galaxies being more luminous and redder, and of earlier morphological type (Sorrentino et al. 2006). However, other studies have shown that void galaxies are similar to field galaxies (Patiri et al. 2006). Based on this, we might expect an elevated SN Ia rate per unit mass in void galaxies consistent with the "A+B" model.

To begin, we define low significance environments (LSEs) in the same manner as HSEs in § 7.1.4. Each LSE is comprised of all galaxies with $\Sigma_P \leq \Sigma_{P,X\%}$, where now $\Sigma_{P,X\%}$

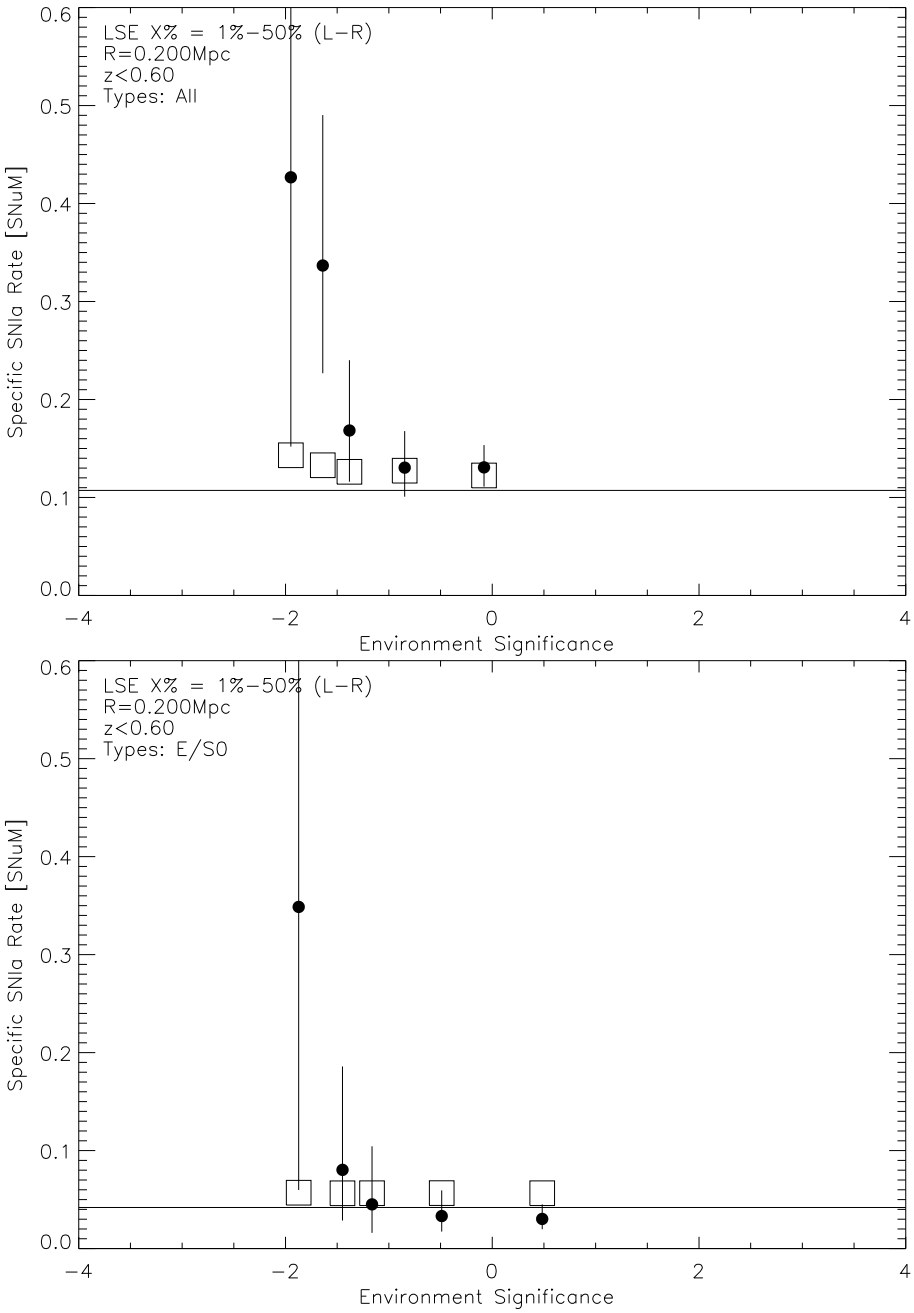

Figure 7.6 Specific SN Ia rates in LSEs for X=1, 5, 25, and 50% (points left to right). Rates based on observations and predictions of the "A+B" model (circles/squares). For galaxies of all SED types and early-type only (top/bottom), and for SNe Ia from the SNLS-2006 sample. Environment radius R_p = 0.2 Mpc.

Table 7.2 SNe Ia Observed and Predicted in Σ_P LSE.

Radius	$\Sigma_{P,10\%}$			$\Sigma_{P,5\%}$			$\Sigma_{P,1\%}$		
(Mpc)	N_{obs}	N_{A+B}	P_{SUM}	N_{obs}	N_{A+B}	P_{SUM}	N_{obs}	N_{A+B}	P_{SUM}
0.10 Mpc	9	7.01	0.27	5	3.52	0.28	0	0.87	0.42
0.20 Mpc	10	7.53	0.23	9	3.50	0.01	2	0.61	0.13
0.50 Mpc	12	7.73	0.09	6	3.60	0.16	0	0.68	0.51
For early-type galaxies only:									
0.10 Mpc	2	2.46	0.55	2	1.23	0.35	0	0.33	0.72
0.20 Mpc	2	2.26	0.61	2	1.26	0.36	1	0.16	0.14
0.50 Mpc	3	2.49	0.45	2	1.07	0.29	1	0.19	0.18

bounds the *least* significant X% of galaxies. Due to the very steep low-significance end of the R_p = 0.05 Mpc, and expecting interloping galaxies to overwhelm any tests at R_p = 1.0 Mpc, we omit our smallest and largest environment radii from this discussion.

Here we make the same analysis of LSEs as we did for HSEs in § 7.1.4. In each LSE we calculate the specific SN Ia rate, and compare it to the rate in the general population and to predictions of the two-component "A+B" model. Figure 7.6 plots the specific SN Ia rate in each LSE as a function of $\Sigma_{P,X\%}$ for X=1, 5, 10, 25, and 50%. In the top graph we include all galaxy SED types, but in the bottom limit to early-types only.

Open squares are predicted SN Ia rates from the two-component "A+B" model. We see for all SED types (top graph) a small SN Ia rate increase predicted by "A+B" in the least significant environments, consistent with slightly elevated star formation rates in void galaxies. Filled circles show the observed SN Ia rates with 1σ error bars. The horizontal line represents the observed SN Ia rate in all galaxies (or X=100%, outside plotting region). There appears to be a SN Ia rate increase over the rate in all galaxies in the least significant environments for R_P = 0.2 Mpc. This is also seen for our other environment radii, but always at the $\lesssim 2\sigma$ confidence level.

This observed rate increase also appears to be inconsistent with "A+B" model predictions in some LSEs. To investigate, we statistically compare the number of SNe Ia observed in each LSE (N_{obs}) to the number predicted by the two-component "A+B" model (N_{A+B}). Resulting summed Poisson probabilities for this comparison are presented the results in Table 7.2 (similar to Table 7.1). Although in many LSEs the observed number is greater than expectations, *most* values of P_{SUM} are > 0.05, indicating good agreement. In general we must conclude there is no solid evidence that residence of a parent galaxy in an under-dense environment affects its specific SN Ia rate.

Table 7.3 SN Ia Rates in Isolated Galaxies

(1) R_p	(2) # SNe Ia[a,b]	(3) Mass[c](Number)	(4) R_{Ia}[a,d]	(5) Ratio[a,e]	(6) N_{A+B}	(7) P_{SUM}
0.50 Mpc	0 (...)	127.7 (73)	...	...	0.12	0.88
0.25 Mpc	14 ($14.78^{+0.00}_{-5.09}$)	18782.4 (13199)	$0.134^{+0.046}_{-0.035}$	$1.09^{+0.38}_{-0.29}$	13.58	0.49

[a] Uncertainties are derived from Poisson errors at the 1σ confidence level, as in Gehrels (1986).

[b] Brackets contain number of SNe Ia corrected for SNLS detection efficiencies as in § 3.2 to be the number which exploded per year of SNLS observations.

[c] Mass units are 10^{10} $M_\odot$; brackets contain number of galaxies in class sample.

[d] SNuM = SNe (100 yr)$^{-1}$ (10^{10} $M_\odot$)$^{-1}$

[e] Ratio over rate in all galaxies.

7.2.1 SNe Ia in Isolated Galaxies

Instead of identifying galaxies in under-dense environments, we here identify a sample of galaxies which are likely to be truly isolated. This is a difficult task, as the spectroscopic redshift catalogs are too incomplete for this task, and we must rely solely on the C09 photometric redshift galaxy catalog. Although one interloper in a cluster is not a large influence, one interloper in an otherwise empty environment will exclude that environment from our sample of isolated galaxies. For this reason our sample of isolated galaxies will be very incomplete, but relatively pure.

We use the same concept of environment as previously in this chapter; a cylinder of radius R_p and depth $\sigma \times (1+z)$. Here we use σ=0.03 and R_p= 0.25, 0.5, 1.0 Mpc, and identify a samples of galaxies with empty environments out to those radii. Again we exclude from consideration all boundary galaxies within $\theta \leq 20''$ of a raw C09 catalog galaxy with Terapix flag=4, as discussed in § 7.1.1.

Here we use our most liberal and largest catalog sample, $z \leq 1.0$ and SNLS-2008. We only find galaxies isolated within our two smallest environment radii, 0.50 and 0.25 Mpc, and only the smallest contains any SNe Ia hosts. For those two environment radii, we list our results in Table 7.3. This includes the SN Ia rate in isolated galaxies, their ratio over the field rate, the number predicted by the two-component "A+B" model, N_{A+B}, and the Poisson probability, P_{SUM}, of having observed N_{obs}.

Observed SN Ia rates in isolated galaxies show no evidence of an enhancement in small-scale empty environments, and are consistent with expectations of the "A+B" model. If we

limit the galaxy catalog to $z \leq 0.6$, although the sample size is smaller, the SN Ia rate ratio between isolated and all galaxies is $1.78^{+0.84}_{-0.61}$ for an environment radius of 0.25 Mpc. This ratio is, however, still consistent with the null result at the 2σ level, and with "A+B". In general, we do not find that parent galaxy residence in under-dense environments affects the SN Ia rate.

7.3 The P_{500} Parameter: Neighbors Within 500 km/s

The concept of probabilistic environment significance, Σ_P, presented and used in the last two sections is derived from the probability that two galaxy redshifts are within 1σ of each other. This parameter was shown to identify members of known groups and clusters, but still allows interloping galaxies to contribute to the clustering strength measurement. Ultimately, we could not draw any robust conclusions. In this section we instead use the probability that two galaxies are physically associated – that they have a radial velocity difference of ±500 km s^{-1} or less – to parametrize clustering in a galaxy's environment. First we will explain how we do this, then examine how well it does in identifying galaxies in known groups and clusters, and finally apply it to the environments of SN Ia host galaxies in § 7.3.1–7.3.3.

7.3.1 Definition of P_{500}

A redshift's uncertainty, $\pm\sigma_{\Delta z/(1+z)}$, is the standard deviation of its Gaussian probability distribution function (PDF) as expressed by:

$$P(dz) = \frac{1}{\sigma\sqrt{2\pi}} \exp\left[-\frac{1}{2}\left(\frac{dz}{\sigma}\right)^2\right]. \tag{7.3}$$

The PDF for the difference between two redshifts, $dz = z_1 - z_2$, has a standard deviation σ_{dz} as given by (Bevington & Robinson 2003):

$$\sigma_{dz} = \sqrt{((1+z_1)\sigma_{\Delta z_1/(1+z)})^2 + ((1+z_2)\sigma_{\Delta z_2/(1+z)})^2}. \tag{7.4}$$

The probability that the two objects of z_1 and z_2 are physically associated (i.e. that they have a velocity difference < ±500 km s^{-1}, or $dz < \pm 0.0017$), is the integral of the normalized Gaussian PDF curve P(dz) from -0.0017 to +0.0017. We refer to the value of this integral as A_{500}. The numerical evaluation of A_{500} is:

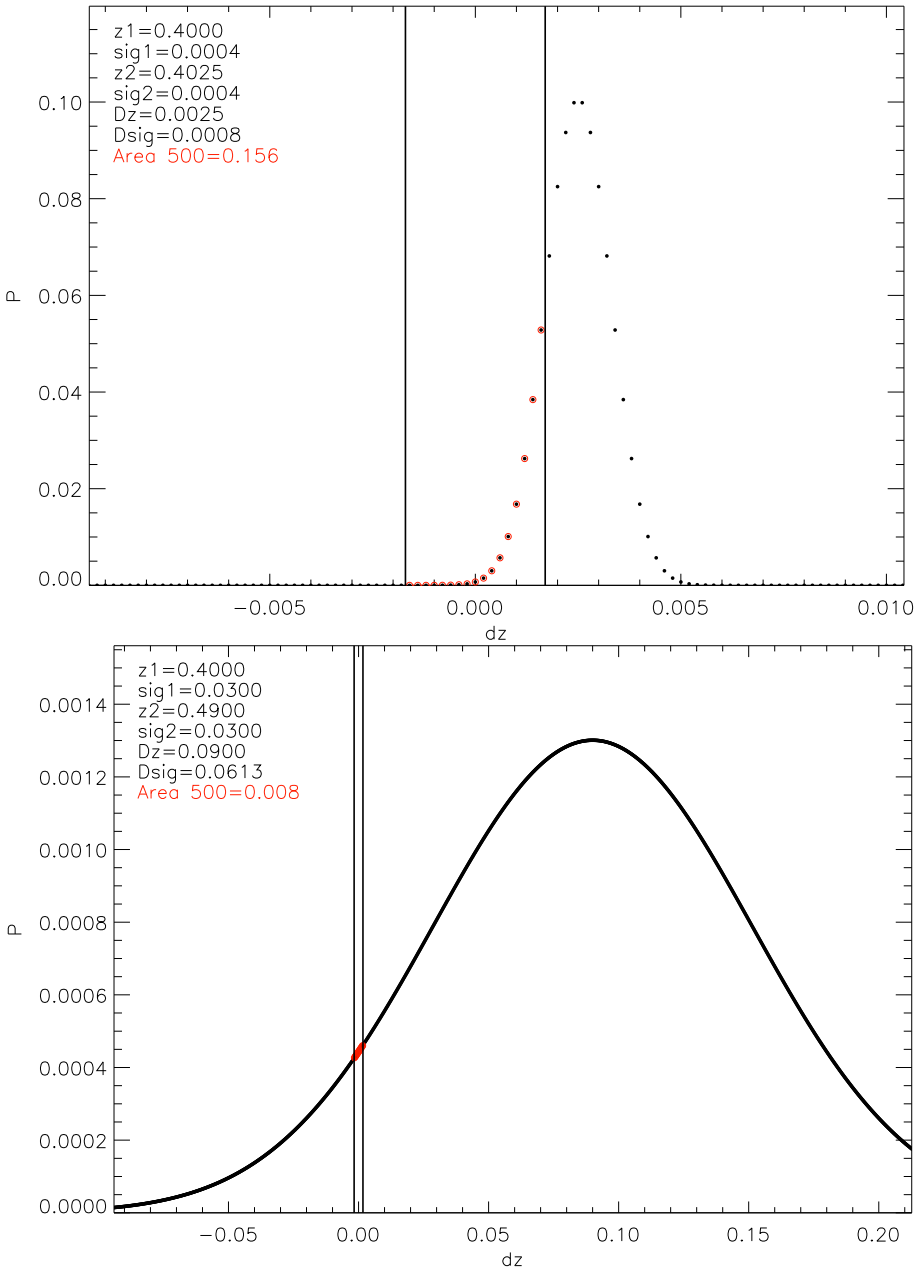

Figure 7.7 Gaussian PDFs for dz = $z_1 - z_2$ used to numerically evaluate A_{500}. Red highlights the points between ±500 km s^{-1} (or $-0.0017 < dz < 0.0017$). The y-axis values are = P(dz) × δ(dz). Top: both z_1 and z_2 are spectroscopic. Bottom: both are photometric.

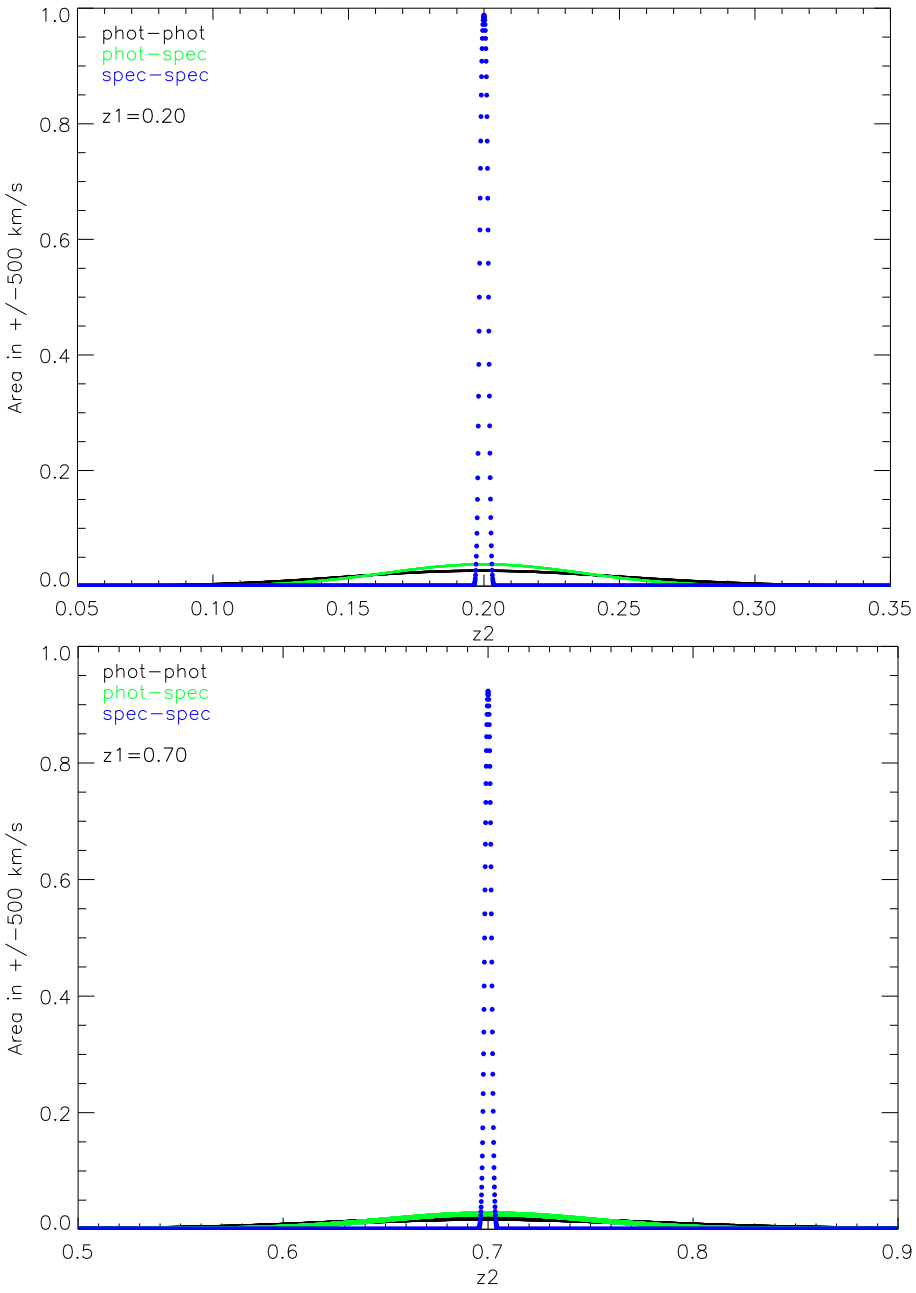

Figure 7.8 Probability A_{500} that two galaxies of redshifts z_1 and z_2 are physically associated, for two sample values of z_1 = 0.2 and 0.7. Plotted for the cases where both z_1 and z_2 are photometric redshifts (black), both are spectroscopic (blue), or one of each (green).

$$A_{500} = \sum_{-0.0017}^{+0.0017} P(dz) \times \delta(dz), \tag{7.5}$$

where δ(dz) is our bin-size. We use $\sigma_{\Delta z/1+z} = 0.03$ for photometric redshifts, 0.001 for spectroscopic redshifts in D1 (LeFèvre et al. 2005), and 0.0004 for spectroscopic redshifts in D2 (Lilly et al. 2009). We plot two examples of P(dz) $\times$ δ(dz) versus dz = $z_1 - z_2$ in Figure 7.7, the cases where z_1 and z_2 are both spectroscopic (top) and both photometric (bottom). The mixed case is very similar to the photometric case.

The value of A_{500} is given in the top left corner of the plots in Figure 7.7. For code speed we have used a bin-size of δ(dz) =0.002, which appears large in Figure 7.7 but actually gives only a $\sim$ 1% error in the value of A_{500} between spectroscopic neighbours (compared to δ(dz) = 0.0001). This is acceptable for our uses of A_{500}.

To show how the value of A_{500} depends on redshift and uncertainty values, we plot A_{500} versus dz for three values of σ_{dz} in Figure 7.8. The proximity of two spectroscopic redshifts is obviously much more significant than when at least one is photometric. The difference in width and peak value at different redshifts (almost unnoticeable on the scale of Figure 7.8) is due to the factor of 1+z from $\sigma_{\Delta z} = (1+z)\sigma_{\Delta z/1+z}$, as expressed in Equation 7.4. The PDF has a larger spread at higher redshift, and thus a lower area under the curve between $\Delta z = \pm 0.0017$. This does not need to be corrected for. Galaxy associations at higher redshift are more uncertain, and the value of A_{500} should and does reflect this.

We use A_{500} to calculate our clustering parameter P_{500} as follows. For every galaxy in the C09 catalog, we calculate the value of A_{500} for every neighbor within a desired physical radius R_p. As shown in Figure 7.8, when dz $> 0.1 \times (1 + z)$, then $A_{500} \sim 0$. To save computing time we include only neighbors with dz $< 0.1 \times (1 + z)$. The clustering parameter P_{500} for a galaxy is the sum of A_{500} from all its neighbors. Essentially, its value is proportional to the probability that on-sky neighbors are within $\pm$500 km s^{-1}.

7.3.2 Assessment of P_{500}

Prior to using P_{500} to evaluate clustering in the environments of SN Ia host galaxies, we must verify its suitability as an environment clustering parameter. We start with a comparison of P_{500} to Σ_P in the top plot of Figure 7.9. The two parameters appear to be generally proportional for low values of P_{500}, but quite different for $P_{500} > 0.3$, which must represent situations of neighbor galaxies in which both have spectroscopic redshifts. That some galaxies with *negative* Σ_P have large values of P_{500} illustrates a potential drawback of Σ_P. If a galaxy with a few close spectroscopic neighbors is in a redshift slice with many spectro-

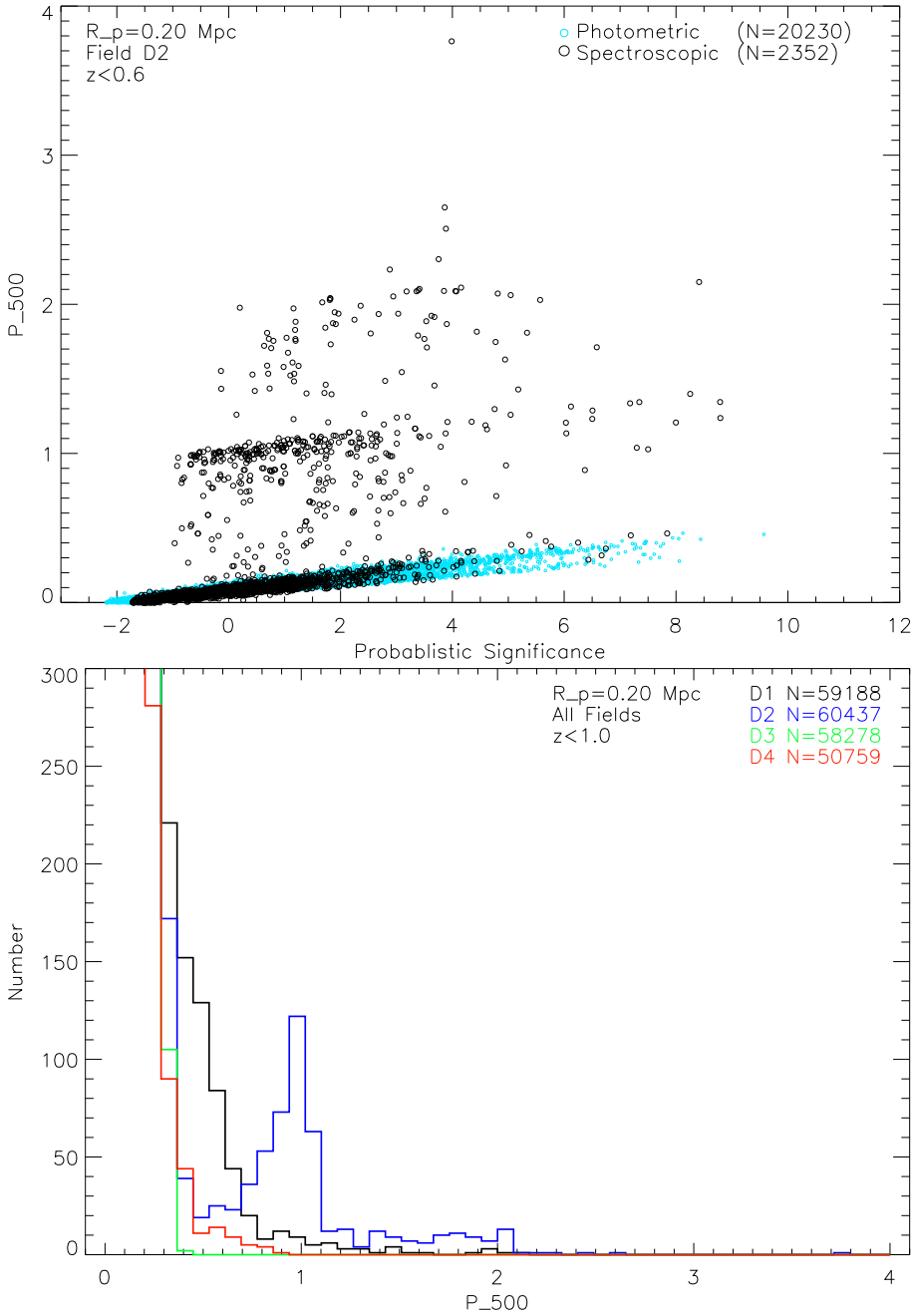

Figure 7.9 The properties of P_{500}. Top: P_{500} versus Σ_P, for photometric redshifts (cyan) and spectroscopic (black). Bottom: the distribution of P_{500} for galaxies in each CFHTLS Deep field. Both plots are for R_p = 0.2 Mpc.

scopic galaxies, the background value P_F will be higher. This will lessen the significance of any real, small groups.

In the bottom graph of Figure 7.9 we display distributions of P_{500} for all CFHTLS Deep fields, and find they are quite dissimilar. This is not surprising because the value of P_{500} depends heavily on spectroscopic redshift uncertainty. Only D1 and D2 contain spectroscopic redshifts, which are higher for the D1 VLT survey and thus yield less certain associations and lower values of P_{500}. However, the actual *value* of P_{500} has the same meaning in all fields: the *probability* that on-sky neighbors are within ± 500 km s^{-1}.

Both graphs in Figure 7.9 clearly show that P_{500} is discretized. This is not a problem, but represents a physical quality of P_{500}: the combination of the steep relation between A_{500} and dz shown in Figure 7.8, and the fact that most galaxy neighbors either *are* physically associated or *are not*; chance encounters are relatively rare. Thus, we would not expect the distribution of P_{500} values to be continuous. This discretization of P_{500} may be enhanced by the bias that brighter galaxies are both more likely to be in groups and pairs, and more likely to be included in the spectroscopic survey. Later we attempt to account for this by limiting analysis samples to only the set of galaxies with spectroscopy.

Galaxy Groups and Clusters Detected by P_{500}

Here we ensure that P_{500} can identify known members of groups and clusters. In Figure 7.10 we plot the normalized regular and cumulative distributions of P_{500} for all $z \leq 0.6$ galaxies in D1 and D2. We also plot the distributions for D1 and D2 galaxies associated with Olsen clusters and Knobel groups. Although the *value* of P_{500} has the same meaning in all Deep fields and at all redshifts, distributions should only be compared within a given Deep field. We perform the KS-test for each field separately (results in lower right corner of plot), and find the P_{500} parametrization identifies known members of groups and clusters just as Σ_P. (The corresponding plot for Σ_P is Figure 7.3). A visual comparison shows Σ_P more clearly distinguishes the cluster member population, whereas the group members are more clearly distinguished from all galaxies by P_{500}. If we limit our sample to galaxies in the spectroscopic catalogs only, the results are equivalent.

We used the term high significance environments (HSEs) in § 7.1.4 to refer to those galaxies with environment significance $\geq \Sigma_{P,X\%}$, where $\Sigma_{P,X\%}$ is defined to enclose the X% most significant environments. Here we extend the term to P_{500}, and also define HSE based on the P_{500} distribution in exactly the same manner (but keep the term "HSE"). We use these P_{500}-based HSE to test whether P_{500} does a better job at placing Olsen cluster and Knobel group members in high significance environments than Σ_P. In Figure 7.11 we plot,

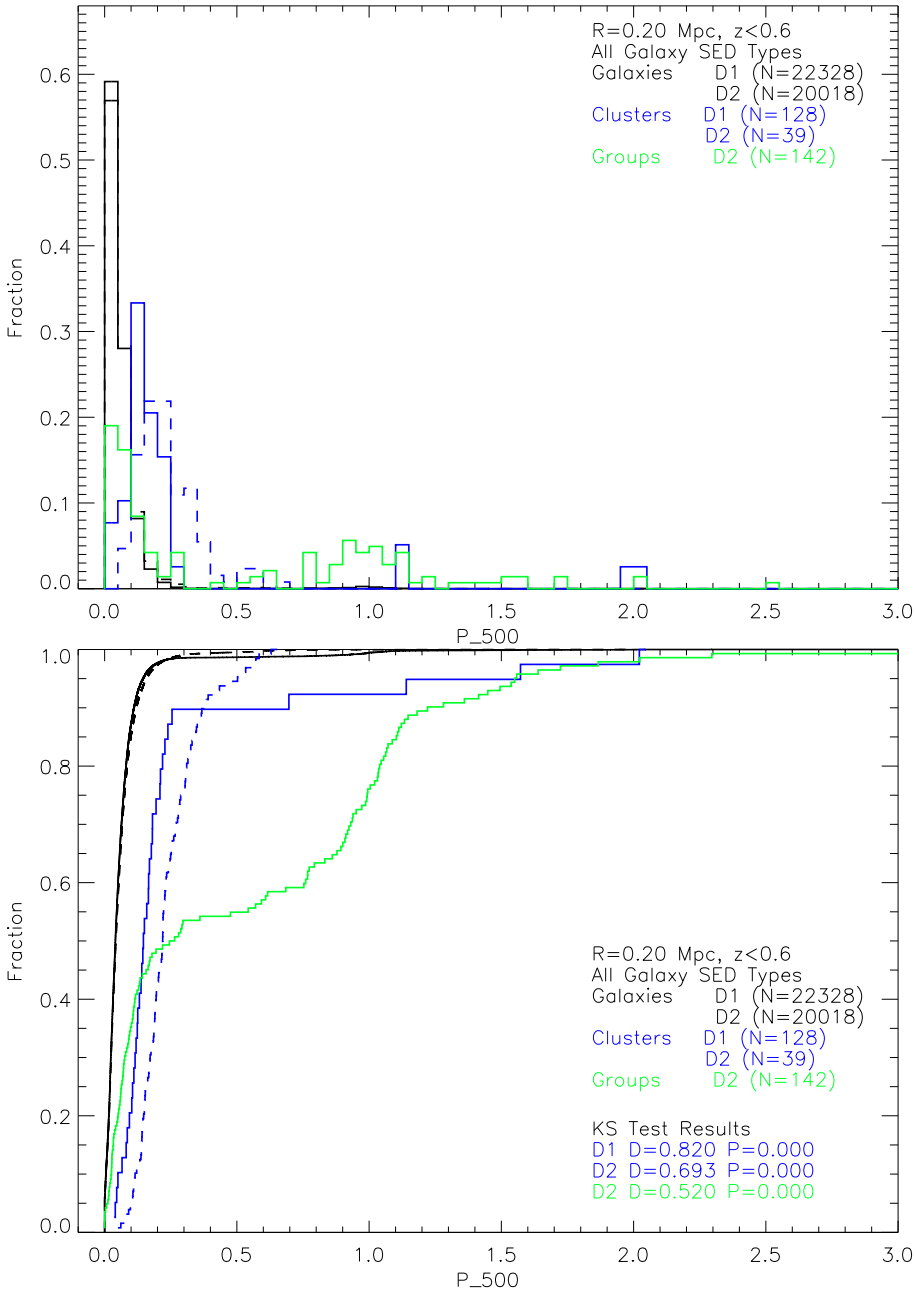

Figure 7.10 Normalized distributions of P_{500}, for all galaxies (black) and members of Olsen clusters (blue) and Knobel groups (green). Shown for environment radius R_p = 0.2 Mpc, for all Deep fields combined (thick solid lines). Distributions for individual CFHTLS Deep fields (dotted, dashed for D2) show field variation.

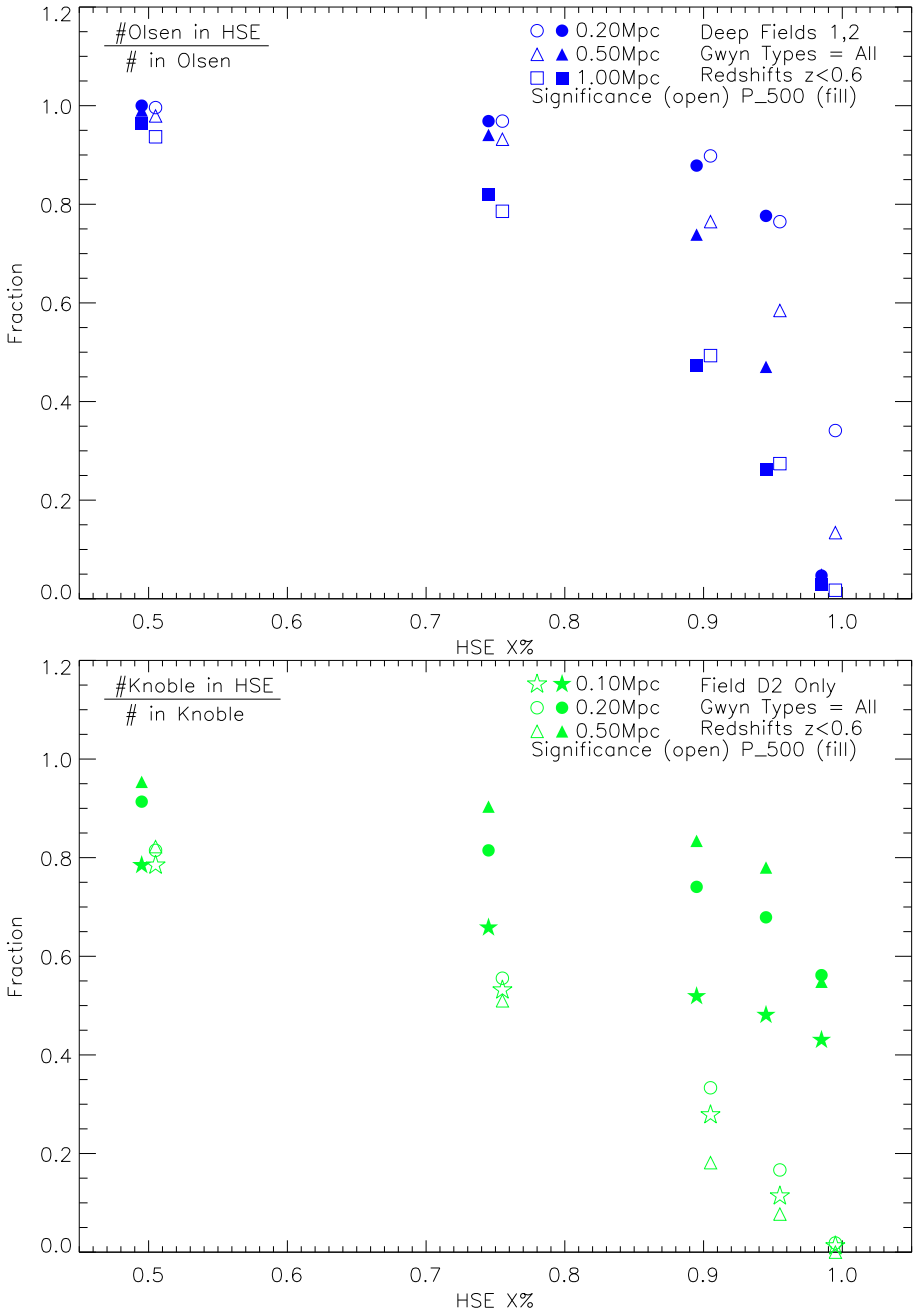

Figure 7.11 Comparing the fraction of cluster (top, blue) and group (bottom, green) members in HSE from the new P_{500} method (filled) to the old Σ_P method (open).

as a function of HSE X%, the fraction of all cluster and group members in that HSE. The open and filled symbols represent Σ_P- and P_{500}-based HSE respectively. We do this for three values of environment radius: 0.2, 0.5, and 1.0 Mpc for clusters, and 0.1, 0.2, and 0.5 Mpc for groups. For galaxy clusters, we see that Σ_P and P_{500} return approximately the same fractions of known cluster members in each HSE, with a few exceptions. For galaxy groups, we see the P_{500}-based HSEs contain a much higher fraction of known group members than the HSEs of Σ_P, suggesting the P_{500} parametrization is much more sensitive to galaxies in groups.

We conclude that the P_{500} parameter does as good a job of identifying galaxies in real clusters as Σ_P, and a much better job of identifying galaxies in real groups. This improvement for galaxy groups might be due in part to the sensitivity of P_{500} to spectroscopic redshifts, combined with the fact that group members are drawn from the spectroscopic survey. However, when we remake these figures based only on the spectroscopic sample of galaxies they look quite similar (though with more scatter), and the same conclusions can be drawn.

7.3.3 The P_{500} of SN Ia Environments

Now that we are satisfied P_{500} is a suitable parametrization of clustering, we compare the distribution of P_{500} values for SN Ia hosts to that of all galaxies in Figure 7.12. This is equivalent to the test for Σ_P in § 7.1.4, except here the KS-test is performed for D1 and D2 separately. In both cases we find that SN Ia host environments have a P_{500} distribution indistinguishable from that of all galaxies, with an environment radius of $R_p = 0.2$ Mpc. The bottom plot of Figure 7.12 verifies this for most environment radii with few exceptions. We find the results are quite similar if we repeat with the smaller spectroscopic sample only. This indicates the agreement is not being heavily influenced by the photometric redshifts and their low P_{500} values.

SN Ia Rates in Environments of High P_{500}

To consider P_{500}-based HSE, we combine the P_{500} distributions of all four CFHTLS Deep fields, and then define the $P_{500,X\%}$ limits identifying the top X% most clustered environments. We must do it this way because the value of P_{500} has the same meaning in all fields: a parameter proportional to the probable number of real, physically associated neighbor galaxies. Unlike the situation with Σ_P, which is normalized to the background of each field, it would be wrong to identify the top X% highest P_{500} environments in each Deep field and

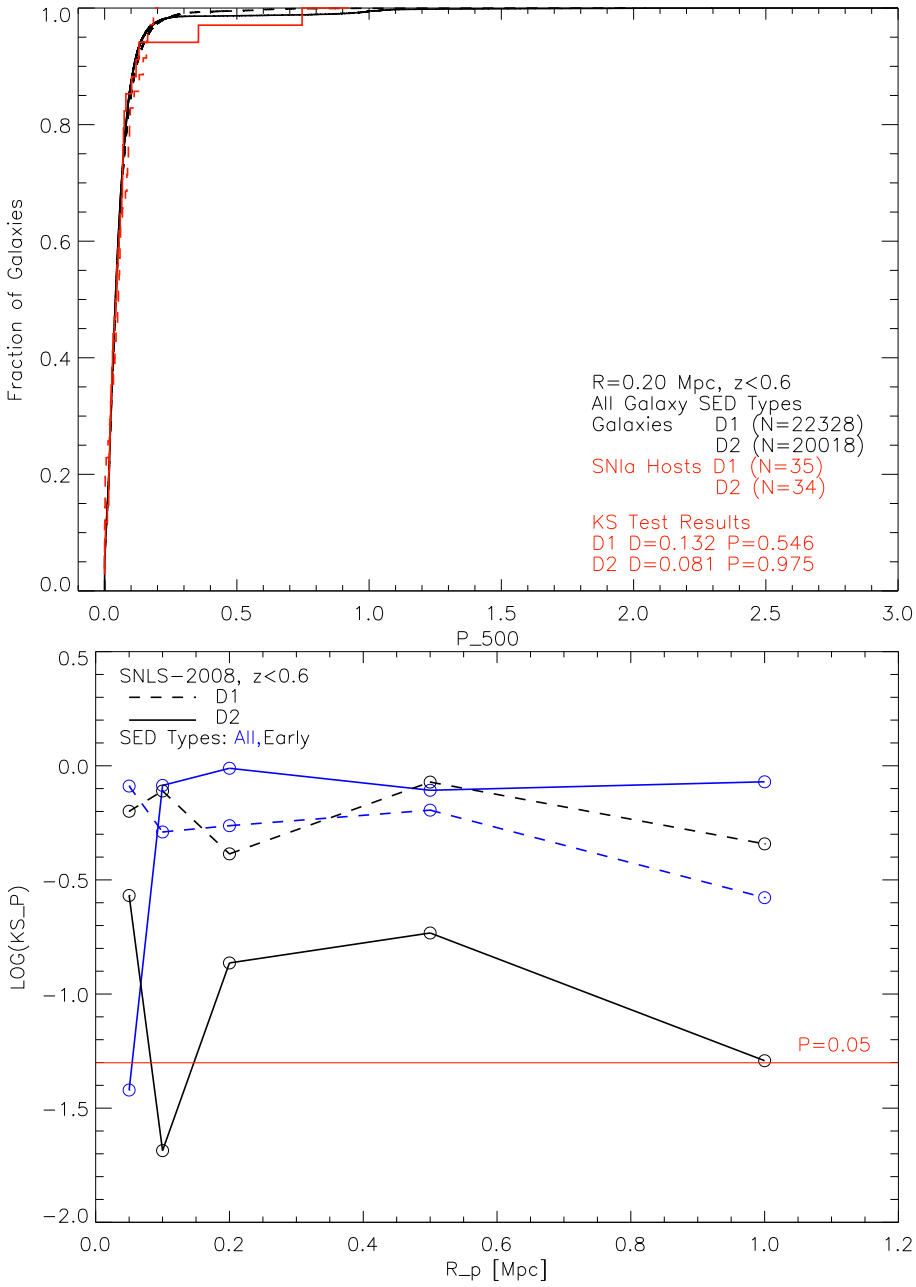

Figure 7.12 Top: Normalized cumulative distributions of P_{500} for all galaxies (black) and SN Ia hosts (red). Bottom: The KS test probability KS_P between SN Ia hosts and all galaxies as a function of environment radius R_p. Though similar to Figure 7.4, note the different line styling.

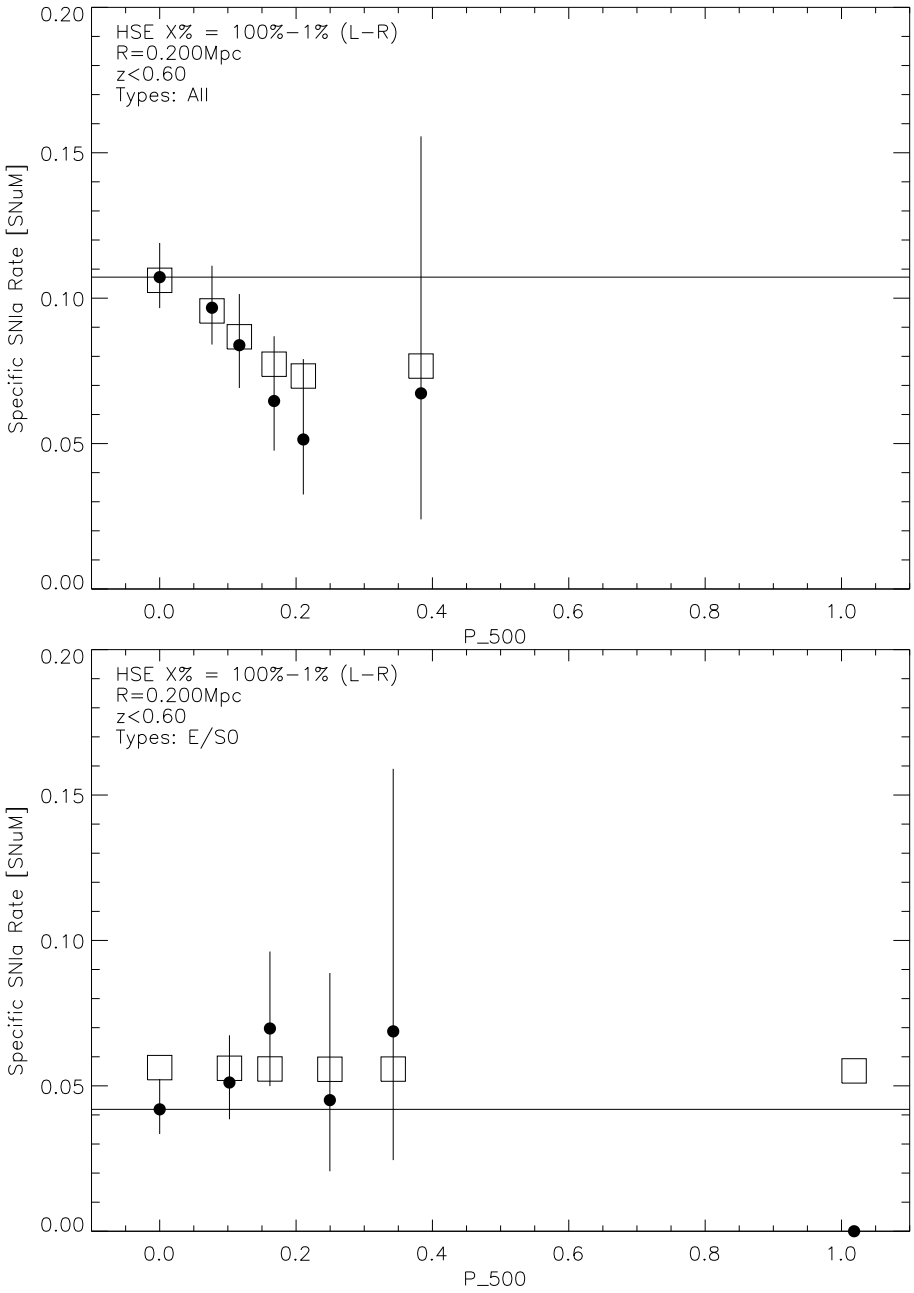

Figure 7.13 Specific SN Ia rates for P_{500}-based HSEs for X=100, 50, 25, 10, 5, and 1% (points left to right). Rates based on observations and predictions of the "A+B" model (circles/squares). For galaxies of all SED types and early-type only (top/bottom), for SNe Ia from the SNLS-2006 sample. Environment radius R_p = 0.2 Mpc.

Table 7.4 SNe Ia Observed and Predicted in P_{500} HSE.

Radius	$P_{500,10\%}$			$P_{500,5\%}$			$P_{500,1\%}$		
(Mpc)	N_{obs}	N_{A+B}	P_{SUM}	N_{obs}	N_{A+B}	P_{SUM}	N_{obs}	N_{A+B}	P_{SUM}
0.05 Mpc	16	13.07	0.24	9	7.41	0.33	1	1.82	0.46
0.10 Mpc	13	14.91	0.37	10	8.42	0.34	2	2.38	0.58
0.20 Mpc	14	15.45	0.42	7	9.16	0.31	2	2.28	0.60
0.50 Mpc	8	14.88	0.04	5	8.63	0.14	3	2.36	0.42
1.00 Mpc	10	13.26	0.23	5	7.44	0.25	2	1.99	0.59
For early-type galaxies only:									
0.05 Mpc	5	3.49	0.27	2	1.86	0.56	0	0.41	0.66
0.10 Mpc	6	3.68	0.17	3	1.91	0.30	1	0.41	0.34
0.20 Mpc	3	3.52	0.53	2	1.61	0.48	0	0.45	0.64
0.50 Mpc	3	3.25	0.59	2	1.64	0.49	0	0.35	0.70
1.00 Mpc	2	2.97	0.43	1	1.53	0.55	0	0.33	0.72

then combine them as an HSE.

In Figure 7.13 we plot the SN Ia rate per unit mass in each P_{500}-based HSE as a function of $P_{500,X\%}$ for X=100%, 50%, 25%, 10%, 5%, and 1%. This is equivalent to Figure 7.5 for Σ_P-based HSE with environment radius R_p =0.2 Mpc, and all results are remarkably similar. Again we see clearly the predicted and observed SN Ia rate decrease in the most clustered environments for all SED types (top) due to the morphology-density relation, and again we find all observed rates are consistent to within 1σ of "A+B" model predictions.

In the discussion for Figure 7.5 we noted a trend in the SN Ia rate when all environment radii are considered: an enhancement in the most significant environments of early-type galaxies at small R_p, and a repression in the most significant environments at large R_p, at the $\lesssim 2\sigma$ confidence level. This *is* seen again for P_{500}-based HSE when we consider all environment radii (and is more obvious with early-type galaxies only), but with even lower statistical significance. Unfortunately, limiting our sample to D1 and D2 (covered by spectroscopic surveys) yields small numbers statistics that greatly increase our uncertainties, such that it becomes impossible to draw any such conclusions.

SNe Ia and "A+B" Predictions in HSEs

As a final experiment, we use summed Poisson probabilities to statistically compare the number of SNe Ia observed in P_{500}-defined HSE to the number predicted by the two-component "A+B" model. Results for X=10, 5, and 1% are presented in Table 7.4, which is

equivalent to Table 7.1 for Σ_P-derived HSE (based on the sample of galaxies with $z \leq 0.6$, and SNe Ia from SNLS-2006). This time, the trend we noted in § 7.1.4, in which the ratio of N_{obs} to N_{A+B} moves from excess to deficit over small to large scale environments, is much less noticeable and not statistically significant. For P_{500}, this is the most obvious in our largest sample of X=10% and all SED types, but the summed Poisson probability remains > 0.05 in all cases (except for X=10%, $R_p = 0.5$ Mpc, where it is =0.04).

No new insight is gained by limiting to the spectroscopic sample of D1 and D2 only, as the small numbers only worsen the statistics. Despite the obvious utility of using the P_{500} environment clustering parameter shown throughout this section, it does not conclusively show whether galaxy clustering in the environments of parent galaxies has an influence on the specific SN Ia rate.

7.4 Summary

This chapter has presented and assessed two different parametrizations of environment clustering, and applied them to the parent galaxies of SNLS SNe Ia. It is expected that the SN Ia rate per unit mass will be lower in large clusters due to the combination of the two-component "A+B" rate model, and the morphology-density relation. We were able to observe this effect. To test for rate effects outside of this known influence, we compared our SN Ia rates in the most clustered environments to predictions of the "A+B" model. With both clustering parameters, we found the number of SNe Ia observed is greater than predicted for environments clustered on small scales, and less than predicted for environments clustered on large scales. In only a few cases this was very statistically significant, and although suggestive, we can only consider our results as inconclusive evidence that galaxy clustering may influence the SN Ia rate per unit mass.

We also measured the SNLS SN Ia rate in under-dense and void environments. We found no evidence that residence of a galaxy in such regions affects its specific SN Ia rate. Our observations were consistent with predictions of the two-component "A+B" model, and in agreement with previous measurements of the SN Ia rate in isolated galaxies (Navasardyan et al. 2001).

Chapter 8

Conclusions

We have assessed the presence of an independent influence from parent galaxy and environment properties on the probability of a Type Ia supernova explosion, outside of the known correlation with star formation rate (SFR). We have explored radio and infrared galaxies, group and cluster members, and galaxies in over- and under-dense environments. In the cases for which we find the specific SN Ia rate is *suggestive* of an enhancement, this is usually with only $\lesssim 2\sigma$ confidence at best. Generally, our results are consistent with previous works to within $\sim$ 1–2σ, and with predictions based on the established correlation between SN Ia rate, mass, and SFR known as the two-component "A+B" model.

We achieved all this by using the intermediate redshift SN Ia database from the Canada-France-Hawaii Telescope Supernova Legacy Survey (CFHT SNLS). There are three main benefits of using this data set. First, the SNLS ran a large follow-up campaign to spectroscopically confirm all SN types, and their analysis includes two independent light-curve fitting techniques which provide the SN Ia stretch values we used in this analysis. Second, the large volume of space sampled by the CFHT Deep fields allowed us to make a simultaneous analysis of SNe Ia in under- and over-dense environments, which is not possible with galaxy or cluster targeted surveys. Third, since SNLS coincides with popular survey fields, we compiled a wide variety of multi-wavelength source and galaxy structure catalogs into the most comprehensive analysis of SN Ia hosts and environments at intermediate redshifts.

The greatest limitation of using the intermediate redshift SNLS database has been incompleteness in the multi-wavelength source catalogs. The VLA radio, Spitzer infrared, and VLT spectroscopic surveys cover only parts of the SNLS volume. Since we are already interested in only the most extreme hosts (e.g. radio-loud), and would have suffered anyway from small number statistics, this reduced coverage has further impaired our analysis by enlarging our uncertainties. Although we made many efforts to assess and avoid biases

introduced by the combination of catalogs with different completeness, this often meant additional limitations which further enlarged uncertainties.

8.1 A Summary of Our Main Results

Despite these limitations – which number less than the benefits – this thesis has successfully examined how host properties and environment density may influence SN Ia rates and properties. Our specific highlights include the following.

- In Chapter 3 we described our synthesis of ten data catalogs in the CFHTLS Deep fields to build the most comprehensive set of host galaxy characteristics for the SNLS database of Type Ia supernovae.

- In Chapter 4 we found no statistically significant evidence that the SN Ia rate in radio-loud elliptical galaxies is enhanced over all ellipticals. However, we did find the stretch values for SNe Ia in radio-loud early-type galaxies are consistent with the established distribution for the "prompt" component, associating SNe Ia in radio-loud ellipticals with an intermediate age stellar population. Also, we made the first calculation that the specific SN Ia rate in luminous infrared elliptical galaxies is enhanced by $\sim$ 2–5$\times$ (with $\lesssim 2\sigma$ significance).

- In Chapter 5 we found the properties of SN Ia host galaxies in small groups are similar to field galaxies in terms of mass, SFR, radio power, and IR luminosity. We also found the SN Ia rate in group galaxies is consistent with the rate in field galaxies, and discovered the N_{Ia}/N_{II} ratio appears to be higher in groups (but within 1σ).

- In Chapter 6 we did not find strong evidence that the specific SN Ia rate in cluster elliptical galaxies may be enhanced over the field, as previously found at lower redshifts. Our results were consistent with predictions of the "A+B" model.

- In Chapter 7, we developed two clustering strength parameters. Our observations showed a systematic deviation from "A+B" model predictions, but were still statistically consistent with them. We also found no evidence that parent galaxy residence in under-dense or void environments affects their specific SN Ia rate.

8.2 A Discussion of Our Main Results

In this thesis we have investigated the influence of parent galaxy and environment on the rates and properties of SNe Ia. Recall that the established correlation between specific SN Ia rate and specific SFR, the two-component "A+B" model (Sullivan et al. 2006a), is consistent with a continuous distribution of delay times (Pritchet et al. 2008), such as are theoretically predicted for the single- and double-degenerate scenarios (Greggio et al. 2008). One of our main motivations was the recent study of Della Valle et al. (2005, DV05) which found the specific SN Ia rate to be higher in early-type galaxies with radio emission. Mannucci et al. (2006) found this is best fit with a bimodal delay time distribution (DTD) in which half of all SNe Ia explode very promptly, within $\leq 10^8$ years.

We did not find a SN Ia rate enhancement in early-type radio-loud galaxies, and our observations were generally consistent with predictions of the two-component "A+B" model. Although we found the SNe Ia stretch values are *not* consistent with them *all* belonging to a uniformly prompt component, we cannot rule out the bimodal DTD of Mannucci et al. (2006). These SNLS stretch values are consistent with DV05's postulate that the root cause of both radio emission and their enhanced SN Ia rate is galaxy interaction/merger induced star formation. We explored this postulate further by determining the SN Ia rate of galaxies in groups and pairs, where interactions and mergers are most common.

We found the SN Ia rate in groups and pairs *may* be enhanced by over field galaxies, but only if we limit our sample to low redshifts, or galaxies with spectroscopic redshifts. For the SNLS data set, we must conclude that the general group SN Ia rate is statistically consistent with the field rate, and with "A+B" model predictions. Considering only galaxies with radio emission, we saw a $\sim 2\times$ SN Ia rate enhancement in group over field radio galaxies. This *might* suggest the effect on SN Ia rate associated with radio emission is independent of any effect in groups and pairs, but small number statistics lead to very large uncertainties on this measurement. The different ratio of N_{Ia}/N_{II} in group and field environments is further tentative evidence that an environmental effect outside of SFR is at work in galaxy groups. To further explore whether environment has an independent influence on SNe Ia, we considered their rate in rich galaxy clusters.

The other main motivation for this thesis work was to verify whether the specific SN Ia rate is $\sim 3\times$ higher in cluster early-type galaxies, as found by Mannucci et al. (2008), contrary to previous low redshift cluster rates. With the SNLS data, we found no strong evidence for an enhancement in cluster over field early-type galaxies, and our observations were also statistically consistent with predictions of the two-component "A+B" model. The

stretch values of cluster SNe Ia were consistent with the "delayed" component, as expected for early-type galaxies; however, association of at least one with the "prompt" component was not statistically unlikely. Ultimately, conclusive evidence of an independent influence on SN Ia rates associated with parent galaxy residence in a rich galaxy cluster can not be found in our data.

Environments can be clustered with different densities on different size scales, and are not actually divided into only "cluster" and "field". For a more robust assessment, we devise and employ two clustering strength parametrizations which are appropriate for our data catalogs, and which can be tailored to examine clustering on any environment size scale. We found an excess of SNe Ia in environments which are significantly clustered on small scales, and an apparent deficit of SNe Ia in environments significantly clustered on large scales. Though very suggestive, these variations were below the statistical level necessary to confirm an influence of clustering on SN Ia rates. We also found no evidence that parent galaxy residence in under-dense or void environments affects their specific SN Ia rate.

8.3 A Review of Our Scientific Impact

The main goal of this thesis was to verify and analyze the influence of parent galaxy and environment characteristics on the rates and properties of SNe Ia. Our investigations included galaxies showing powerful radio and infrared emission, members of known groups and rich clusters, and galaxies in over- and under-dense regions on a continuum of environment size scales. This thesis marks the first time all such properties have been considered simultaneously.

In general we have found the specific SN Ia rate *may* be enhanced by some of these galaxy and environment properties at the $\lesssim 2\sigma$ level. Where available, our results were in agreement with previous works to within $\sim$ 1–2σ. In all cases where a potential rate discrepancy was seen, our results were still consistent with predictions of the two-component "A+B" model. This was true also when we incorporated IR-derived SFR in very active star-forming systems such as Luminous Infrared Galaxies, despite the fact the model was founded on optically-derived properties in less extreme galaxies. Such broad agreement with the "A+B" model demonstrates its flexibility, and reinforces it as a very useful parametrization which applies to a wide range of galaxy types and environments.

In Chapter 2 we discussed how the progenitor scenario(s), delay time, and correlation between stretch and the host population's age and metallicity remain open questions

beyond the scope of this thesis. In retrospect, we consider whether this work can place independent constraints on the character of SN Ia progenitor systems. At least in terms of nature versus nurture, our results point to nature. The SN Ia rate has the same dependency on stellar population age in all types of special galaxies ("A+B"), and does not appear to be influenced by factors associated with parent galaxy environment such as AGN winds, the binary fraction, or other hitherto unsuspected phenomena. Based on this work, we see no reason to discontinue their use as cosmological standard candles.

Many of the results reviewed above have already been released to the scientific community. The contents of Chapter 4 were presented in Graham et al. (2010), which currently has 1 citation and $\sim$ 200 total reads on NASA ADS. The work in Chapter 6 and a rudimentary version of the environment significance parameter in Chapter 7 were published in Graham et al. (2008), which currently has 16 citations and $\sim$ 450 total reads on NASA ADS. As discussed in the summary of Chapter 6, better constraints on the SN Ia rate in clusters are still important. To help provide this, we have devoted a significant amount of our time to the CFHT Multi-Epoch Nearby Cluster Survey (MENeaCS). In Appendix A, we provide a description of the MENeaCS science goals, survey strategy, real-time analysis pipeline for SN detections, and detection efficiencies which are necessary for our MENeaCS cluster rates calculations.

The field of supernova studies continues to expand, and its future is bright. Large scale automated surveys for supernovae such as PanSTARRS and the Palomar Transient Factory are now monitoring our skies, and should find hundreds of transients every month. With respect to the work of this thesis, there are many advantages of wide area low-redshift samples of SNe Ia, including better completeness – both for supernovae and for the multi-wavelength properties. Their biggest strengths will be in the sheer number of SNe they can find. Considering the rarest 1% of environments is a more statistically productive exercise when the starting sample is 5000 instead of 500, and with projects such as the Large Synoptic Survey Telescope slated to come on-line within the decade, the sky itself will be the limit.

Appendix A

The Multi-Epoch Nearby Cluster Survey

The Canada-France-Hawaii Telescope's Multi-Epoch Nearby Cluster Survey (MENeaCS) began monthly observations of 60 x-ray luminous, low redshift galaxy clusters in February 2008, and finished primary observations in January 2010. It will provide both the deepest set of cluster data, and the largest sample of cluster supernovae, yet observed. MENeaCS has multiple science goals and a great deal of data, but a relatively small team led by principal investigator Henk Hoekstra at the University of Leiden. While Henk was planning a deep imaging survey to do weak lensing in clusters, David Sand was devising an extended imaging survey to constrain the SN Ia rate in low redshift galaxy clusters. As MENeaCS legend goes, while attending the same conference and chatting over beers – where so many truly great plans in human history are hatched – they decided to combine their projects. The core MENeaCS collaboration now consists of: Dennis Zaritsky, an expert in intracluster light (ICL) measurements; Chris Pritchet, an expert in supernova detection pipelines; Chris Bildfell, experienced in studies of brightest cluster galaxies; and myself, experienced in SN Ia rates, hosts, and environments.

This chapter focuses on my role in MENeaCS: to build, run, and maintain our automated pipeline for data management, supernova detection, flux calibration, and detection efficiency. It should be a useful read for anyone starting their own supernova survey. It contains a brief outline of the MENeaCS science goals and survey strategy, an outline of the supernova detection pipeline, and a description of detection efficiencies calculations in § A.1–A.3.

A.1 Science Goals and Survey Strategy

This section describes the main science goals of the MENeaCS survey, and presents a brief outline of its technical observing strategy. Though I had minimal involvement in the MENeaCS planning stages, the information here is necessary to motivate the content of the following two sections.

A.1.1 Science Goals

Galaxy clusters are scientifically valuable because baryons cannot escape their deep gravitational potential well. Clusters are a Universal equivalent of Las Vegas: what happens in a galaxy cluster stays in the galaxy cluster. The forensic evidence generated during its evolutionary history remains there for the astronomer to study.

The radial profile of dark matter sub-halos around elliptical cluster galaxies helps constrain cold dark matter theory (CDM). This profile is observed via the weak lensing signal of background galaxies, whose shape is distorted by the mass of elliptical cluster members. If tidal stripping of elliptical galaxies in the cluster's large dark matter halo is responsible for their current radial profile, then CDM theory must also predict the fraction of intracluster light (ICL) between the galaxies. This is because tidally stripped stars cannot escape the cluster.

Observations to quantify the ICL fraction are difficult due to the ICL's low surface brightness. The ratio between cluster hosted and hostless supernovae is presumed proportional to the amount of mass in ICS, but has so far only constrained the ICL fraction to within 10-40% (Gal-Yam et al. 2003). The intracluster medium (ICM) is well known to be an iron enriched environment, yet the current rate of SNe Ia in cluster galaxies is too low to account for this (Maoz & Gal-Yam 2004). It is also too low – and currently too uncertain – to avoid the requirement that galaxies eject a very large ($\sim$ 80%) of their metals into the ICM (Sivanandam et al. 2009). This is true also for the SN rate in the ICS.

The three science goals of the MENeaCS survey work in concert to establish clear constraints on these issues. MENeacs will measure the radial profile of cluster ellipticals; quantify the fraction of light in between the cluster galaxies; and measure the SN Ia rate in the ICS and cluster galaxies. The first two require very deep, uniform imaging of a large sample of clusters, and the third goal simply requires extending this imaging program over time.

A.1.2 Survey Strategy

The MegaCam instrument on the Canada-France-Hawaii Telescope was chosen for several reasons. First, CFHT's 3.6 meter primary mirror and optimal site on Mauna Kea in Hawaii is most suitable for achieving the required image depth and quality. Second, MegaCam's one square degree field of view is large enough to contain a cluster in a single image, and it is a stable, well-calibrated instrument operated with queue service observing (QSO). Third, CFHT has proved successful both for SN Ia surveys (SNLS) and cluster surveys such as the Canadian Cluster Comparison Project (CCCP).

The MENeaCS survey monitored 60 clusters within $0.05 < z < 0.15$ every month (when possible) in 2008 and 2009, for a total of $\sim$ 12 epochs for each cluster surveyed. Each epoch of observation is comprised of 4 exposures taken on the same night, referred to as one "observing group": 2 each in filters g and r, with integration times of 120 seconds, and dithered to fill in the gaps between MegaCam's 6 chips. The MENeaCS dither pattern includes 12 unique pointings in order to get uniformly deep stacks and a good astrometric solution. With overheads, the entire survey has amounted to > 120 hours of observation.

MegaCam is mounted on CFHT for $\gtrsim$ 2 weeks every month. At the beginning of each of these "queue runs", we simply provide a prioritized list of the observations to be done that month; the service observers work to complete them when the conditions are right. Though we lost some epochs due to weather, $\sim$ 12 epochs were achieved for each cluster. During the queue run we had next-day access to the data, which were immediately processed and searched for new supernovae. This method of observing is commonly referred to as real-time analysis (RTA), and is described in detail in the next section.

Since SNe are typed based on the elements present in their spectra – and also to some extent the shape of their light curve – SN surveys such as MENeaCS require follow-up observations to confirm and classify the detected transients. Dave Sand was primarily responsible for our triple-tiered follow-up observations. First, a classical imaging campaign was scheduled on the 2.3 meter Bok Telescope at Steward Observatory to verify transients, and furnish their light curves in between MegaCam queue runs. Second, classical runs with Hectospec at the MMT Observatory were scheduled to coincide with the end of MegaCam queue runs, to obtain spectra of as many detected transients as possible. Third, a target-of-opportunity program at Gemini was approved to obtain immediate spectra of any intracluster supernova candidate.

A.2 MENeaCS Real-Time Analysis

The section describes the MENeaCS real-time analysis (RTA) pipeline to detect new supernovae in CFHT exposures. It is not meant to be an exhaustive description of MegaCam data reduction. Rather, it is intended to provide an RTA pipeline template for SN surveys, and to give special attention to issues particular to time-sensitive reductions. It assumes a basic knowledge of common image quality parameters and reduction processes.

Although I constructed, tested, and ran the RTA pipeline, this was done with much assistance from the MENeaCS team and many of the pipeline's individual components were written by them. Where appropriate I credit the subroutines to their author by name, or to the Image Reduction and Analysis Facility (IRAF)[1], but otherwise continue to write in first person plural.

CFHT runs its three primary instruments in queue service observing (QSO) mode. All accepted programs for a semester are ranked, and service observers at the summit take exposures for the highest ranked program given current weather conditions. QSO mode results in more data being taken for all programs, a higher fraction of programs reaching completeness, and better data quality overall as exposures are taken and monitored by experts. With QSO, large long term projects such as the SNLS and MENeaCS are greatly facilitated.

In April 2009, the NRC's student travel grant allowed me to travel to CFHT during a MegaCam queue run. I visited both the headquarters in Waimea and the telescope on Mauna Kea, first learning how the QSO mode is set up and administered, and then helping to acquire data at the telescope, including some for MENeaCS. I was able to impress the service observers with images of new supernovae the very next night after using the the data reduction and candidate detection pipeline outlined in § A.2.1 and A.2.2.

A.2.1 Data Acquisition and Reduction

CFHT MegaCam exposures are reviewed every morning by staff astronomers to ensure they meet the image quality restrictions of their program. Those that do are validated and listed on the CFHT Night Reports webpage. A whole observing group (OG: two dithered exposures in each filter, g and r) is required for SN detection, so human interaction is required to flag validated exposures from incomplete OG's as unusable (a few minutes). If multi-

[1]IRAF is distributed by the National Optical Astronomy Observatories, which are operated by the Association of Universities for Research in Astronomy, Inc., under cooperative agreement with the National Science Foundation.

Table A.1 Approximate human and machine hours for the RTA pipeline.

Human Task	Hours
checking CFHT night report	0.2
starting scripts for new epochs	0.3
human review of candidate triplets	0.3
TOTAL	0.8

Machine Task	Hours
downloading and pre-processing	1
creating single epoch images	1
detecting & culling transients	2
deriving photometric corrections	2
updating database & creating finders	0.3
TOTAL	6.3

ple OG's are obtained in a night, they are automatically identified as a single epoch. The final list is used to sort exposures into epochs, highlight clusters with new data requiring processing, and update our progress websites.

Since MENeaCS is a real-time survey, CFHT automatically partially reduces (bias subtracts and flat-fields) the data and makes it available for download the following morning. Our automated data acquisition codes check for new data, download it, and convert it to the multi-extension format (MEF) required by the RTA pipeline. As an example, if CFHT obtains 5 epochs of MENeaCS data in a night ($\sim$ 30 Gigabytes), data acquisition completes within an hour with minimal human interaction. An approximate accounting for all the human and machine processing hours discussed in this section, for our example of 5 new epochs of data, is given as an example in Table A.1. At the end of every MegaCam queue run, data fully processed by the CFHT Elixir reduction software is also automatically downloaded.

Each individual exposure of an epoch can be searched individually for transients, or combined into a single image and then searched. We choose to combine, mostly to save time during later processing steps. To combine exposures we use three software packages by Emmanual Bertin[2]. First, SExtractor (Bertin & Arnouts 1996) generates a catalog of bright stars for each exposure. Next, SCAMP (Bertin 2006) simultaneously uses

[2]http://www.astromatic.net/

every exposure's catalog to create header files of astrometric and photometric solutions, by comparing to external star catalogs (we use 2MASS (Skrutskie et al. 2006)). Third, SWarp (Bertin et al. 2002) uses these headers to combine all epoch exposures into a single 20000x20000 image, free of chip gaps and centered on the brightest cluster galaxy. Optimal values for SExtractor, SCAMP, and SWarp input parameters were determined with CFHT MegaCam images prior to MENeaCS, confirmed to work well for the first MENeaCS data, and used consistently throughout the survey.

These three packages are automatically run in series by a single script written with Interactive Data Language (IDL)[3]. The final step adds several parameters essential to later processing to the epoch image headers: the sky background, the full-width half-max (FWHM) of the point spread function (PSF), and the SCAMP *fluxscale*. The sky background is eponymous, mathematically equivalent to the mode pixel value. The FWHM of the PSF is the apparent size of a point source's image disk, also known as the *seeing* when the crowning influence on FWHM is atmospheric turbulence. Both are common measures of image quality. The SCAMP *fluxscale* is a multiplicative factor which forces the SWarp output image zeropoint to 30; since actual zeropoint calculations can be complicated, this is convenient for RTA pipelines. Typically, epochs for 5 clusters are processed to single epoch images in $\lesssim 1$ hour and require no human interaction.

A.2.2 Candidate Detection

Subtracting a cluster's first epoch image from its newest epoch image results in a difference image containing only sources which have appeared, brightened, or since faded from view during the time between epochs. However, weather conditions such as light cloud layers, sky background, and seeing change the profile of *every* source. The resulting difference image is full of strange residuals, prohibiting the identification of real transients. To avoid this we degrade the quality of the better image to match the worse one. This common practice is called PSF-matching, and is well explained elsewhere (Alard & Lupton 1998). The basic method is to determine the PSF profiles of stars in each image, and from them the kernel which, when convolved with the better-seeing PSF, results in the worse-seeing PSF. This kernel is then convolved with the better-seeing image, and used in the subtraction to produce a clean difference image.

For transient detection we use a set of Fortran codes and IRAF scripts written by Chris Pritchet to align and PSF-match images, create difference images, extract transient sources

[3]http://www.ittvis.com/ProductServices/IDL.aspx

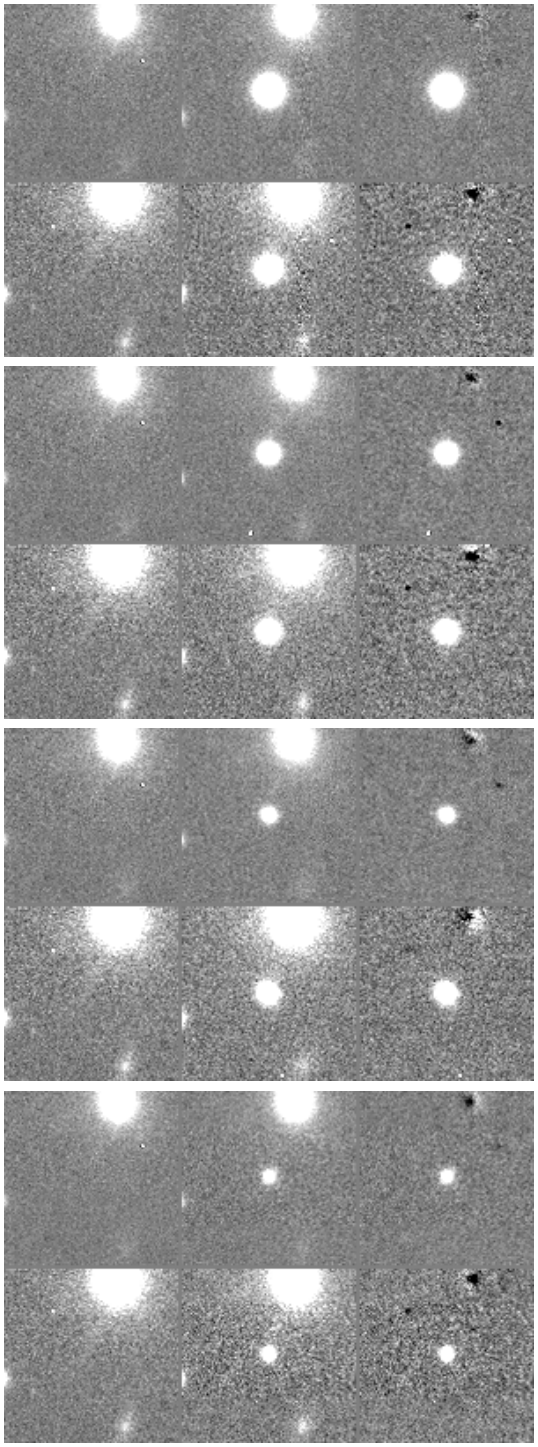

Figure A.1 A series of detection triplets for an IC SN candidate in Abell 399 from November 2008 to January 2009 (top to bottom). Each triplet is comprised of three columns displaying the first epoch, detection epoch, and PSF matched difference image (left to right), and one row each for the g- and r-band filters (top and bottom).

with the IRAF task DAOfind, and automatically reject objects unlikely to be real. This includes sources which are in the noise, are in groups (i.e. in diffraction spikes around foreground stars), are not round, and/or have negative sources very nearby (i.e. products of misalignments). The culling parameters were determined from the first few epochs of MENeaCS and then used consistently.

The resulting list contains up to hundreds of transients per square degree, and requires further automated culls before human review. We run an aperture photometry code written by Chris Pritchet on each transient to return fluxes in four apertures (2, 4, 8, and 16 pixels), an integrated flux from a best fitting PSF, and a χ^2 value representing its goodness-of-fit. Based on these, we impose the following five condition: a) simultaneous detection in g- and r-band filters; b) apparent g-band magnitude < 23.5; c) a positive peak flux; d) an increasing flux in each successively larger aperture; e) $\chi^2 < 50$. For all transients which survive these cuts we create detection triplet image stamps (Figure A.1) for review.

All of these steps, from image alignment to the generation of triplet stamps, are run automatically by high level scripts which format the data, input it to the programs, run the routines in series, and monitor their progress. For our example of 5 new epochs, this entire process takes a few hours and requires minimal interaction. The triplet review stage flags for discard any transient which is obviously not real (such as cosmic ray hits, exposure flaws, and PSF-match artifacts). Human review of 5 epochs worth of transients typically requires only 15 to 20 minutes. Information on successful candidate sources from each detection and culling level are stored in separate files, but disk space demands all processing product images be deleted.

For every candidate, we use a routine written by Dave Sand to identify a host in the galaxy catalogs generated by Chris Bildfell for each cluster field. This host finder is based on the algorithm presented in Sullivan et al. (2006a). It also queries the NASA/IPAC Extragalactic Database (NED) for known cluster members, non-cluster galaxies, and/or variable sources coincident with the candidate.

The Candidate Database

As soon as the data is reduced, we compile information on all candidates, from every cluster and epoch, in a single database. For this we use an IDL structure for its convenient arrays-within-arrays format. For each candidate we store their coordinates, cluster details, host galaxy information from Dave Sand's codes (including host offset and NED information), and the dates, fluxes, and magnitudes from all epochs of detection.

When two or more sources are coincident within 0.5″we identify them as the same

candidate. This is crucial in helping to exclude "SN impostors" such as variable stars, novae, and active galactic nuclei from our follow-up target lists (associations with NED known variables helps also). For every truly new candidate, a finder chart is automatically created from the first epoch image. Updating the database and making the finder charts for our example of 5 new epochs takes only about 15-20 minutes.

During database creation, we apply photometric corrections to candidate apparent magnitudes so all are in the Sloan Digital Sky Survey (SDSS) filter system (Fukugita et al. 1996). The details are unique to the survey design and will not be useful to readers outside of MENeaCS, but we will outline steps that would apply to any similar SN survey.

Only ~half of our clusters are covered by the SDSS, but that is enough to derive a reliable zeropoint for each MegaCam queue run. Our basic procedure is to derive a suite of internal adjustment factors for each epoch which correct it to the most photometric epoch, and then use queue run zeropoints of the most photometric epoch to correct to the SDSS filter system. The internal adjustments include an airmass term, color terms, aperture corrections, atmospheric attenuation, and the inverse of the SCAMP *fluxscale*. All are derived by internal comparisons of foreground star magnitudes, and use star-isolation and aperture photometry routines written by Chris Pritchet. It is important to note that since candidate magnitudes are measured on difference images made from PSF-matched images, the appropriate corrections are those for the *worse-seeing* epoch.

The derivation of photometric corrections for ~ 5 new epochs takes a couple of hours, but is generally run prior to updating the candidate database. Correcting to SDSS filter apparent magnitudes is very important because it allows us to combine imaging detections from CFHT and the Bok Telescopes to identify and prioritize candidates for follow-up, and set exposure times for spectroscopy.

A.3 SN Detection Efficiencies

In order to determine SN Ia rates from the MENeaCS survey, we must have a measure of our detection incompleteness. To do this we generate a population of fake SNe with realistic intrinsic properties, add them to our data, and repeat the SN detection pipeline. We can then consider the fraction of fake SNe recovered as a function of the properties, and derive corrections to our actual recovered supernovae to account for those missed. This section contains enough detail to be useful to anyone needing to perform a detection efficiency analysis for their SN Ia survey. Properties of the population of fake SNe Ia, methods of planting and recovering them, and our basic recovery statistics are presented in § A.3.1–

Table A.2 Clusters and epochs used for detection efficiencies.

Cluster Name	Epochs Used	Number of Epochs	Number of Fake SNe
Abell1068	4,5	2	356
Abell119	7,8,9,10,11	5	316
Abell1361	7,8,9	3	453
Abell1650	6,7,8	3	437
Abell1781	6,7,8,9,10	5	363
Abell2029	4,5,6,7	4	430
Abell21	2,3,4	3	445
Abell2440	5,6,7,8,9,10	6	314
Abell2443	6,7,8,9,10	5	380
Abell2597	9,10,11,12,13	5	285
Abell2627	6,7,8,9,10	5	340
Abell401	2,3,4,5,6	5	404
Abell644	4,5,6	3	466
Abell646	4,5,6	3	317
Abell754	9,10,11	3	450
RXCJ0132m08	3,4,5,6,7	5	265
RXCJ0736p39	6,7,8,9,10	5	343
ZwCl0628	2,3,4,5	4	554
Total = 18		74	6918

A.3.2.

A.3.1 Population of Fake SNe Ia

This section describes the characteristics of the population of fake SNe Ia, including the clusters and epochs used, their distribution on the sky and within their host galaxies, their intrinsic properties, and how observer-frame light curves are derived from rest-frame templates. Our goal was to create as realistic a sample of fake SNe Ia as possible, to obtain the most robust detection efficiencies.

Set of Clusters and Epochs

For a robust evaluation of our detection efficiencies, we wanted to ensure the fake SNe Ia were planted in clusters and epochs with a variety of properties. To cover our whole redshift range, we simply sorted the clusters by redshift and selected every third (approximately)

Table A.3 Host situation and sub-type for the fake SNe Ia.

Host Situation	SN Ia Subtype			
	Normal	SN 91bg-like	SN 91T-like	Total
Red-Sequence Hosted	1169	275	26	1470
Non-Red-Sequence Hosted	2655	788	19	3462
Cluster Hostless	477	75	8	560
Background Hosted	775	190	11	976
Background Hostless	367	68	15	450
Total	5443	1396	79	6918

for a total of 18 clusters. We then chose 2-6 consecutive epochs from each of these clusters to cover a range of seeing, sky background, and date. The chosen clusters and their epochs are listed in Table A.2. Note that we use only the central 24x24 arcminutes of the field for planting and recovery. Each cluster has catalogs, created by Chris Bildfell, of all galaxies in the field and the red-sequence galaxies only. The number of fake SNe Ia planted in a given cluster is proportional to the number of galaxies in the following way.

Spatial Distribution of Hosted and Hostless Fake SNe Ia

Five host categories are used for the fake SNe, three of which are associated with the cluster: SNe hosted by red-sequence cluster members, by other non-red-sequence (blue) cluster members, and hostless cluster SNe Ia. These fake SNe are given the redshift of their cluster. The two additional host categories are SNe hosted by background galaxies, and hostless SNe Ia in the background. The fake SNe in these categories are given a random redshift $0.3 < z < 0.5$.

We set the number of red-sequence hosted fake SNe at half the total number of red-sequence galaxies, and the number of cluster hostless is 25% of this. The number of non-red-sequence (blue) hosted fake SNe is equal to 1% of the total number of non-red-sequence galaxies. The number of background hosted and hostless fake SNe are 25% and 10% of this number, respectively. This aspect of the fake SN Ia catalog is certainly not realistic, but we plant far more SNe Ia than would be observed in order to get good statistics on our detection efficiencies. Table A.3 contains the number of fake SNe of each hosting type, and Figure A.2 contains the resulting redshift distribution.

All hosted fake SNe are distributed proportional to the light in galaxies by a code written by Chris Pritchet. Given the coordinates for the potential host galaxies and the number

of desired fake SNe, the code returns coordinates which are radially distributed around galaxies in a manner proportional to their radial light profiles. Hostless fake SNe are distributed randomly, and we do not allow a 'hostless' fake SN to be within 10 effective radii (R_{eff}) of any catalog galaxy. Once all fake SNe have their pixel coordinates, any within 100 pixels of another are rejected. Table A.2 contains the total number fake SNe for each cluster in column 4.

Fake SN Ia Properties: Sub-types, Stretch, Peak Brightness, and Phase

The four main characteristics of a SN Ia are its sub-type (normal, underluminous, or overluminous), its light curve stretch value s (see Equations A.1 and A.2), its intrinsic peak B-band magnitude $M_{B,peak}$, and its phase in days (time from peak magnitude). Based on these four properties, the magnitude of a fake SN Ia can be determined from templates (as explained in the next section). To generate a realistic population of fake SNe Ia, we use the observed distributions of these four properties.

We distribute the SN Ia sub-types as described in Richardson et al. (2002), with $\sim$ 20% of the total number of planted SNe Ia assigned as underluminous (SN 91bg-like) and $\sim$ 1% as overluminous (SN 91T-like). In Table A.3 we show the resulting number of fake SNe Ia of each SN Ia sub-type. As discussed above, the fake SNe's redshift is dictated by whether it's in the cluster or background. Phase, or day of the light curve since explosion, is randomly selected between -10 and +40 days. We use this as the *observer frame* day, as described below. One of the cluster epochs from the list in Table A.2 is randomly chosen to be the epoch for that phase, and the phase for other epochs are set accordingly. In Figure A.2 we plot the redshift and phase distributions for fake SNe.

The intrinsic peak B-band magnitude for normal SNe Ia is ~ -19.3 (Astier et al. 2006). We use a Gaussian distribution centered at -19.3 with $\sigma = 0.15$ and limited to $-19.6 \leq M_{B_{peak}} \leq -19.0$ (Perrett et al. 2010). The stretch distribution for normal SNe Ia is a Gaussian distribution centered at 1.0 with $\sigma = 0.1$; we do not correlate the stretch with host type (Sullivan et al. 2006a; Perrett et al. 2010). The intrinsic peak B-band magnitudes for SN 91bg-like events is set to -17.0 (Richardson et al. 2002), and for SN 91T-like events is -19.85 with no intrinsic variation (also unrealistic, but suitable for our purposes)
(Saha et al. 2001). The stretch values for all underluminous and overluminous SNe Ia is 1.0. Although underluminous SNe Ia are low stretch normal SNe Ia, we use the 1991bg-like template (discussed below) and thus do not extend our normal-SN Ia stretch distribution down that far, and do not need a stretch distribution for sub-luminous SNe Ia. Figure A.2 shows the distributions of $M_{B_{peak}}$ and stretch for the normal population of fake SNe Ia.

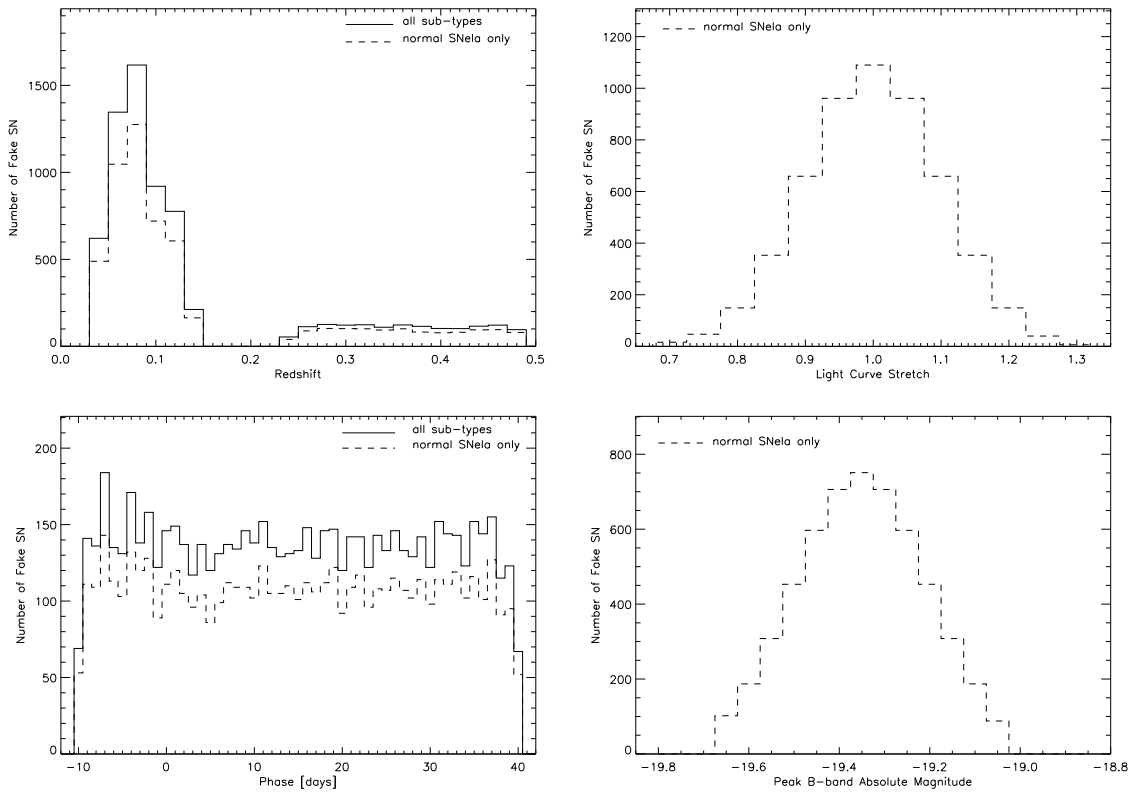

Figure A.2 Properties of the population of fake SNe Ia. At left, redshift (top) and phase (bottom) distributions for all fake SNe Ia (solid) and those of sub-type “normal” only (dashed). At right, light curve stretch (top) and intrinsic peak B-band apparent magnitude for fake SNe Ia in the “normal” sub-type only (dashed).

Generating Observer-Frame Light Curves

These four intrinsic properties must be converted to observable qualities, and for this we use the template light curves of Nugent et al. (2002). These SN Ia light curve templates include one each for normal, subluminous, and overluminous SN Ia types[4]. They are given in Vega magnitudes and normalized to $M_{B_{peak}}(t = 0) = 0$. We use Johnson B-band ($\sim$ 4450Å) and V-band ($\sim$ 5510Å) light curves, as these wavelengths correspond roughtly to MegaCam's g-band ($\sim$ 4620Å) and r-band ($\sim$ 6360Å) in the redshift range of MENeaCS clusters, $0.05 \leq z \leq 0.15$. This is less appropriate for the background sample of fake SNe, but we use a proper *K*-correction at all times. The first step is to convert the template's time axis from rest-frame days t_{rest} to observer-frame days t_{obs} with Equation A.1, and hereafter deal just with observer-frame days.

$$t_{obs}(d) = s\,(1+z)\,t_{rest}(d) \tag{A.1}$$

The next step is to convert the value of the appropriate Nugent template at the appropriate phase, which we express as $MT_{F_{peak}}(d)$, into an apparent magnitude m_f. Here we use F to denote rest-frame filter (B or V), and f for observed-frame filter (SDSS g or r). This conversion is given by Equation A.2,

$$m_f = [MT_{F_{peak}}(d) + M_{B_{peak}}(0) + \alpha(1-s)] + 5\log D_L(z) + 25 + K_{Ff} + A_f + m_{f,AB}(Vega), \tag{A.2}$$

where $M_{B_{peak}}(0)$ is the intrinsic peak B-band magnitude; $\alpha(1 - s)$ accounts for the relationship between stretch and peak brightness, and we use $\alpha = 1.5$ from Astier et al. (2006); $5 \log D_L(z) + 25$ is essentially the distance modulus where $D_L(z)$ is the luminosity distance in megaparsecs and z is the SN redshift; K_{Ff} is the *K*-correction from restframe filter F to observed filter f, and is calculated with an appropriate code from the SNLS IDL routines; A_f is the Galactic extinction in observed filter f for the coordinates of the SN; and $m_{f,AB}$(Vega) is the AB-system magnitude of Vega which converts from the Vega-system (which the Nugent templates are in) to the AB-system (which we want to use), where $m_{g,AB}(Vega) = -0.08$ and $m_{r,AB}(Vega) = 0.16$ [(5,6)].

The resulting distributions of apparent SDSS magnitudes for all fake SNe Ia are plotted in Figure A.3. The graph shows the distribution of brightest apparent magnitude reached in

[4]http://supernova.lbl.gov/ nugent/nugent_templates.html
[5]http://www.sdss.org/DR5/algorithms/sdssUBVRITransform.html
[6]http://dls.physics.ucdavis.edu/calib/vegaab.html

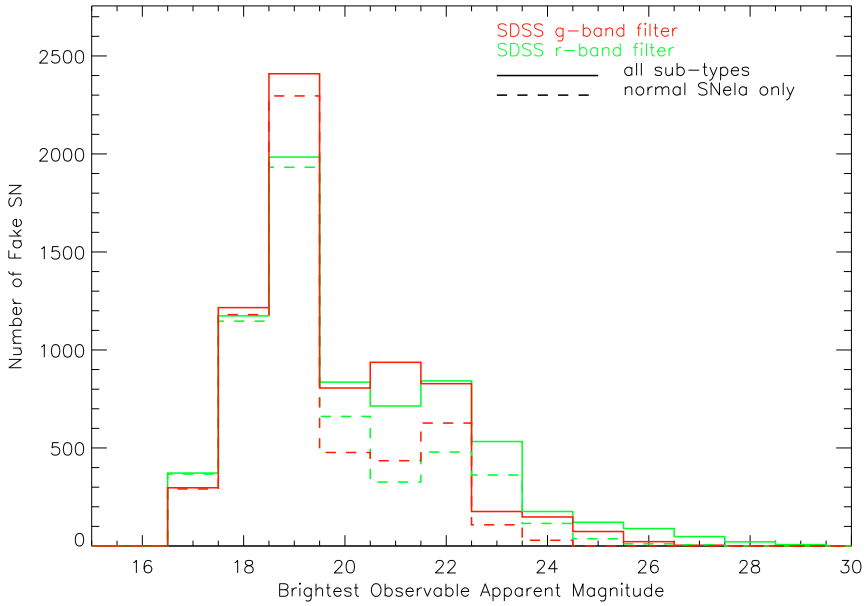

Figure A.3 Distribution of brightest observable apparent magnitude for the fake SN Ia population. Plotted for g- and r-band SDSS magnitudes (green and red), for all fake SNe Ia (solid), and the normal sub-type only (dashed).

any epoch, or brightest *observable* magnitude, has many bright and a tail of faint sources which, though perhaps not entirely realistic, are very useful for testing detection efficiencies as a funtion of magnitude. The apparent SDSS magnitudes of fake SNe Ia in each epoch are coverted to raw instrumental MegaCam magnitudes by applying, in reverse, all the photometric corrections we mention at the end of § A.2.

Planting and Recovering the Fake SNe Ia

We use a Fortran code written by Chris Pritchet to make a fake image containing only Moffat profile fake sources of specified instrumental magnitudes, planted at the given coordinates and with the FWHM PSF of the epoch image. Then we simply add this perfect image of fake sources to the epoch image. From there, transient detection and culling is done as described in § A.2.2, except that triplets are not made for visual review. Recall the only transients flagged for discard are those which are *obviously* not real, so no fake SN would ever be rejected at this stage. If a fake SN Ia survives the automated culling routine at least for one of its epochs, we consider it 'recovered'.

A.3.2 Recovery Statistics

Here we present our recovery statistics for all 6918 fake SNe Ia. In Figure A.4 we plot the number and fraction of fake SNe Ia recovered as a function of their brightest apparent magnitude in any epoch. Our first priority was to ensure the detection efficiency for hosted and hostless SNe Ia in clusters was equivalent, as this directly influences the ICL fraction measurement. From Figure A.4 we see they are mostly equal but diverge for faint fake SNe Ia (although, with small numbers statistics in the faint magnitude bins they are technically consistent).

There is also a difference in recovery fraction for faint ($m > 22$) hosted fake SNe Ia in red-sequence members and in non-red-sequence members. In Figure A.5 we plot the recovered fraction of cluster hosted fake SNe Ia as a function of their host offset for two bins of brightest observable fake SN Ia magnitude: $m_g < 22$ and $m_g > 22$. Host offset is in units of host effective radius (defined to contain half of a galaxy's luminosity). The interesting part of this graph is at small host offset, $R_{eff} < 1.5$, where we evidently have trouble detecting faint SNe Ia in brighter red-sequence galaxies. However, in general we do not consider these inefficiencies for faint fake SNe Ia to present an immediate problem for our SN Ia rates, as they represent a relatively small portion of our fake (and real) SN Ia populations.

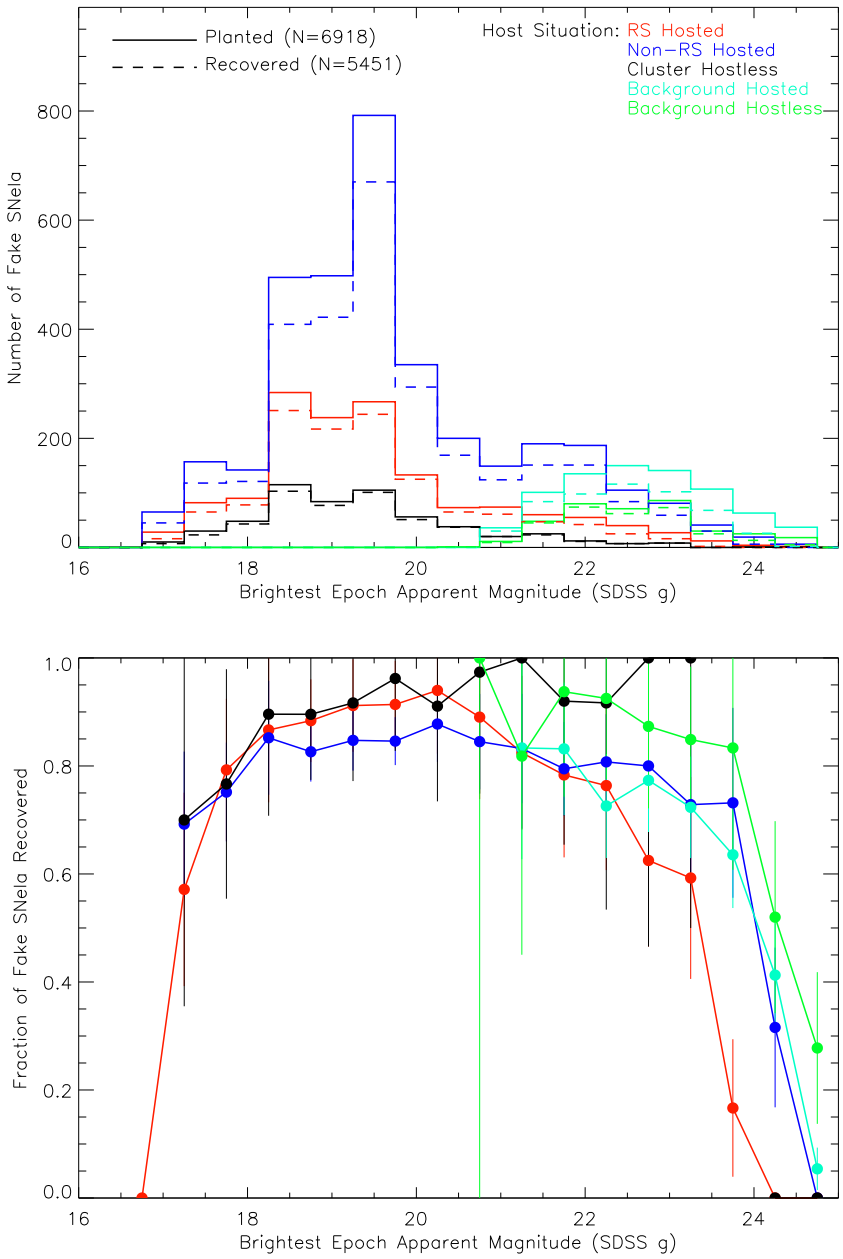

Figure A.4 Top: number of fake SNe Ia planted (solid) and recovered (dashed) as a function of planted apparent g-band magnitude in its brightest epoch. Bottom: fraction of fake SNe Ia recovered in each magnitude bin, with $\sqrt{N}$-derived error bars. Color corresponds to hosting situation.

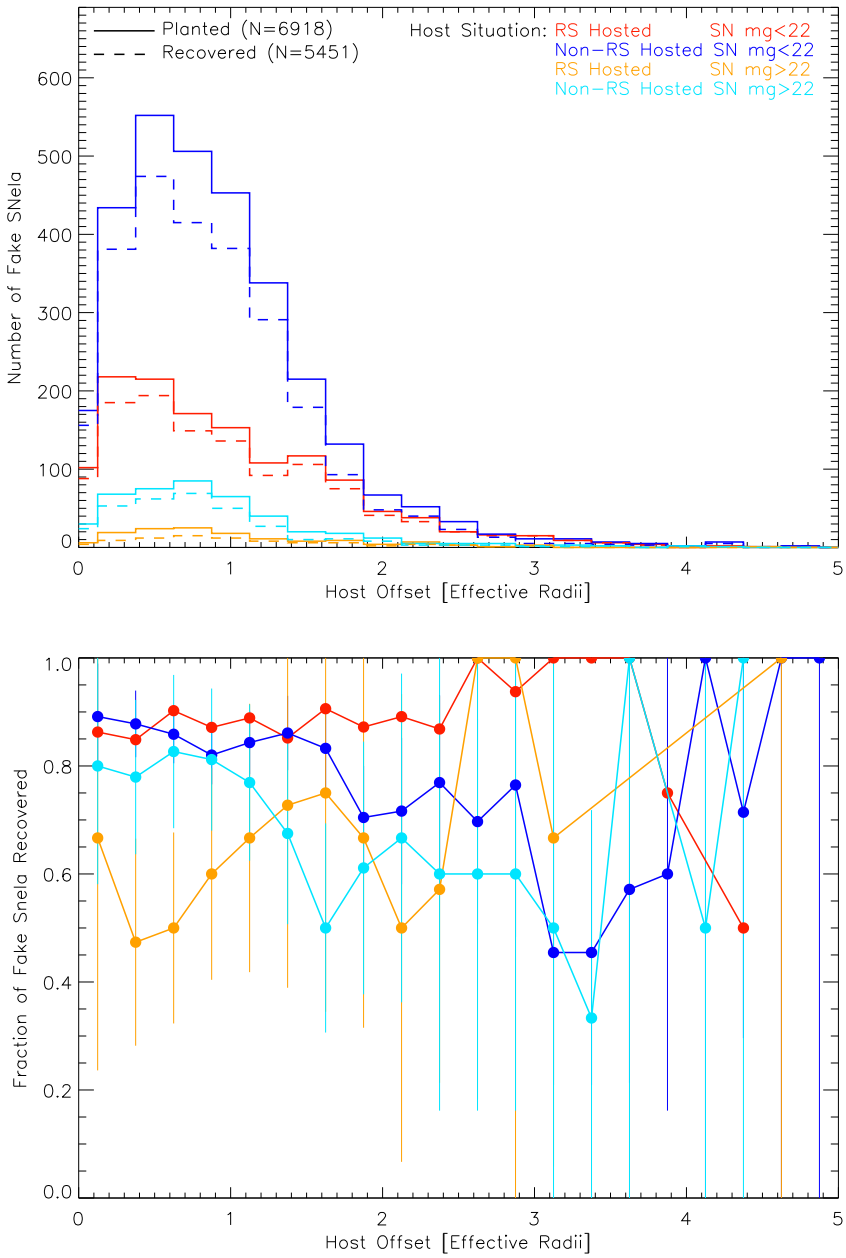

Figure A.5 Top: number of fake SNe Ia planted (solid) and recovered (dashed) as a function of host offset in units of host effective radii. Bottom: fraction of fake SNe Ia recovered in each host offset bin. Color corresponds to hosting situation *and* brightest observable magnitude of the fake SNe Ia.

A.4 Summary

This section has introduced the main science goals and technical specifications of the MENeaCS survey, described our RTA pipeline and candidate database, and presented our main detection efficiencies. Our first paper to present the four IC SNe Ia and their implications regarding the ICL fraction is slated for publication during the summer as Sand et al. (2010). However, my involvement with MENeaCS will not end there. We are working on the full cluster SN Ia rates paper and are also looking at the properties of cluster host galaxies, the paper for which will likely incorporate some of the science goals and methods discussed in Chapters 4–6.

Bibliography

[Alard & Lupton 1998] Alard, C. & Lupton, R. H. 1998, ApJ, 503, 325

[Arnett 1982] Arnett, W. D. 1982, ApJ, 253, 785

[Astier et al. 2006] Astier, P. et al. 2006, A&A, 447, 31

[Baade & Zwicky 1934] Baade, W. & Zwicky, F. 1934, Proc. N. A. S., 20, 254

[Barbary et al. 2010] Barbary, K. H. et al. 2010, AAS, 21534303B

[Bazin et al. 2009] Bazin, G. et al. 2009, A&A, 499, 653

[Becker et al. 2007] Becker et al. (2007) ApJ, 669, 905

[Bertin & Arnouts 1996] Bertin, E. & Arnouts, S. 1996, A&AS, 317, 393

[Bertin et al. 2002] Bertin, E. et al. 2002, ASPC, 281, 228

[Bertin 2006] Bertin, E. 2006, ASPC, 351, 112

[Bevington & Robinson 2003] Bevington, P. & Robinson, R. Data Reduction and Error Analysis for the Physical Sciences. New York: McGraw-Hill Companies Inc., 2003

[Binney & Merrifield 1998] Binney, J. & Merrifield, M. Galactic Astronomy. Princeton: Princeton University Press, 1998.

[Bondi et al. 2003] Bondi, M. et al. 2003, A&A, 403, 857

[Branch et al. 1993] Branch, D., Fisher, A. & Nugent, P. 1993, AJ, 106, 2383

[Buzzoni 2005] Buzzoni, A. 2005, MNRAS, 361, 725

[Capetti 2002] Capetti, A. 2002, ApJ, 574, 25

[Cappellaro et al. 1993] Cappellaro, E., Turatto, M., Benetti, S., Tsvetkov, D. Yu., Bartunov, O. S., & Makarova, I. N. 1993, A&A, 268, 472

[Cappellaro et al. 1997] Cappellaro, E., Turatto, M., Tsvetkov, D. Yu., Bartunov, O. S., Pollas, C., Evans, R. & Hamuy, M. 1997, A&A, 322, 431

[Cappellaro et al. 1999] Cappellaro, E., Evans, R., & Turatto, M. 1999, A&A, 351, 459

[Carlberg et al. 2008] Carlberg, R. G. et al. 2008, ApJ, 682, 25

[Chary & Elbaz 2001] Chary, R. & Elbaz, D. 2001, ApJ, 556, 562

[Ciliegi et al. 2005] Ciliegi, P. et al. 2005, A&A, 441, 879

[Coleman et al. 1980] Coleman, G. D., Wu, C. C., & Weedman, D. W. 1980, ApJS, 43, 393

[Condon et al. 1998] Condon, J. J., Cotton, W. D., Greisen, E. W., Yin, Q. F., Perley, R. A., Taylor, G. B., & Broderick, J. J. 1998, AJ, 115, 1693

[Conley et al. 2008] Conley, A. et al. 2008, ApJ, 681, 482

[Coupon et al. 2009] Coupon, J. et al. 2009, A&A, 500, 981

[Dahlen et al. 2004] Dahlen, T. et al. 2004, ApJ, 613, 189

[Dawson et al. 2009] Dawson, K. S. et al. 2009, AJ, 138, 1271

[Della Valle et al. 2005] Della Valle, M., Panagia, N., Padovani, P., Cappellaro, E., Mannucci, F., & Turatto, M. 2005, ApJ, 629, 750

[Dilday et al. 2010] Dilday, B. et al. 2010, ApJ, 715, 1021

[Evans et al. 1989] Evans, R., van den Bergh, S., & Clure, R. D. 1989, ApJ, 345, 752

[Filippenko 1997] Filippenko, A. V. 1997, ARA&A, 35, 309

[Fullmer & Lonsdale 1989] Fullmer, L. & Lonsdale, C. J. 1989, Cataloged Galaxies and Quasars Observed in the IRAS Survey, Version 2, Jet Propulsion Laboratory (JPL D-1932)

[Fukugita et al. 1996] Fukugita, M., Ichikawa, T., Gunn, J. E., Doi, M., Shimasaku, K., & Schneider, D. P. 1996, AJ111, 1748

[Gallagher et al. 2005] Gallagher, J. S., Garnavich, P. M., Berlind, P., Challis, P., Jha, S., & Kirshner, R. P. 2005, ApJ, 634,210

[Gallagher et al. 2008] Gallagher, J. S., Garnavich, P. M., Caldwell, N., Kirshner, R. P., Jha, S. W., Li, W., Ganeshalingam, M. & Filippenko, A. V. 2008, ApJ, 685, 752

[Gal-Yam et al. 2002] Gal-Yam, A., Maoz, D., & Sharon, K. 2002, MNRAS, 332, 37

[Gal-Yam et al. 2003] Gal-Yam, A., Maoz, D., Guhathakurta, P. & Filippenko, A. V. 2003, AJ, 125, 1087

[Gal-Yam et al. 2008] Gal-Yam, A., Maoz, D., Guhathakurta, P., & Filippenko, A. V. 2008, ApJ, 680, 550

[Gehrels 1986] Gehrels, N. 1986, ApJ, 303, 336

[Graham et al. 2008] Graham, M. L. et al. 2008, AJ, 135, 1343

[Graham et al. 2010] Graham, M. L. et al. 2010, AJ, 139, 594

[Greggio et al. 2008] Greggio, L., Renzini, A., & Daddi, E. 2008, MNRAS, 388, 829

[Gregory et al. 1996] Gregory, P. C., Scott, W. K., Douglas, K., & Condon, J. J. 1996, ApJS, 103, 427

[Griffith & Wright 1993] Griffith, M. R. & Wright, A. E. 1993, AJ, 105, 1666

[Guy et al. 2010] Guy, J. et al. 2010, A&A, accepted

[Gwyn 2001] Gwyn, S. D. J. The Evolution of Galaxies in the Hubble Deep Fields. Ph.D.T. 2001

[Hakobyan et al. 2008] Hakobyan, A. A., Petrosian, A. R., McLean, B., Kunth, D., Allen, R. J., Turatto, M., & Barbon, R. 2008, A&A, 488, 523

[Hamuy et al. 1996] Hamuy, M., Phillips, M. M., Schommer, R. A., Suntzeff, N. B., Maza, J., & Aviles, R. 1996, AJ, 112, 2391

[Hickson 1997] Hickson, P. 1997, ARA&A, 35, 357

[Hillebrandt & Niemeyer 2000] Hillebrandt, W. & Niemeyer, J. C. 2000, ARA&A, 38, 191

[Hirata et al. 1987] Hirata, K. et al. 1987, Physical Review Letters, 58, 1490

[Höflich et al. 2003] Höflich, P., Gerardy, C., & Linder, E. 2003, LNP, 635, 203

[Hogg 1999] Hogg, D. W. 1999, (arXiv:astro-ph/9905116)

[Hogg et al. 2002] Hogg, D. W., Baldry, I. K., Blanton M. R., & Eisenstein, D. J. 2002, (arXiv:astro-ph/0210394)

[Howell et al. 2001] Howell, D. A. 2001, ApJ, 554, 193

[Howell et al. 2005] Howell, D. A. et al. 2005, ApJ, 634, 1190

[Howell et al. 2006] Howell, D. A. et al. 2006, Nature, 443, 308

[Howell et al. 2007] Howell, D. A., Sullivan, M., Conley, A., & Carlberg, R. 2007, ApJ, 667, 37

[Howell et al. 2009] Howell, D. A. et al. 2009, ApJ, 691, 661

[Ilbert et al. 2006] Ilbert, O. et al. 2006, A&A, 457, 841

[Kinney et al. 1996] Kinney, A. L., Calzetti, D., Bohlin, R. C., McQuade, K., Storchi-Bergmann, T., & Schmitt, H. R. 1996, ApJ, 467, 38

[Knobel et al. 2009] Knobel, C. et al. 2009, ApJ, 697, 1842

[Komatsu et al. 2009] Komatsu, E. et al. 2009, ApJS, 180, 330

[Lacy et al. 2004] Lacy, M., et al. 2004, ApJS, 154, 166

[Ledlow & Owen 1996] Ledlow, M. J. & Owen, F. N. 1996, AJ, 112, 9

[LeFèvre et al. 2005] LeFèvre, O. et al. 2005, A&A, 439, 845

[Li et al. 2007] Li, W. et al. 2007, ApJ, 661, 1013

[Lilly et al. 2007] Lilly, S. J. et al. 2007, ApJS, 172, 70

[Lilly et al. 2009] Lilly, S. J. et al. 2009, ApJS, 184, 218

[Livio et al. 2002] Livio, M., Riess, A., & Sparks, W. 2002, ApJ, 571, L99

[Lonsdale et al. 2003] Lonsdale, C. J. et al. 2003, PASP, 115, 897

[Madrid et al. 2007] Madrid, J. P., Sparks, W. B., Ferguson, H. C., Livio, M., & Macchetto, D. 2007, ApJ, 654L, 41

[Magliocchetti et al. 2007] Magliocchetti, M., & Brüggen, M., 2007b, MNRAS, 379, 260

[Magliocchetti et al. 2008] Magliocchetti, M., Andreani, P., & Zwaan, M. A. 2008, MNRAS, 383, 479

[Mainieri et al. 2008] Mainieri, V. et al. 2008, ApJS, 179, 95

[Mannucci et al. 2003] Mannucci, F. et al. 2003, A&A, 401, 519

[Mannucci et al. 2005] Mannucci, F., Della Valle, M., Panagia, N., Cappellaro, E., Cresci, G., Maiolino, R., Petrosian, A., & Turatto, M. 2005, A&A, 433, 807

[Mannucci et al. 2006] Mannucci, F., Della Valle, M., Panagia, N. 2006, MNRAS, 370, 733

[Mannucci et al. 2007] Mannucci, F., Della Valle, M., & Panagia, N. 2007, MNRAS, 377, 1229

[Mannucci et al. 2008] Mannucci, F., Maoz, D., Sharon, K., Botticella, M. T., Della Valle, M., Gal-Yam, A. & Panagia, N., 2007, MNRAS, 383, 1121

[Maoz & Gal-Yam 2004] Maoz, D. & Gal-Yam, A. 2004, MNRAS, 347, 951

[Mazzali et al. 2007] Mazzali, P. A., Röpke, F. K., Benetti, S., & Hillebrandt, W. 2007, Science, 315, 825

[McGee & Balogh 2010] McGee, Sean L. & Balogh, Michael L. 2010, MNRAS, 403, 79

[Milkeraitis et al. 2010] Milkeraitis, M., Van Waerbeke, L., Heymans, C., Hildebrandt, H., Dietrich, J. P. & Erben, T. 2010, MNRAS, tmp, 701

[Moshir et al. 1992] Moshir, M., Kopman, G. & Conrow, T. A. O. 1992, Explanatory Supplement to the IRAS Faint Source Survey, version 2, JPL D-10015 8/92 (Pasadena: JPL)

[Navasardyan et al. 2001] Navasardyan, H., Petrosian, A. R., Turatto, M., Cappellaro, E., & Boulesteix, J. 2001, MNRAS, 328, 1181

[Neill et al. 2006] Neill, J. D. et al. 2006, AJ, 132, 1126

[Nomoto et al. 1984] Nomoto, K., Thielemann, F.-K. & Yokoi, K. 1984, ApJ, 286, 644

[Nugent et al. 2001] Nugent, P., Aldering, G., Hook, I., Permutter, S. & Wang, L. 2001, IAU Circ. 7612

[Nugent et al. 2002] Nugent, P., Kim, A. & Perlmutter, S. 2002, PASP, 114, 803

[Olsen et al. 2007] Olsen, L. F. et al. 2007, A&A, 461, 810

[Patiri et al. 2006] Patiri, S. G. et al. 2006, MNRAS372, 1710

[Perlmutter et al. 1997] Perlmutter, S. et al. 1997, ApJ, 483, 565

[Perlmutter et al. 1999] Perlmutter, S. et al. 1999, ApJ, 517, 565

[Perrett et al. 2010] Perrett, K. et al. 2010, AJ, accepted (arXiv:astro-ph/1006.2254)

[Phillips 1993] Phillips, M. M. 1993, ApJ, 413, 105

[Phillips et al. 2003] Phillips, M. M. et al. From Twilight to Highlight: The Physics of Supernovae: Proceedings of the ESO/MPA/MPE Workshop. Editors Hillebrandt, W. & Leibundgut, B. Springer-Verlag, 2003, 193

[Postman & Geller 1984] Postman, M. & Geller, M. J. 1984, ApJ, 281, 95

[Pritchet et al. 2008] Pritchet, C. J., Howell, D. A., & Sullivan, M. 2008, ApJ, 683, 25

[Richardson et al. 2002] Richardson, D., Branch, D., Casebeer, D., Millard, J., Thomas, R. C., Baron, E. 2002, AJ, 123, 745

[Riess et al. 1998] Riess, A. et al. 1998, AJ, 116, 1009

[Riess et al. 2007] Riess, A. et al. 2007, ApJ, 659, 98

[Röpke & Hillebrandt 2004] Röpke, F. K. & Hillebrandt, W. 2004, A&A, 420, 1

[Ruiz-Lapuente et al. 2004] Ruiz-Lapuente, P. et al. 2004, Nature, 431, 1069

[Saha et al. 2001] Saha, A., Sandage, A., Thim, F., Labhardt, L., Tammann, G. A., Christensen, J., Panagia, N., Macchetto, F. D. 2001, ApJ, 551, 973

[Sajina et al. 2005] Sajina, A., Lacy, M., & Scott, D. 2005, ApJ, 621, 256

[Sanders & Mirabel 1996] Sanders, D. B. & Mirabel, I. F. 1996 ARA&A, 34, 749

[Sanders et al. 2007] Sanders, D. B. et al. 2007, ApJS, 172, 86

[Schinnerer et al. 2007] Schinnerer, E. et al. 2007, ApJS, 172, 46

[Scannapieco & Bildsten 2005] Scannapieco, E. & Bildsten, L. 2005, ApJ, 629, L85

[Sharon et al. 2007] Sharon, K., Gal-Yam, A., Maoz, D., Filippenko, A. V., & Guhathakurta, P. 2007, ApJ, 660, 1165

[Sivanandam et al. 2009] Sivanandam, S., Zabludoff, A. I., Zaritsky, D., Gonzalez, A. H. & Kelson, D. 2009, ApJ, 691, 1787

[Skrutskie et al. 2006] Skrutskie, M. F. et al. 2006, AJ, 131, 1163

[Smartt 2009] Smartt, S. J. 2009, ARA&A, 47, 63

[Sorrentino et al. 2006] Sorrentino, G. et al. 2006, A&A, 460, 673

[Sullivan et al. 2006a] Sullivan, M. et al. 2006a, ApJ, 648, 868

[Sullivan et al. 2006b] Sullivan, M. et al. 2006b, AJ, 131, 960

[Tago et al. 2008] Tago, E., Einasto, J., Saar, E., Tempel, E., Einasto, M., Vennik, J., & Mller, V. 2008 A&A, 479, 927

[Takeuchi et al. 2005] Takeuchi, T. T., Buat, V., & Burgarella, D. 2005, A&A, 440, L17

[Thanjavur et al. 2009] Thanjavur, K., Willis, J. & Crampton, D. 2009, ApJ, 706, 571

[Timmes et al. 2003] Timmes, F. X., Brown, E. F., & Truran, J. W. 2003, ApJ, 590, 83

[Tristram et al. 2009] Tristram, K. R. W. et al. 2009, A&A, 502, 67

[Wood-Vasey et al. 2007] Wood-Vasey, M. et al. 2007, ApJ, 666, 694

[Woosley & Weaver 1986] Woosley, S. E. & Weaver, T. A. 1986, ARA&A, 24, 205

[Zamfir et al. 2008] Zamfir, S., Sulentic, J. W., & Marziani, P. 2008, MNRAS, 387, 856